POLITECNICO DI TORINO

Master of Science in Biomedical Engineering

Master Thesis

Bioactive glass scaffolds reinforced with tailor-made polyurethane coatings for Bone Tissue Engineering

SUPERVISORS

Prof. Gianluca Ciardelli

Prof. Aldo R. Boccaccini

Dr. Monica Boffito

CANDIDATE

Lucia Servello

December 2018

"Cento volte al giorno ricordo a me stesso
che la mia vita interiore e esteriore
sono basate sulle fatiche di altri uomini, vivi e morti,
e che io devo sforzarmi al massimo
per dare nella stessa misura in cui ho ricevuto"
Albert Einstein

Ai miei genitori

Table of content

Abstract

In the last decades, bioactive glasses have gained great importance in bone tissue engineering (BTE) applications due to their chemical similarity to the inorganic phase of bone and their excellent bioactivity. In fact, this class of biomaterials not only provides a biocompatible surface, but can also lead and enhance the deposition of new bone tissue. However, their relatively low mechanical properties, low resistance to fracture under loads and high brittleness limit their application in BTE approaches, which require robust mechanical structure and high resistance to applied stress. For this reason, extensive researches have been focused on the field of Polymer-Bioactive glasses composites.

The aim of this work was the design and characterization of 45S5 Bioglass®-based scaffolds (BG) coated with tailor-made polymers. The coating is expected to improve the mechanical resistance and stiffness of the scaffolds, with no significant changes in biocompatibility and bioactivity. In detail, the scaffolds were fabricated by the foam replica technique and coated by a dipping procedure with a custom-made poly(urethane-urea)s (PUs) or commercial poly(ε-caprolactone) (PCL) (80000 g/mol) which was used as control. Two polyurethanes were used as coatings, differing in their soft segment: poly(ε-caprolactone) (2000 g/mol) for KHC2000 polyurethane and a mixture of poly(ε-caprolactone) (2000 g/mol) and polyethylene glycol (2000 g/mol) (PEG) in 70/30 weight ratio for KHC2000E2000. For what concerns PU hard segment, both the materials were based on 1,6-hexamethylene diisocyanate and L-lysine ethyl ester. Concerning the characterization of the synthesized polyurethanes, they were thoroughly characterized in terms of their degradability by studying their hydrolytic and enxymatic degradation, which was assessed in terms of weight loss, changing of molecular weight (through Size Exclusion Chromatography) as well as morphological modification of the surface (evaluated by Scanning Electron Microscopy).

PCL showed almost no degradation during immersion in PBS, due to its hydrophobic nature. Moreover, no changing of surface or cross section morphologies were observed through SEM images even after 21 days of immersion. On the contrary, enzymatic degradation leads a drastically modification of the morphology through the gradually surface erosion. KHC2000 resulted the much stronger of the tested polymers against both hydrolytic and enzymatic degradation. In fact, also SEM images showed almost the same surface after 21 days of hydrolytic degradation, while the surface presented some broken sites after immersion in PBS containing Lipase. KHC2000E2000 presented the much complex degradation behaviour, and even if it able

to maintain its shape after 21 days of enzymatic degradation the final molecular weight was extremely low (5600 g/mol). Moreover, in addition to the enzymatic degradation the presence of PEG allows the entrance of water into the inner part of film leading a concomitantly bulk degradation. However, the enzymatic degradation is less dramatically in this case respect to PCL because of the less amount of ester groups present in the chains.

The foam replica scaffolding technology allowed the fabrication of highly porous scaffolds (>90%) with interconnected porosity that are expected to be easily colonized by cells. But, this highly porous structure is one of the contributors to the poor mechanical properties of this kind of matrices. In previous works scaffold dipping procedure has been optimized in terms of concentration of the polymeric solution prepared in chloroform and immersion time: 1% w/v concentration and 2.5 minutes for poly(ε-caprolactone), 0.5%w/v concentration and 1 minute for KHC2000 and 1%w/v and 1 minute for KHC2000E2000. In this work, in order to increase the amount of polymer, and subsequently enhance the overall scaffold mechanical properties, the dip coating procedure was repeated three times on each scaffold. Coated and uncoated scaffolds were characterized in terms of morphology by Scanning Electron Microscopy (SEM) that revealed a high porous structure even after three coatings. Moreover, results showed that the polyurethanes provide a more homogenous coating with respect to PCL.

Scaffold bioactivity was investigated after immersion in Simulated Body Fluid (SBF) by SEM, Fourier Transform Infrared Spectroscopy (ATR-FT-IR) and X-Ray Diffraction (XRD) to assess the successful deposition of hydroxyapatite. Moreover, to better clarify how the presence of polymeric coating affect the bioactivity, also Bioglass® pellets were soaked for 1 week in SBF and analysed through ATR-FT-IR and SEM. Use pellets instead of scaffolds allows to investigate directly the coated surface that contains higher amount and thicker layer of polymer. The results showed that the presence of polymers did not inhibit the well-known bioactivity of 45S5 Bioglass®.

Concerning mechanical properties, compressive tests were carried out in dry and wet conditions, to better simulate the *in-vivo* conditions. Scaffolds compressive strength was considerably increased by coating them with both polyurethanes and PCL. In fact, the compressive stress of uncoated 45S5 Bioglass® scaffolds was determined to be 0.13 ± 0.04 MPa, while it reached 0.33 ± 0.1 MPa, 0.32 ± 0.1 MPa and 0.27 ± 0.07 MPa for the scaffolds coated with KHC2000, KHC200E2000 and PCL, respectively. KHC2000-coated scaffolds showed a similar improvement in mechanical properties compared to both KHC2000E2000- and PCL-coated ones, but the amount of polymer coating was different, being around 0.9 mg/scaffold for KHC2000 and 1.5 mg/scaffold for KHC2000E2000 and PCL. In addition, KHC2000-coated scaffolds retained they mechanical property in wet conditions much better than KHC2000E2000-coated ones probably because of its higher stability in aqueous environment.

Furthermore, compressive tests were carried out after 3, 7, 14 and 21 days of immersion in SBF to investigate the effect of the degradation and the hydroxyapatite deposition on the mechanical behaviour. After immersion in SBF for up 21 days, coated scaffolds showed well-maintained mechanical properties thanks to the slower rate of dissolution of the crystalline phase, never-

theless for all the three coated samples the compressive strength after 21 days was found to be in the range 0.09 – 0.16 MPa which was in the same range of the compressive strength of as-sinterd scaffolds without immersion in SBF.
Degradation tests were carried immersing the samples for up 21 days in PBS to analyse the percentage of weight loss and the pH variation during the degradation. All the coated scaffolds exhibited almost the same degradation rate of pure Bioglass® scaffolds. Only KHC2000-coated scaffolds, despite the initial burst release, provide more stability after 14 days of immersion.
Biological tests using MG-63 cells showed that the synthesized polyurethanes were cytocompatible, and the coating with KHC2000 worked significantly better than that based on commercial PCL. In details, after WST-8 analysis cell viability of KHC2000- and PCL- coated scaffolds was 114 ± 3% and 88 ± 1%. (using uncoated scaffold as control), respectively. Fluorescence analysis revealed a good colonization of the scaffolds even in the inner part thanks to the high porous structure, and the cells were well spreaded on the surface in both uncoated and coated scaffolds. Thus, the coating layer did not influence the good biocompatibility of the parent 45S5 Bioglass® scaffolds that is well known to promote the adhesion ad proliferation of osteoblasts.
Altogether, the results of the present investigation showed that 45S5 Bioglass®-scaffolds coated with custom-made poly(urethane-urea)s have promising potential for application in bone tissue engineering. In fact, thanks to their multi-block structure this class of biomaterials allows a fine tuning of their characteristics which results in the possibility to modulate the properties of the resulting matrices at a larger extent with respect to commercially available materials.

1 . Introduction

1.1 Bone Tissue Engineering

1.1.1 Bone

Bone is a very complex tissue that provides mechanical support and protection from damages and injuries to the internal organs. It stores approximately 85% of the body's phosphorus and 99% of calcium [1] and plays an important role within their homeostasis in the circulating body fluids.

At the macroscopic level, it is possible to distinguish two types of bone tissue, namely cortical and cancellous bone, which are characterized by different micro-level organization and, as a consequence, different functions and mechanical properties (Tab. 1.1). All the bones inside the body contain both he cortical and the cancellous bone, but their distribution and ratio vary based on the anatomical site [2].

Table 1.1: *Mechanical properties of cortical and cancellous bone [12]*

Property	**Cortical bone**	**Cancellous bone**
Compressive strength	100-230 MPa	2-12 MPa
Tensile strength	50-100 MPa	10-20 MPa
Strain to failure	1-3%	5-7%
Fracture toughness	2-12 $MPa\sqrt[2]{m}$	-
Young's modulus	7-30 GPa	0.5-0.05 GPa

The structural unit of the cortical bone is called osteon and it is formed by concentric lamellae around a central canal, called Haversian canal, which is run through by blood vessels and nerves (Fig. 1.1a). Cortical bone possesses a very low porosity, around 2-13%, and high average density of 1.8 g/cm^3 [12]. Because of its properties, the compact bone is present under the periosteum and in the diaphysis, where it provides support and protection. On the other hand, cancellous bone has a porosity of 50-90% and low average density, around 0.2 g/cm^3 [12] as a consequence of its sponge-like structure. In the cancellous bone the lamellae forms trabeculae that grow on the same direction of applied maximum stress.

From a material science point of view, bone is a composite material consisting of 20% of water and 80% of solid matrix that is made up of:

- Organic phase (30-35% dry weight) in which the principal component is type I collagen. It is a structural protein very well organized in fibers, as showed in Fig. 1.1b, that gives viscoelasticity to the bone, stabilizes the extracellular matrix and supports the mineral deposition. The other types of non-collagenous proteins present in the organic phase (such as albumin, fibronectin, decorin, osteonectin) are important for matrix organization, cell signalling, metabolism and mineralization [3].
- Inorganic phase of hydroxyapatite $C_{10}(PO_4)(OH_2)$ (65-70% dry weight). These crystals grow in an orderly way on the collagen fibers providing structural reinforcement; indeed, they are responsible of bone hardness and stiffness.

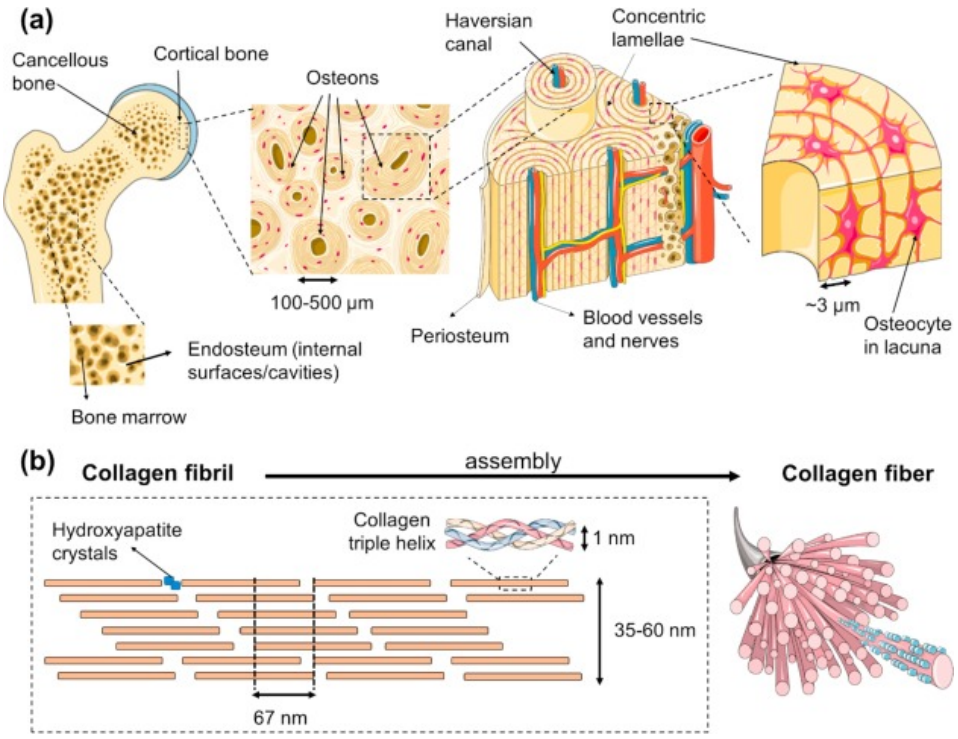

Figure 1.1: *Interscale representation of bone: a) A macroscopic-to-microscopic view of cancellous and cortical bone and b) Bone tissue is constituted at the nanometric scale by collagen fibers that contain the mineral phase. [2]*

In the calcified matrix four different types of bone cells with different functions are present, osteogenic cells, osteoblasts, osteocytes and osteoclasts. Bone is highly dynamic tissue that is constantly created and replaced and the cells have a crucial role in this process called remodeling. Osteoblasts, differentiated from mesenchymal cells, are located on the surface of the tissue and their main function is to produce new bone and induce mineralization. At the end of the process they undergo apoptosis, or they are encapsulated into the matrix and become osteocytes. Osteocytes are the primary cells of mature bone, responsible for the maintenance of the mineral concentration of the bone and the modulation of the activity of osteoclasts and osteoblasts during the remodeling process [7]. Each osteocyte is embedded into the matrix in a place called lacuna and can communicate and exchange substances with the surrounding cells through the

canaliculi [1, 2]. The primary role of osteoclasts, differentiated from hematopoietic stem cells, is the localized degradation of the matrix during bone remodeling. Hence, the proper balance between osteoclast and osteoblast activity plays a key role in the maintenance of a healthy condition. For instance, in case of disproportionate resorption concomitant with a decreased osteoblastic activity, the bone mass is reduced and the bone becomes osteoporotic. On the other hand, when osteoblast activity prevails over osteclast one, hypercalcification phenomena occurs.

Bone tissue exhibits a high capacity of remodelling and self-regeneration thanks to the combined action of the bone cells depending which can be finely tuned by applying different mechanical stimuli [1].

Bone healing is a complex process divided into three sequential stages (Fig. 1.2):

1. *Inflammatory phase*: during the first phase of the healing process a hematoma forms due to broken blood vessels after the trauma. Necrotic cells release danger signals that lead to the activation of the inflammatory response and the coagulation cascade that replace the hematoma with a temporary fibrin network [4]. In the meantime, macrophages remove bone fragments and induce the recruitment of mesenchymal and osteogenic cells.

2. *Soft callus formation*: because of the lack of vascularization, the fracture site is hypoxic. Hence, mesenchymal cells become chondrocytes and they produce cartilage that bridges across the fracture site to hold the bone fragments [4]. The soft callus provides mechanical stability and a template for vascularization and then mineralization. By a process called endochondral ossification, bone cells replace soft tissue with woven (or immature hollow) bone.

3. *Remodelling*: over months or even years, woven bone and the cartilage matrix are removed by osteoclasts and the bone begins to remodel based on the mechanical stress it is subjected to [4].

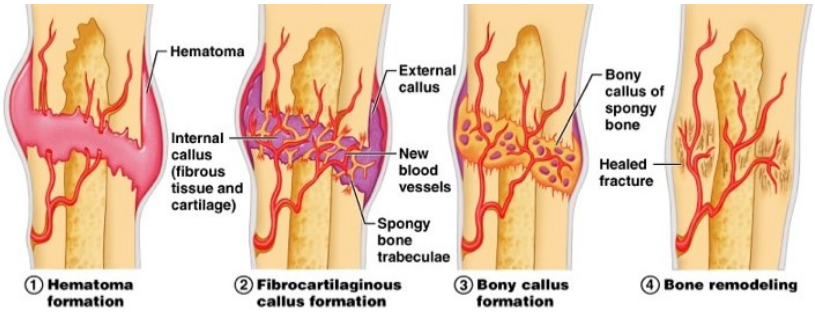

Figure 1.2: *Schematic rapresentation of bone healing process*

1.1.2 Biomateriales in Bone Tissue Engineering

As discussed previously, bone exhibits a high regenerative capacity. Hence, when the injury is smaller than "the critical size defect", bone is able to repair itself and the newly formed tissue

is indistinguishable from the healthy one. The critical size defect is defined as “the smallest size intraosseous wound in a particular bone and species of animal that will not heal spontaneously during the lifetime of the animal” (Schmitz & Hollinger 1986, Hollinger & Kleinschmidt 1990) [8]. It is not possible to exactly define the critical size or volume as critical size, but as a general guideline the literature proposes to consider as critical a size with length greater than 1–2 cm and a loss of the circumference of the bone greater than 50% [9].
In these cases, usually resulting from trauma, osteoporosis, bone neoplasia, infection, tumour resection, orthopaedic surgery, oral and maxillofacial surgery, a bone replacement is required to support the impaired or insufficient regeneration processing of the tissue.
Nowadays, the gold standards for bone reconstruction are autografts, in which cancellous iliac bone is taken from the same patient and used as graft. Autogenous bone ensures high regeneration and integration within the injured bone without risk of immunogenic response, since it is perfectly biocompatible [10]. However, this procedure has some drawbacks, such as the limited availability, donor site morbidity, and the extra surgery often causes more pain to the patient and requires longer periods of rehabilitation [11].
An alternative to solve the above-mentioned problem is represented by allografts, where bone is taken from a living human donor or from cadaver (freeze-dried bone), or xenografts (animal origin). However, they exhibit some disadvantages concerning their low revascularization and integration, their different kinetics of remodelling, the large immunogenic response and the non-negligible risk of transmission of viral pathologies [12].
A different option is the implantation of biomaterials to replace the tissue. The term "biomaterial" has been defined by the American National Institute of Health as “substance or combination of substances, other than drugs, synthetic or natural in origin, which can be used for any period of time, which augments or replaces partially or totally any tissue, organ or function of the body, in order to maintain or improve the quality of life of the individual” [13]. In the last years, great attention has been focused on this field since the implantation of biomaterials guarantees major availability, reproducibility, international standard and reliability [14] with respect to the transplantation of autologous and allogenic bone.
In Bone Tissue Engineering, biomaterials can be divided into three categories.
First generation biomaterials, developed during the 1960s and 1970s, were designed to match the mechanical properties of the host tissue in order to avoid stress shielding phenomena and the consequent bone resorption. These biomaterials, such as Titanium, Alumina, Zirconia and Poly(methyl methacrylate), were bioinert, meaning that the goal was to replace the defect without inducing any foreign body response of the host’s immune system. The implantation of such materials into the body promotes the pro-inflammatory process that leads to the encapsulation of the inert material into an acellular collagenous bag [15]. The thickness of the fibrous layer between the tissue and the material is related to the condition of the material, the tissue and the mechanical load.
The emphasis of the *second generation* of biomaterials was the creation of a stable interface with the host tissue, without formation of the fibrous layer, thus enhancing bone growth. Therefore,

biomaterials became bioactive, namely they "elicit a specific biological response at the interface of the material which results in the formation of a bond between the tissues and the material" [17].

Since 1984, a large research has been carried out in this field and many new materials have been discovered: bioactive glasses (45S5 Bioglass®) and glass-ceramics, A/W glass ceramics, machinable glass-ceramics, dense calcium phosphate ceramics (synthetic hydroxyapatite), bioactive composites and bioactive coatings. Each of these materials exhibits a different mechanism, strength and thickness of the bonding with the bone tissue (Fig. 1.3) [16]. In particular, it was reported that the thickness of the bonding zone between the material and the tissue is related to an Index of Bioactivity (I_B) [23] defined by Hench:

$$I_B = \frac{100}{t_{0.55bb}} \tag{1.1}$$

Where $t_{0.55bb}$ is the time required to bind more than 50% of the implant interface to bone [23].

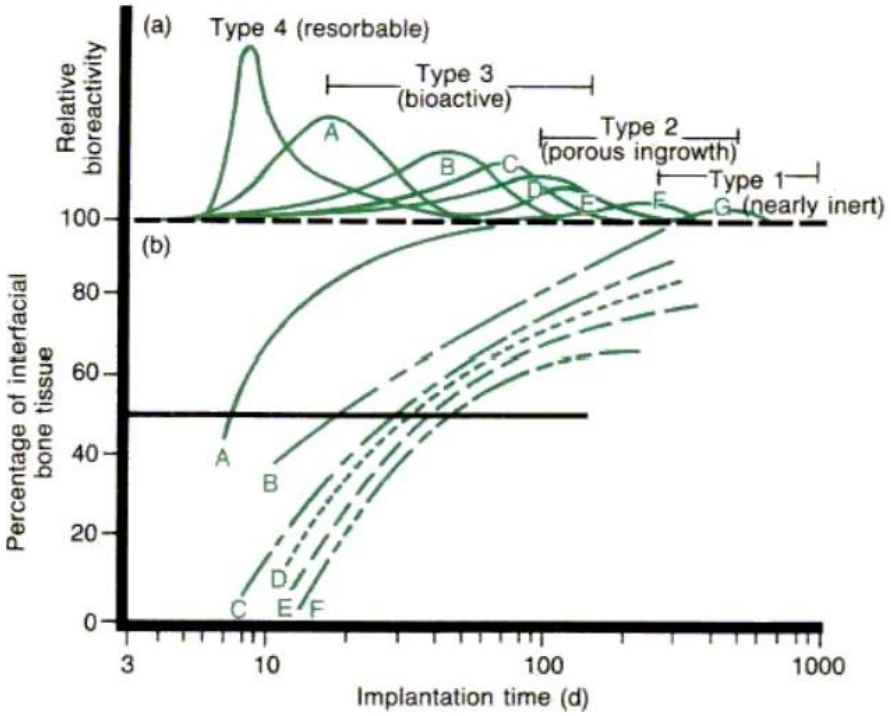

Figure 1.3: *Bioactivity spectrum for various bioceramic implants: (a) relative rate of bioactivity and (b) time dependence of formation of bone bonding at an implant interface. [(A) 45S5 Bioglass®, (B) Mina13 Cerevital®, (C) 55S4.3 Bioglass®, (D) A/W glass-ceramic, (E) HA, (F) KGy213 Cerevital®] [16]*

Thanks to this value it is possible to estimate the bioactivity level in terms of interactions with the host bone and, consequently, to classify the bioactive materials:

- *Class A: osteoproductive (or osteoinductive) materials.* These materials, like bioactive glasses, interact with the osteogenic cells realising ions that promote bone growth. Moreover, they are able to bind to either bone and soft tissues [53].

- *Class B: osteoconductive materials.* They present a non-specific response; they only provide a biocompatible interface and a bioconductive pathway that allow bone to grow. Ceramic materials, such as synthetic hydroxyapatite and tri-calcium phosphate (TCP), belong to this category [53].

Second generationbiomaterials also include the resorbable biomaterials, which degrade and resorb upon implantation, thus, allowing the seeding and the proliferation of the osteogenic cells. Then, the cells secrete their own extracellular matrix and finally the material is totally replaced by new bone. Since the products of the degradation are realised into the body they must be biocompatible and biologically accepted by the body [19]. Moreover, the degradation rate of the resorbable implant should match the repair rate of the bone in order to guarantee an optimal support during the regeneration process [16].
The newest materials, belonging to the *third generation*, are bioactive and resorbable biomaterials, namely "bioactive materials are being made resorbable and resorbable polymers are being made bioactive" [18]. Through molecular modifications of polymers, bioactive glasses, glass-ceramics and composites, it is possible to induce specific reactions directly to the cells that stimulate the regeneration of the tissue.

1.2 Bioactive glasses

As general concept, a glass is a liquid with an amorphous structure that has lost its ability to flow and it is obtained by a very fast cooling of the liquid in order to inhibit the nucleation of the crystalline phase. A silicate-based glass presents a continuous network of silicon-oxygen tetrahedral units (short range order) randomly linked to each other in terms of degree and length of the bond, as showed in Fig. 1.4a. In addition to the primary glass former, it is possible to incorporate intermediate (Al_2O_3, ZnO, ZrO_2) and modifying oxides (alkali and alkaline earth elements, such as Na_2O, K_2O, CaO, BaO) [20]. They are not able to form a glass network by themselves, but they can change the structure and subsequently the property of the glass. For instance, in multicomponent silicate glasses, some silica is replaced by the intermediates, meanwhile the modifiers broke the Si – O – Si units and create ionic bonds with oxygen (Fig. 1.4b). Furthermore, using a heat treatment on the glass, called devitrification, it is possible to elicit the growing and nucleation of the crystalline phase, thus, obtaining a glass-ceramic that exhibits better thermo-physical properties and higher strength and wear resistance [20].

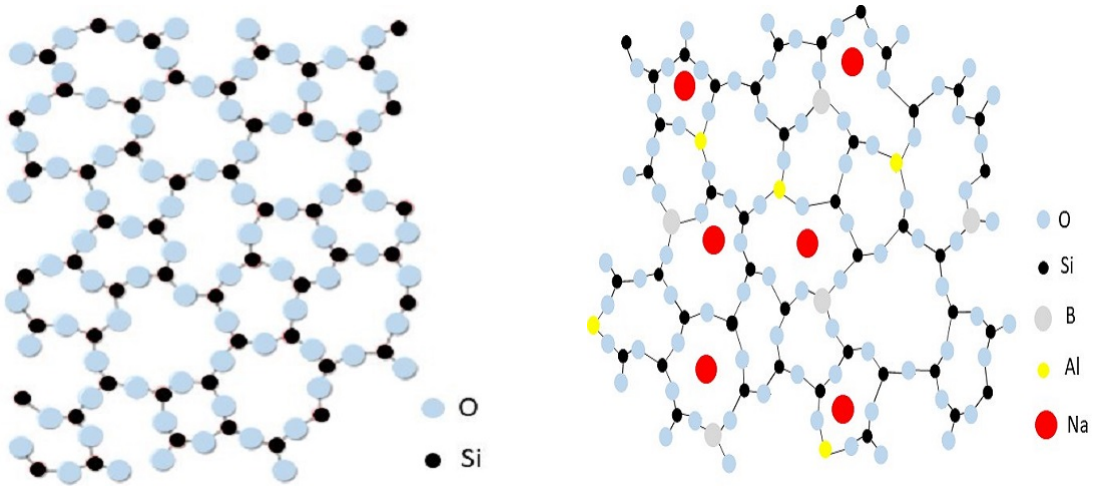

(a) (b)

Figure 1.4: Two-dimensional structure model of a) a silicate glass and b) an alkali-silicate glass with disrupted network

Thanks to the possibility to finely tune their properties, glasses and glass-ceramics have gained great attention for biomedical applications especially after the discovery of the bioactivity property of the second generation biomaterials. Obviously not all the glasses exploit the possibility to form a strong bond with the bone through a bone-like hydroxyapatite layer and the mechanism of bioactivity also depends on the glass composition. Hench and colleagues [22], the pioneers into bioactive glasses field, proposed a compositional diagram of the silicate glass system (SiO_2–CaO–Na_2O–P_2O_5), reported in Fig. 1.5, that allows the definition of different types of glass. In the diagram the percentage of P_2O_5 is fixed at 6%, since the characteristics and the possibility to make a glass only depend on the amount of silica and on the molar ratio Na_2/CO.

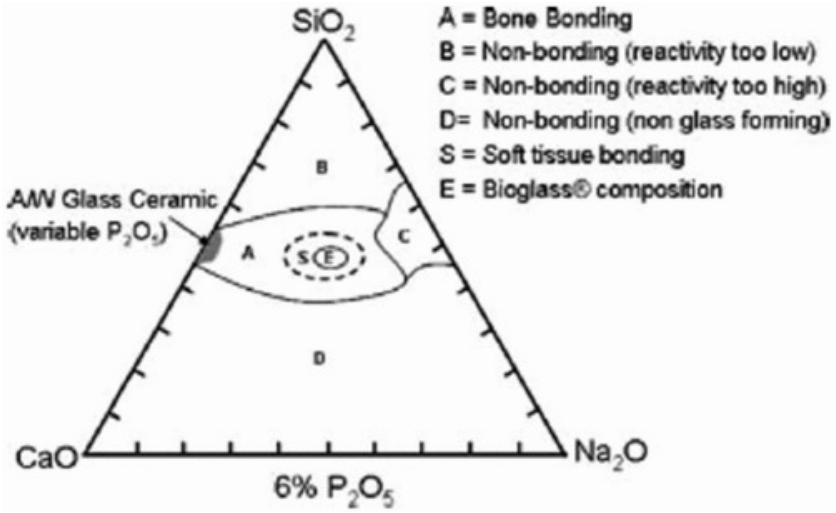

Figure 1.5: *Compositional diagram representing the bone bonding properties of bioactive glasses. [29]*

The broader is the presence of silica, the higher is the possibility of vitrification; hence, the compositions in region D do not allow the formation of a glass network since the precence of silica is not enough. On the other hand, the compositions containing an excess of silica (>70% mol) are poorly reactive and they are not able to create the hydroxyapatite layer; hence, the glasses that fall in region B are inert and they are encapsulated by fibrous tissue after implantation into the body [21]. The glasses with compositions in region C are resorbed in a few days after implantation (10-30 days) [29]. The glasses in region A are characterized by an high bioactivity index ($I_B > 8$) and they belong to class B, thus they are able to bond either hard and soft tissues. Finally, region E includes the composition of 45S5 Bioglass®, the first composition invented and the most used and investigated even today.

The story of **45S5 Bioglass®** started in the summer of 1967 during the U.S Army Material Research Conference about radiation resistant materials, when Colonel Klinker asked Larry Hench, one of the pioneers of modern biomaterials science, if it could be possible to create also a material able to survive to the biological environment in the human body [23]. In detail, he said "We can save lives, but we cannot save limbs. We need new materials that will not be rejected by the body" [22].
This stimulating question lead Hench to develop a new material with a composition closer to the bone that can bond the living tissues with no encapsulation in an acellular collagenous bag. Therefore, Hench investigated the silicate-based bioglasses belonging to the SiO_2 – Na_2O – CaO system and the first and the most popular bioactive glass, known as 45S5 Bioglass®, was discovered, starting a very intensive research in that field.
Bioglass® is produced by a conventional melt-derived synthesis route. 45S5 Bioglass® is commercially available in the form of a powder with a composition of 45% SiO_2, 24.5% Na_2O, 24.5% CaO, 6% P_2O_5 (in wt%) and it is characterized by three compositional features that are responsible for its bioactivity. Silicon is the primary glass former and its low content (<60% mol) plays an important role on the dissolution rate of the glass, meanwhile the high content of glass network modifiers (CaO - Na_2O) and the high CaO/P_2O_5 ratio provide high reactivity to the glass surface, thus inducing the formation of a surface layer of crystal hydroxyl-carbonate-apatite in a very short time. Furthemore, the CaO/P_2O_5 ratio was chosen to simulate the fisiological ratio into the hydroxyapatite minerals.
When the glass is implanted into the human body activated physiological cascade is quite complex and involves protein adhesion, cell proliferation and differentiation [23]. The bonding to hard and soft tissue through the formation of bone-like apatite is due to several reactions [22, 23], as reported in Fig. 1.6.

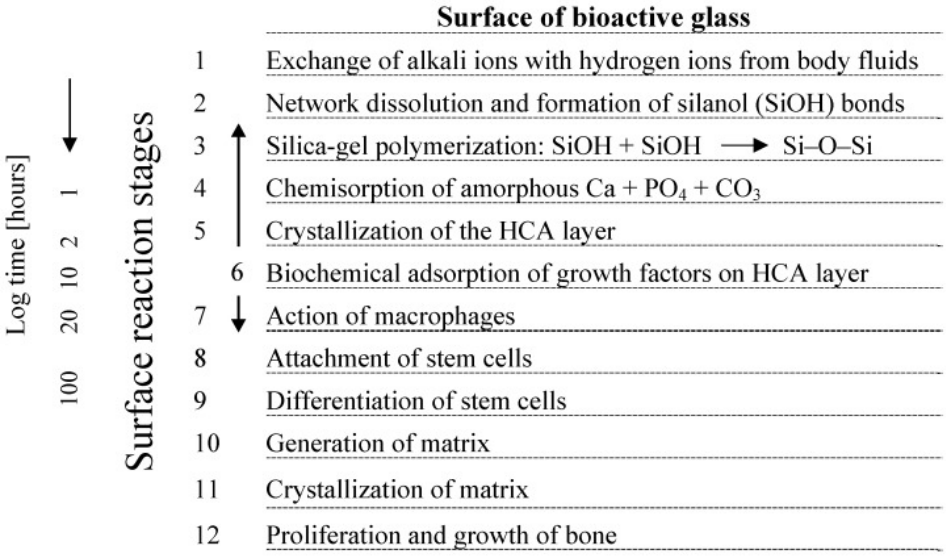

Figure 1.6: *Sequence of reactions on the bioactive surface after implantation into the human body [24]*

The first five stages lead to a quick release of ions and the formation of a calcium-deficient carbonate phosphate surface layer, Fig. 1.7.

Stage 1: Ion exchange between H^+ from the solution and the glass network modifiers. These ions (Na^+ and Ca_{2+}) are easily released, from the structure to the solution, because they are bonded with the non-bridging oxygen, thus they are replaced by H^+. This rapid exchange causes the hydrolysis of the silica group, leading to the formation of silanols (Si – OH):

$$\mathrm{Si-O-Na^+ \;+\; H^+ \;+\; OH^- \longrightarrow Si-OH \;+\; Na^+ \;+\; OH^-(aq)}$$

As a consequence, the pH of the solution increases.

Stage 2: Due to the pH increase, also the bonds between Si and the bonding-oxygen break, leadingto the release of soluble silica $Si(OH)_4$ in the solution. At the same time, silanols continue to condense at the glass/fluid interface:

$$\mathrm{Si-O-Si \;+\; H_2O \longrightarrow Si-OH \;+\; OH-Si}$$

Stage 3: Condensation and repolymerisation of a poor in cations and silica-rich layer on the surface of the glass (silica gel). Typically, the thickness of this layer is 1-2 µm [28].

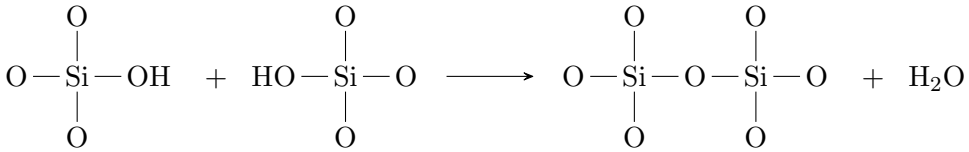

Stage 4: Diffusion of the Ca^{2+} and $(PO_4)^{3-}$ groups through the amorphous $CaO\text{-}P_2O_5$ layer and consequent formation of an amorphous calcium phosphate (ACP) layer.

Stage 5: Crystallisation of the amorphous film and formation of a mixed hydroxycarbonate apatite (HCA) layer, structurally similar to the mineral phase of bone, resulting from the incorporation of OH^- and $(CO_3)^{2-}$ anions from the solution [27].

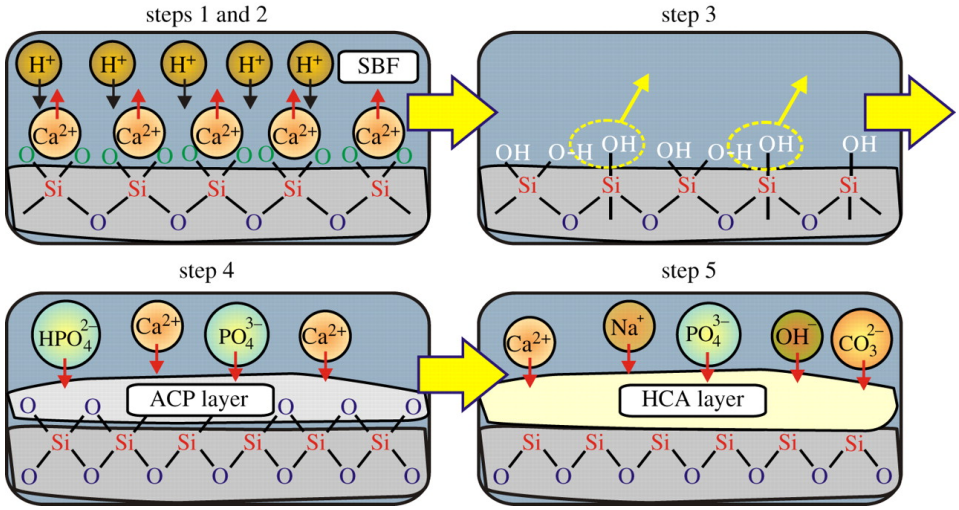

Figure 1.7: *Formation of HCA layer [26]*

The biological process of bone-bonding starts with the formation of the HCA layer. First of all growth factors are adsorbed into the layer (*Stage 6*), followed by the activation of macrophages that are required to begin the tissue repair process (*Stage 7*). Then, attachment (*Stage 8*) and differentiation (*Stage 9*) of osteoblasts occur and they start to generate the organic bone matrix (*Stage 10*). During crystallization, mature osteocytes are encased into the matrix and gradually the bioactive glass is absorbed with increasing bone ingrowth. [22, 28]

According to Kokubo et al [90], the key requirement in the bonding between the living bone and bioactive glasses is the formation of the HCA layer. These first five steps of the mechanism of bioactivity are independent of the presence of the tissue; therefore, the in vivo bioactivity of the material can be predicted from the apatite formation, which could be assessed *in-vitro* using a solution mimicking the composition of blood plasma.
Various protocols have been considered to assess *in-vitro* the nucleation and precipitation of crystalline hydroxyapatite, such as soaking the material in acellular simulated body fluid (SBF) [90], in TRIS buffer solution[43], in phosphate solution [46, 34] or in cell culture medium (Dubecco's Modified Eagle's Medium, DMEM) [44, 33]. The effect of the different aqueous solution has been studied in the literature and an ISO standard was suggested in order to enhance the comparison between results of different studies. According to the ISO standards, an acellular and protein-free SBF solution buffered with TRIS should be used at a fixed mass per solution volume ratio of 75 mg in 50 ml [29].
SBF is a solution highly supersaturated with respect to apatite and it has higher concentration of Cl^- ions and lower concentration of $(HCO_3)^-$ ions with respect the human blood plasma [90]. The nominal ion concentration of SBF compared to human blood plasma is shown in Tab. 1.2 [90].
Furthermore, dissolution products of 45S5 Bioglass® are reported to up-regulate the expression of genes that are responsible for osteogenesis and to enhance angiogenesis. The release of Si induces the formation and the calcification of new bone, leading to the precipitation of

Table 1.2: *Nominal ion concentration of SBF and human blood plasma*

Ion	**Blood plasma (mM)**	**SBF (mM)**
Na^+	142.0	142.0
K^+	5.0	5.0
Mg^{2+}	1.5	1.5
Ca^{2+}	2.5	2.5
Cl^-	103.0	147.8
HCO_3^-	27.0	4.2
HPO_4^{2-}	1.0	1.0
SO_4^{2-}	0.5	0.5

hydroxyapatite. Moreover, it is essential for metabolic processes [35]. Maeno et al. [36] reported that as far the concentration level of calcium is lower than the toxic one (10 mmol), it has positive effects on osteoblast proliferation and the expression of some growth factors. Thus, the release of ions is the crucial step for the formation of strong bond between material and bone, more than the deposition of the HCA layer [22].

For this reason, several studies were carried out to modify 45S5 Bioglass® properties through the addition of trace elements, such as calcium (Ca), phosphorous (P), silicon (Si), strontium (Sr), zinc (Zn), boron (B), vanadium (V), cobalt (Co) and magnesium (Mg). In general, many ion-doped bioactive silicate based glasses were investigated to improve the bioactivity through a specific biological response [35].

In the last years, great attention has been addressed to the antibacterial property of the material to prevent post-surgical infections. Silver has well known ability to inhibit bacterial growth, therefore different solutions have been proposed using sol-gel technique [37, 38, 39, 40]. Boccaccini et al. [41] developed a 45S5 Bioglass®-based scaffold doped with Ag using molten salt ion-exchange technique,which allows the addition of Ag^+ ions directly on the surface rather than in the bulk during the glass formation. Since silver ions were added on the surface, they were easily released acting as an initial barrier against bacteria. However, high concentration of Ag ions or their fast release may result in cytotoxic effects on the cells.

Magnesium was also used as doping element for bioactive glasses since it stimulates bone formation, increases bone cell adhesion [42] and improves the dissolution of the glass network. However, a better investigation of its specific osteogenic and cytotoxic effect is required.

Boron is a trace element that enhances RNA synthesis in fibroblast cells and it has been used not only as doping element but also as primary glass former instead of silica [43, 44]. Boron-doped and borate-based bioactive glasses show faster in-vitro degradation with respect to the undoped glasses, which result in a faster and more complete formation of the hydroxyapatite layer [45]. Huang et al. [46] confirmed that the reaction rate increased with increasing B_2O_3 content.

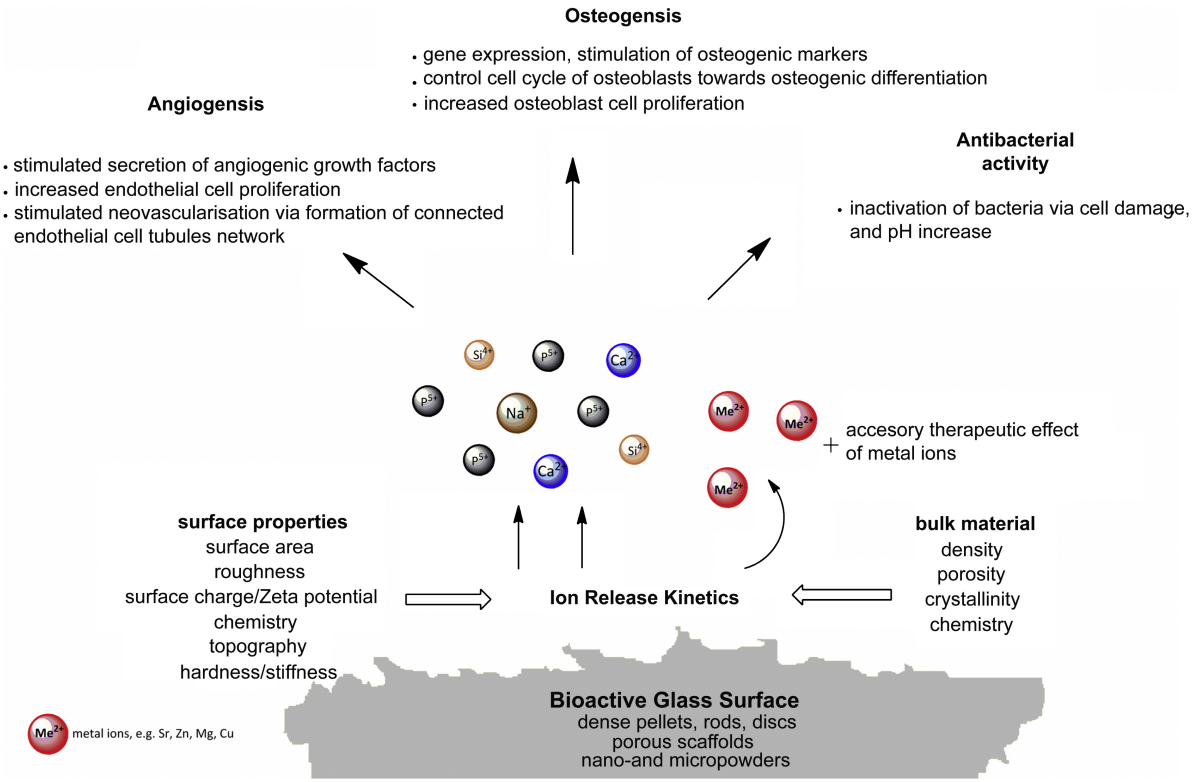

Figure 1.8: *Biological response to ionic dissolution products of bioactive glasses [35]*

1.3 Application of Bioglass®

After its discovery, 45S5 Bioglass® has gained great attention and even reached many clinical applications. The first commercial device, approved by FDA (Food and Drug Administration) in 1985, was called "Bioglass® Ossicular Reconstruction Prosthesis" or "Middle Ear Prosthesis" MEP®. The device was a compact truncated cone produced by a melt-quenching technique, implanted to replace the middle ear bone and to transmit sound from the tympanic membrane to the cochlea [47]. MEP® was used because of its capability to bond with soft collagenous tissues as well as calcified tissues, instead of metals and plastics that are encapsulated in a fibrous tissue [48].

The second clinical application Endosseous Ridge Maintenance Implant (ERMI®), was designed to replace tooth roots and to provide stable support after tooth extraction [49].

However, these two devices have not been widely used in clinics, firstly because of their fixed shape that limits the possibility to customize the product; secondly because orthopaedic surgeons and dentists preferred to use particles or granules that can be more easily implanted [48]. Thus, monolithic shapes were substituted by Bioglass® particles, that were placed on the market with the trade-name of Perioglas® and NovaBone®. PerioGlas® has a particle size in the range 90 – 710 µm and it has been used in dental field as substitute in periodontal disease [48]. Instead, the goal of NovaBone® was to repair maxillofacial and cranial bone defects and non-load-bearing sites in orthopaedic applications. Moreover, NovaBone® particles have been also used to

coat porous polyethylene orbital implants [47]. During application, PerioGlas® or Novabone® particles are usually packed randomly allowing the tissue ingrowth into the free spaces [48]. In recent years a new commercial product, based on 45S5 Bioglass® composition, has been approved for oral care (NovaMin®). These small particles, around 18 µm, are often added to the toothpaste for treating tooth hypersensitivity since they allow the deposition of HCA layer on the exposed dentinal tubules, thus reducing pain [49].

1.3.1 Bioglass® based scaffolds

Considering that scaffolds have a key role in bone tissue engineering, intensive research has been carried out in the last years in this field. Although it is not easy to design a scaffold that could serve as universal template for tissue repair [19], some criteria for an ideal scaffold for bone tissue engineering have been proposed in the literature [82]:

1. Besides biocompatibility, that is essential for all implantation into the human body, the scaffold shall have bioactive property to lead the deposition of the HCA layer and the later formation of a strong bond to the bone without encapsulation in an acellular collagenous bag [48].

2. Three-dimensional highly porous (80-90%) structure mimicking the architecture of cancellous bone and interconnected porosity that promotes cells penetration as well as oxygen, nutrient and waste exchange [51]. The pore size should be suitable for infiltration, colonization and migration of cells into the inner structure. Moreover, pores with diameter ranging from 200 to 400 µm [52] are required to promote faster vascularization, thereby the site is no longer in hypoxic condition and the newly bone might be formed via direct osteogenesis without osteochondral formation [12]. However, pores with smaller diameter ($\sim$ 2-10 µm) are needed to promote the interaction between cells [53].

3. The crucial step for the success of the implanted device is protein attachment on implant surface that determines the attachment and the shape of cells. This in turn depends on the surface property, such as roughness, topography and chemistry that must be carefully controlled.

4. All the materials considered for bone tissue engineering are biodegradable; hence they are expected to be completely replaced by the newly formed tissue. The products released during the degradation have to be biocompatible in order to be eliminated through natural pathways from the body [12]. Nevertheless, scaffold should have similar degradation and resorption rate to the tissue remodeling.

5. Robust mechanical structure and high resistance to applied stress are required to elicit bone healing. Here again it is required that the scaffold matches as closer as possible the mechanical properties of the native tissue. If too weak, it is not able to serve its purpose to promote the regeneration, while if it possesses too high mechanical properties

its implantation may lead to stress shielding phenomena [51]. Moreover, mechanical properties are related to porosity, as the porosity increases the mechanical strength decreases.

6. A further requirement to consider regards the change of mechanical properties due to the progessive degradation. A well-defined balance between degradation rate and the need to maintain a sufficient stiffness to support the regeneration for at least 3-6 months [19].

7. Scaffolds should be processed to obtain irregular shapes.

8. Finally, in order to obtain a potential saleable device, it is important to meet the International Standards Organisation (ISO) or Food and Drug Administration (FDA) standards.

45S5 Bioglass®-based scaffolds are promising devices for bone tissue engineering and they fulfil most of the above-mentioned criteria, although this material has not reached its full potential yet. As widely discussed in previous sections, 45S5 Bioglass® is a material belonging to class A, thus it is osteoconductive and osteoproductive. It is not only able to allow the adhesion and proliferation of osteogenic cells that form extracellular matrix, but even to elicit the deposition of new tissue through biomolecular signalling. The bioactive behaviour of 45S5 Bioglass® depends on its composition and its high reactivity makes it easily resorbed by the body. Its degradation products have osteogenic and angiogenesis potential. Moreover, thanks to the possibility to easily incorporate trace elements [48], it is possible to obtain scaffolds that induce specific body's responses. Several manufacturing techniques (detailed in the next sections) have been proposed in order to produce high porous scaffolds with high surface area and well interconnected structure. The main disadvantages of 45S5 Bioglass® scaffolds, that limit their application in load-bearing sites, are the low mechanical properties resulting from the highly porous structure and the brittle nature of the material. Indeed, dense 45S5 Bioglass® shows fracture toughness of 0.7–1.1 $MPa\sqrt[2]{m}$, meanwhile for cancellous bone is in the range 2–12 $MPa\sqrt[2]{m}$ [50]. To overcome this limitation great attention has been focused on composite materials (discussed in Section 1.3.3).

1.3.2 Fabrication methods of Bioglass® based scaffolds

Before the thorough description of the different manufacturing methods reported in the literature to produce 45S5 Bioglass®-based scaffolds, an important issue has to be pointed out. To enhance mechanical properties and biochemical stability of the fabricated scaffolds, all the techniques presented in this section involve a sintering process that could induce devitrification and subsequently the formation of a glass-ceramic [48]. Sintering takes place at temperature between glass transition (T_g) and crystallization ($T_{c\ onset}$) temperature in order to merge the particles between each other and to obtain densification without fully crystallization of the material [48].
The formation of the HCA layer on the bioactive surface depends on the residual glassy phase

after the heat treatment and Li et al. [54] found that if the percentage is greater than 5% the bioactivity of the material might not be totally suppressed. However, Clupper and Hench [82] reported that the crystal phase present in the glass-ceramic is $Na_2Ca_2Si_3O_9$ that should not completely inhibit the bioactive property of the glass.
45S5 Bioglass® scaffolds have been produced using several techniques.
Gel cast foaming is a direct foaming method to produce scaffolds from melt-derived glasses. This method involves the incorporation of bubbles in a slurry made up of 45S5 Bioglass® particles [55] and organic monomers (usually acrylates) dispersed in aqueous solution. Under vigorous agitation a surfactant, an initiator and a catalyst are added to stabilize temporarily the entrapped air that forms bubbles [56]. Finally, the in-situ polymerization of the monomers stabilises the foam and leads to the production of a composite Bioglass® containing air bubbles stabilized by the polymer. The so produce samples are called green bodies and they were sintered to provide mechanical stability and to create the porosity. Varying the amount of surfactant, it is possible to easily control the size and the interconnectivity of the pores. As expected, by increasing the amount of surfactant also the porosity increases, while the mechanical strength slight decreases [55, 56]. Gel cast foaming of 45S5 Bioglass® allows to produce scaffolds with opened and interconnected porosity (70-80%), with pores dimensions in the range 100-500 µm, that are suitable for BTE, and mechanical strength of around 1.2 MPa [55].
The properties of 45S5 Bioglass® are listed in Tab. 1.3; it is possible to notice that the sintering windows is very small, thus the process must be finely controlled.

Table 1.3: *Termal properties of melt-derived 45S5 Bioglass® [48]*

Glass transition temperature	538°C
Onset of crystallization	677°C
Thermal expansion coefficient	15.1×10^{6}°C^{-1}

Polymer burn out is a high cost-effectiveness method as well as a simple technique. In fact, the technique involves the addition of a porogen to the glass slurry that will be eliminated during sintering at high temperature. The porogen is an organic phase, such as sucrose, gelatine, or polymeric microbeads, that influences the morphology of the final structure [53]. Because of its environment friendly nature, Wu el a. [57] selected rice husk as porogen, that is a waste material from rice production. It allowed the fabrication of mechanically strong scaffolds with compressive strength in the range 5.4–7.2 MPa and low porosity (approx. 45%) which made them unsuitable for bone tissue engineering applications. Bellucci et al. [58] proposed the use of polyethylene (PE) as porogen with two different dimensions of the particles. Large (300–500 µm) PE particles conferred high porosity to the scaffolds, in the range 60-70%, meanwhile small particles (90–150 µm) allowed the production of highly interconnected structures to promote bone tissue ingrowth, as well as angiogenesis, nutrient and waste exchange and cell-cell cross-talk. The well interconnected structure produced using this technique was proved by Deb and co-workers [59] through rhodamine dye infiltration test.
The most investigated technique to produce 45S5 Bioglass scaffolds that fulfil almost the all

criteria aforementioned is the *polymer-sponge method* (or replication technique) proposed by Chen et al. [82]. Polyurethane or natural marine sponges [60] with the desired structure are used as sacrificial template to produce scaffolds with shape similar to that of cancellous bone. The foam is covered with a Bioglass® slurry containing poly(vinyl alcohol) as binder to enhance the adhesion of the particles to the sponge. The excess slurry is squeezed by hand to ensure homogeneous coating of the sponge avoiding the risk pore obstruction that causes a drastically decrease of the porosity. The green body than undergoes the thermal treatment that will eliminate the sponge while sintering the particles. As discussed before, this is a crucial step since extensive densification is desired to improve mechanical properties but at the same time, high percentage of the glassy phase is required to do not suppress completely the bioactive behaviour. For this reason, a double step heat treatment (Fig. **??**) has been optimized:

1. Heating at 400°C for 1 hour using a heating rate of 2°C/min to pyrolyze the sacrificial template.

2. Sintering at 1050°C for 2 hours with the same heating rate and then natural cooling.

Chen et al. produced scaffolds with high interconnected porosity (aprrox. 90%) and pores in the range 510-720 µm. This kind of scaffolds was well characterized in terms of morphology, bioactivity and cytotoxicity in several studies reported in literature [82, 83, 85, 109, 110, 60]. The main disadvantage of this technique regards the mechanical properties of the fabricated scaffolds, as a consequence of the brittle nature of the Bioglass® and high scaffolds porosity. Moreover, the removal of the sacrificial template creates an hole in each strut that can causes the decreasing of the mechanical properties. Indeed, the scaffolds have compressive strength of 0.3-0.4 MPa, that lies closer to the lower bextreme of the compressive strength of spongy bone (0.2- 4 MPa) [82]. Therefore,it is mandatory to finely define a balance between the required mechanical properties to match closer those of cancellous bone, and the high porosity to enhance cell colonization of the scaffolds [61].
These conventional methods the fabrication of scaffolds with structure similar to that of cancellous bone; however, the results depend on the amount of surfactant used, water content, agitation rate, dimension and amount of the pore-creating additives and all the other boundary conditions [48]. Thus, the produced scaffolds are never identical between each other. To overcome these limitations rapid prototype techniques have been proposed since they allow a finely control of the porous structure and repeatable results. However, in the specific case of 45S5 Bioglass® the available literature is still incomplete due to the difficulties in the sintering and the high cost of the starting powders [64]. Computerized Tomography (CT) or Magnetic Resonance Imaging (MRI) can be exploited to create a 3D CAD computer model and reproduce the exactly shape of the patient's defect with high resolution.
Tesavibul et al. [62] employed *Lithography-based additive manufacturing* to fabricate cellular structures. 45S5 Bioglass® slurry was made photosensitive with the addition of an organic solvent, a light absorber and a photoinitiator, and it was photo-cured layer by layer through the light, following a bottom-up approach. This is a Solid Free Form fabrication (SFF), as the non-

solidified slurry works as support for the layers above. Afterwards a heat treatment is performed to remove the polymer and sintering the slurry. The samples showed uniform structure and high density; however, their mechanical strength (0.33 MPa) resulted very low compared to highly porous scaffolds produced by the foam replication method [64] and also compared to other materials microfabricated with the same process, meaning that an optimization of the process is required [62].
An alternative rapid prototyping technique is *Robocasting* in which the solution, with appropriate viscosity, is directly extruded drawing the shape of the CAD model. A complet characterization of 45S5 Bioglass® scaffolds fabricated by robocasting is reported elsewhere [63, 64]. 45S5 Bioglass® powders were mixed with a dispersant/binder to provide the required density for the extrusion [63] and after the deposition the samples were sintered at 1000°C to obtain a crystalline glass-ceramic. This technique allows to produce scaffolds with compressive stress of almost 10 MPa, well maintained bioactive behaviour of the parent glass and no cytotoxic effect on cells in vitro [64].
Another type of SFF method is the *Direct Selective Laser Sintering* (SLS) that was used by Liu et al. [65] to produce for the first time 45S5 Bioglass based scaffolds. Setting the appropriate parameters, such as laser power, thickness of layer, scanning speed, and scanning spacing, the laser beam is moved under the control of the CAD software to reproduce the customized shape by sintering the powders. Also this technique has a bottom-up approach and the final geometry is produced layer-by-layer; however, in this case the final step of heat treatment to sinter the samples is not required andthe process is carried out directly on glass powder with no need to add other components. Additionally, they found that the selection of the proper focused beam allows to control the formation of the desired crystal phase ($Na_2Ca_2Si_3O_9$).

1.3.3 Polymer-Bioactive Glasses Composites

With the final aim of improving the poor mechanical properties of bioactive glasses scaffolds, great attention has been addressed on composite materials made up of Bioglass® and polymers. Polymers offer advantages such as toughness, high ductility, plasticity, processability and the possibility to work as a carrier for drug release, while bioactive glasses confer bioactivity, stiffness and adequate mechanical strength to the composite [24].A possible approach consists in the desing of a polymeric matrix containing bioactive glasses as filler; these scaffolds have been produced by several techniques such as thermally induced phase separation (TIPS), solvent casting, particle leaching, solid freeform fabrication techniques (FFT) and microsphere sintering [66]. However, mechanical properties of polymers are not suitable for bone tissue engineering applications, hence these compositesl do not possess the required stiffness to replace load-bearing sites. Additionally, the lower amount of bioactive glass might be insufficient to guarantee bioactivity [66].
To mimic closer the composite nature of bone, that is mainly composed of inorganic phase, the most promising solution consists in the reinforcement of the ceramic matrix with polymers at a mineral/organic ratio similar to that of natural bone [66]. The most promising approach

consists in coating the brittle bioactive glass scaffolds with a polymeric layer. The goal is to improve the toughness of the composite through the infiltration of the polymer into the bioceramic matrix while filling the cracks formed during the sintering process [67].
Natural polymers such as chitosan, gelatine or collagen have great biocompatibility, indeed their degradation products are nontoxic and provide a low inflammation. However, they present hard processability, risk of disease transmission, batch-to-batch variability and difficulty in tuning their properties [68]. Excellent processing flexibility and reproducibility can be obtained by using synthetic polymers, such as poly(ε-caprolactone) (PCL), poly(ethylene glycol) (PEG), poly(lactic acid) (PLA), poly(glycolic acid) (PGA), poly(hydroxyalcanoate)s (PHA) or poly(urethane)s. Indeed, since they are produced in a controlled manner, tensile strength, elastic modulus and degradation rate are predictable and reproducible [66].
Both natural and synthetic polymers have been investigated to coat 45S5 Bioglass®-based scaffolds produced by foam replication method improving mechanical properties, rate of biodegradation, surface functionalization as well as drug release.
Gelatine [69] used as coating improved the mechanical strength and resistance to fracture of highly porous Bioglass® scaffolds. Moreover, like other polymers, it allows the easy incorporation of therapeutic agents that can be released with a controlled kinetics.
Poly(D,L-lactide) (PDLLA) has been extensively investigated as alternative coating of Bioglass scaffolds®. Chen et al. [88] found that the homogenous coating of the struts slightly retarded the growth of the HCA layer. On the other hand, the presence of the polymeric layer improved the mechanical stress of the scaffolds as well as the maintenance of mechanical performance even after several weeks in SBF.
Bretcanau et al. [70] produced Bioglass scaffolds coated with poly(3-hydroxybutyrate) (PHB). In addition to good biocompatibility and biodegradability, PHB shows piezoelectric properties, that could be exploited to enhance the bone healing process [67]. The polymeric coating increased the work of fracture of uncoated scaffold, without affecting their initial porosity ($\sim$ 85%). Moreover, the samples showed a good bioactive behaviour thanks also to the presence of small non-coated regions where, due to the direct contact between glass and SBF, the nucleation of HA probably started. Polyhydroxyalkanoates were also investigated by Li and co-workers [71], that used the copolymer poly(3-hydroxybutyrate-co-3-hydroxyvalerate) (PHBV) to guarantee a controlled release of vancomycin, that is an antibiotic widely used during implantation to treat possible infections. The compressive stress of uncoated 45S5 Bioglass® scaffolds was determined to be 0.02 $\pm$ 0.01 MPa, while it reached 0.10 $\pm$ 0.09 MPa with the coating.
45S5 Bioglass® scaffolds were coated by Fereshteh et al. [86] using PCL to confer higher mechanical properties, meanwhile controlled drug delivery was achieved through zein that is a natural polymer largely used in pharmaceutical applications. By varying zein content a fine tuning of degradation was achieved, whereas increasing the amount of PCL higher toughness was obtained. Compressive strength of uncoated scaffolds (0.004 $\pm$ 0.001 MPa) was considerably increased in composite PCL/zein/BG scaffolds (0.15 $\pm$ 0.02 MPa); however, these values were still quite low for bone tissue engineering due to the fact that the porosity was almost 96%.

PCL was also used at the same time as a filler into the glass slurry and as coating for the drug release [72]. Vancomycin loaded directly into the scaffold was completely released after 24 hours of immersion in PBS, while the scaffolds coated with PCL and chitosan showed a lower release rate since the polymeric film worked as a barrier against the well-known burst release of Bioglass®.

2 . Aim of the work

Moving from the previously discussed drawbacks of Bioglass-based porous scaffolds, the final aim of this work was the reinforcement of 45S5 Bioglass® scaffolds by coating them with ad hoc synthesized synthetic polymers that belong to the wide family of poly(urethane)s. Polyurethanes (PUs) represent a promising category of synthetic polymers, they allow a fine tuning of their characteristics thanks to their multi-block structure. PUs show a two-phase structure characterized by the presence of hard segments embedded in a soft matrix (Fig. 2.1. The hard glassy phase is made up of a diisocyanate and a chain extender and it has a crucial role in determining the mechanical strength of the resulting material. These hard domains act as filler in the amorphous matrix of soft segments (macrodiol) that confers compliance and elasticity to the material [73].

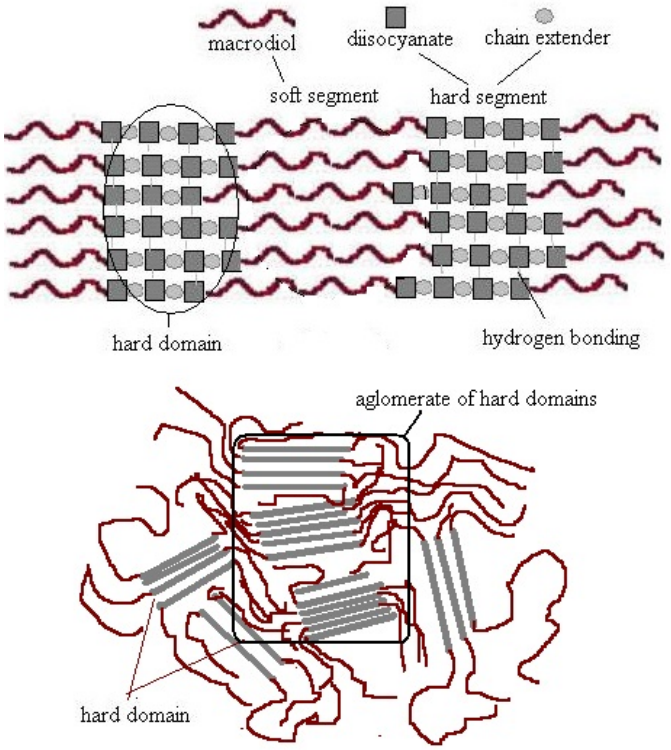

Figure 2.1: *Schematic rapresentation of polyurethane microphase [74]*

In particular, two different PUs have been synthesized at the Biomedical Laboratory of Po-

litecnico di Torino and then used to coat Bioglass scaffolds after a thorough physico-chemical characterization (through for example Fourier Transformed Infrared Spectroscopy, Size Esclusion Chromatography, degradation tests). They differed only in the composition of their soft segment: poly(ε-caprolactone) (2000 g/mol) for KHC2000 polyurethane and a mixture of poly(ε-caprolactone) (2000 g/mol) and polyethylene glycol (2000 g/mol) in 70/30 weight ratio for KHC2000E2000. For what concerns PU hard segment, both the materials were based on 1,6-hexamethylene diisocyanate and L-lysine ethyl ester.
1,6-hexamethylene diisocyanate (HDI) (Fig. 2.2) is an aliphatic diisocyanate with low molecular weight that releases non-toxic products during the degradation. Moreover, thanks to its symmetrical structure it possesses higher mechanical properties with respect to other asymmetrical diisocyanates [75].

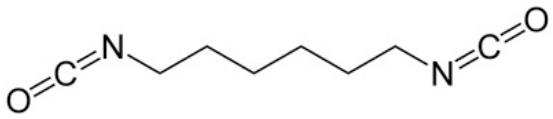

Figure 2.2: *Chemical structure of HDI*

L-Lysine Ethyl Ester (Fig. 2.3) was selected as chain extender for its biocompatibility properties and for its capability to produce a final polymer with elastomeric mechanical properties and high tensile strength, as already reported by Sartori et al. [78].

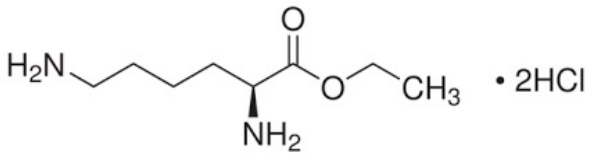

Figure 2.3: *Chemical structure of L-Lysine Ethyl Ester dihydrochloride*

Poly(ε-caprolactone) (PCL) (Fig. 4.8) is an aliphatic polyester with a glass transition temperature (T_g) around -60°C. It is a semi-crystalline material and its crystallinity tends to decrease as the molecular weight increases. It exhibits good solubility in a wide range of organic and inorganic solvents, low melting point (59–64°C), which enables easy formability at relatively low temperatures, and an exceptional blend-compatibility [76]. In-vivo biodegradation of PCL is quite long and can take up to 2 or 3 years. PCL may undergo two different mechanism of degradation, surface or bulk degradation. Surface erosion takes place when the release rate of oligomers and monomers, created by the random scission of ester bonds, is faster than water uptake into the polymeric matrix. This results in a decrease in sample thickness, accompanied by no significant changes in the molecular weight. On the other hand, when water penetrates the inner part of the samples, bulk degradation occurs, chains scisson is more drastic and a decrease of the molecular weight can be observed [77].

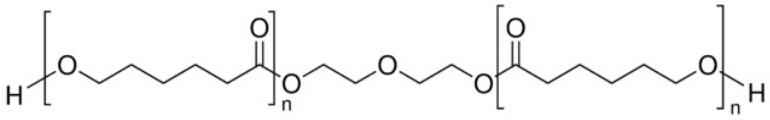

Figure 2.4: *Chemical structure of PCL-diol*

Poly(ethylene glycol) (PEG) (Fig. 2.5) is a crystalline thermoplastic polyether that undergoes an oxidative degradation mechanism. Moreover, thank to its high-water solubility and hydrophilicity it is extensively used, as in this work, to enhance the wettability of PCL.

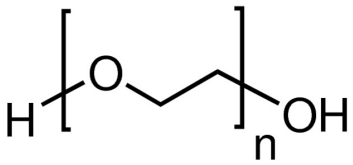

Figure 2.5: *Chemical structure of PEG*

Since mechanical properties and wettability of the synthesized poly(urethane-urea)s have been extensively investigated in previous works [87, 101], in this study the as synthesized PUs were thoroughly characterized in terms of their degradability by studying their hydrolytic and enxymatic degradation, which was assessed in terms of weight loss, changing of molecular weight (through Size Exclusion Chromatography) as well as morphological modification of the surface (evaluated by Scanning Electron Microscopy).
45S5 Bioglass® (BG) based scaffolds have been fabricated at Biomaterial Laboratory of Friedrich-Alexander-Universität Erlangen-Nürnberg, using the polymer-sponge method in order to obtain samples with high porosity (above 90%) and suitable pore size (400 – 500 µm). The polymer layer was added through dip-coating technique using protocols already optimized [87, 101]. However, to enhance the mechanical stability, the coating procedure was performed three times on each scaffold. Pure BG and PCL/BG scaffolds have been also fabricated and used as control. The obtained composites have been characterized in terms of bioactive and degradation behaviour as well as mechanical properties before and after immersion in Simulated Body Fluid. Moreover, biological tests using MG-63 were conducted to assess cytocompatibility.

3 . Materials and Methods

3.1 Materials

The synthesis of polyurethanes required PCL diol and PEG, both with a number average molecular weight M_n=2000 g/mol, that were used as diols. They were purchased from Acros Organics, Germany and from Sigma Aldrich, Italy. The diisocianate 1,6–hexametilen diisocyanate (HDI, M_n=168.19 g/mol), the chain extender L-lysine ethyl ester dihydrochloride (M_n=247.16 g/mol), triethylamine (TEA) and the catalyst dibutiltin dilaurate (DBTDL) were purchased from Sigma Aldrich, Italy. All solvents used during the synthesis were purchased from CarloErba Reagents, Italy in the analytical grade.
Concerning scaffold production, the slurry was obtained from melt-derived 45S5 Bioglass® powder with particles size of approximately 2 µm, purchased from Schott, Germany and polyvinyl alcohol (PVA) as binder acquired from Merck KGaA, Germany. The sacrificial template was a fully reticulated polyester-based polyurethane foam with 45 ppi (pores per inch), purchased from Recticel UK, Corby [82].

3.2 PU nomenclature

The nomenclature of the synthesized poly(urethane urea)s is based on the constituent segments:

- The first letter indicates the chain extender, K for L-lysine ethyl ester;
- The second letter identifies the diisocyanate, H corresponds to 1,6-hexamethylen diisocyanate;
- The last part stands for the macrodiol, C2000 refers to PCL with average number molecular weight 2000 g/mol and E2000 indicates PEG with M_n=2000 g/mol.

3.3 Synthesis of PCL-based Polyurethane

The PUs used in this work were synthesised following the procedure described in [78]. A two steps procedure in solvent was carried out in order to obtain a controlled reaction, higher molecular weight of the polymer and consequently good mechanical properties.

Before the synthesis reagents, solvents and glassware were prepared as follows. In particular, PCL diol was dried under reduced pressure at 100°C for 8 hours and then it was kept at 30°C, in order to remove residual water, which could lead to undesired side reactions during the polymerization. L-lysine ethyl ester dihydrochloride, was stored under reduced pressure at room temperature until use. 1,2-dichloroethane (DCE) was dried by pouring it under nitrogen over activated molecular sieves (Sigma Aldric, Italy) overnight.1,6-hexamethylene diisocyanate (HDI) was distilled under reduced pressure and stored at room temperature. The glassware was completely dried at 120°C overnight before use.
The synthesis occurs in controlled atmosphere (N_2) and in anhydrous conditions.
PCL diol was first solubilized in DCE in a round-bottom flask at 40% w/v (200-250 rpm). In order to keep the temperature constant around 80°C the flask was immersed in heated silicone oil. Then, the diisocyanate HDI was added to the solution, in 2:1 molar ratio with respect to PCL diol. HDI reacted with the macrodiol in the presence of the catalyst dibutylin dilaurate (DBTDL), at 0.1% w/v with respect to the diol, to form, after 2.5 hours, the NCO terminated prepolymer. The second step occured at room temperature and it started with the addition of the chain extender at 1:1 molar ratio with respect to the macrodiol. Before addition, the chain extender was dissolved in anhydrous DCE (3% w/v) and triethylamine (TEA) was also added to induce neutralisation of the chain extender. A previously optimized protocol provides to add 2 ml of TEA every 15 g of macrodiol.
The reaction was stopped after about 16 hours by adding methano.After 20-30 minutes the polymer was collected by precipitation in petroleum ether (in 4:1 volume ratio with respect to the total amount of DCE used) an dried overnight. In order to purify the synthesized PU, the polymer was solubilized in dimethylformammide (DMF) at a concentration of 20% w/v and precipitated in methanol in 5:1 volume ratio with respect to DMF. The purification procedure was performed twice.

3.4 Synthesis of PCL/PEG-based Polyurethane

The procedure followed for the synthesis of the PCL/PEG-based polyurethane was the same previously described for the synthesis of KHC2000 polyurethane. A simple explanation of the reaction is showed in Fig. 3.1 [79]. In this case the macrodiol was composed by by a mixture of PCL diol and PEG at 70/30 weight ratio, while in terms of protocol the only difference concerned the purification step. Since PEG is soluble in methanol, purification was carried out by precipitating the polymer in a mixture of diethyl ether (DEE) and methanol (97:3) in a volume ratio of 5:1 with respect to DMF. The procedure for purification was performed twice.

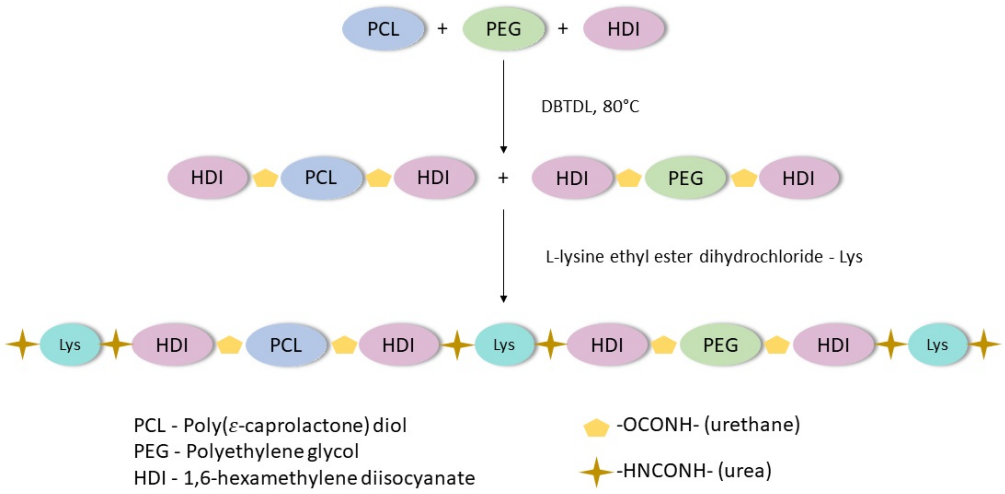

Figure 3.1: *Synthetic scheme for poly(ether ester urethane)urea synthesis*

3.5 Polyurethane Characterisation

3.5.1 Attenuated Total Reflectance Fourier Transform Infrared Spectroscopy

Fourier Transform Infrared Spectroscopy (FTIR) analysis was performed to assess the successful synthesis of polyurethane-urea and to confirm the formation of urethane-urea groups. An attenuated total reflection (ATR) accessory operates by measuring the changes that occur in a totally internally reflected infrared beam when the beam meets a sample. The source generates an infrared radiation, one per time, in the spectral range from 4000 to 600 cm^{-1} with a resolution of 4 cm^{-1}. The radiation passes through an optically dense crystal with a high refractive index with a certain angle; if this angle is bigger than a critical value the Attenuate Total Reflection phenomenon occurs (Fig. 4.19). When the radiation interacts with the sample the bonds start to vibrate, this occurs at resonant frequencies which are characteristic of its structure. Hence, the material absorbs energy and the amount of light at the end is lower than the light provided to the sample. The light finally passes to the detector and it is sent to the software where the Fourier Transformation takes place. In this way an easily understandable spectrum is obtained, in which the wavenumbers of the peaks correspond to the frequencies of vibrations between the bonds of the atoms making up the material, while the peak width is an indication of the amount of bond present. For the technique to be successful, the following two requirements must be met:

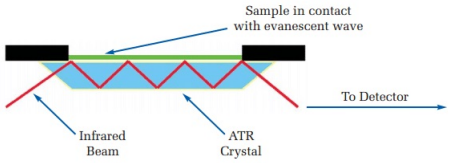

Figure 3.2: Schematic rapresentation of a multiple reflection ATR system (www.perkinelmer.com) [80]

- The sample must be in direct contact with the ATR crystal, because the evanescent wave only extends beyond the crystal 0.5 µm - 5 µm.

- The refractive index of the crystal must be significantly greater than that of the sample otherwise internal reflectance will not occur

In this work polyurethane-urea samples in the form of powder were analysed using a Perkin-Elmer Spectrum 100 equipped with an ATR accessory with diamond crystal. Attenuated Total Reflection Fourier Transform Infrared (ATR-FT-IR) spectra were obtained as a result of 16 scans with a resolution of 4 cm^{-1}, in the spectral range from 4000 to 600 cm^{-1} at room temperature using a germanium crystal. The spectra were analysed using the Perkin-Elmer Spectrum Software.

3.5.2 Size Exclusion Chromatography

Number average and weight average molecular weight (M_n and M_w) and the molecular weight distribution M_w/M_n of the custom-made poly(urethane-urea)s were estimated by Size Exclusion Chromatography (SEC) (Agilent Technologies 1200 Series, USA). The polymer was dissolved (2mg/ml) in a solution of dimethylformammide (DMF HPCL grade, Carlo Erba reagents) and Lithium Bromide (Sigma -Aldrich) at 0.1%w/v. To prevent damages to the machine because of the impurities present in the polymer, the polymeric solution was filtered using a 0.45 µm syringe filter (Lab logistics Group GmbH, USA). Analysis was performed at 55 °C with a flow rate of 0.5 ml/min through two Waters Styragel columns (HT2 and HT4). The columns are filled with spherical porous beads that allow polymer chain separation based on the size; in fact, large molecules do not interact with the pores and they are eluted quickly. In contrast, smaller molecules exhibit great diffusion within the column media; thus, they are eluted last.
The chromatography peaks were converted (Agilent ChemStation Software) into a molar mass distribution by a calibration curve [81] obtained using nine polymethylmethacrylate (PMMA) standards ranging in M_n from 4000 to 200000 g/mol.

3.5.3 Degradation/dissolution Tests

In this study hydrolytic and enzymatic degradation tests were carried out on the two polyurethanes, KHC2000 and KHC2000E2000, and on PCL homopolymer (M_n=80000 Da) for comparative purposes. In order to prepare thin samples, film casting technique was performed using chloroform and DMF as solvents for PCL and the synthesized poly(urethane)s, respectively. The solution was stirred continuously at room temperature until complete solubilization and then cast into glass Petri dishes (diameter 12 cm). The solvent was evaporated and then the films were dried at room temperature under a fume hood for 1 day. The films for the degradation experiments were 10 mm x 10 mm in size and 20-30 mg in weight (w_0). Hydrolytic degradation was performed in Phosphate Buffered Saline (PBS) solutions (pH 7.4, Sigma Aldrich, Italy), while enzymatic degradation was carried out in PBS containing Lipase from Pseudomonas cepacia (Sigma-Aldrich, Italy) at 0.1% w/v. All tests were performed at a constant temperature

of 37°C to recapitulate in vitro physiological conditions. Salt concentration of PBS is reported in Tab. 3.1

Table 3.1: *Composition of PBS*

Salt	**Concentration (mM)**
NaCl	137
KCl	2.7
Phosphate Buffer	10

Each sample was weighted and appropriate amount of solution was added (300 µl of solution every 5mg of polymer) according to Table 3.2 and they were incubated at 37°C. The degradation medium was completely refreshed every 3 to 4 days in order to keep the pH of the solution constant and to maintain the enzymatic activity.

Table 3.2: *Volume of degradation medium*

Samples' weight	**Volume of PBS**
12 mg - 16 mg	1 ml
16 mg - 18 mg	1.1 ml
18 mg - 20 mg	1.2 ml
21 mg - 27 mg	1.4 ml
28 mg - 30 mg	1.7 ml
30 mg - 35 mg	2 ml

After 1, 3, 5, 7, 14 and 21 days three films were picked out, rinsed using deionised water, freeze-dried, and then weighted again (w_t). Degradation/dissolution was expressed as percentage of weight loss after immersion in in the degradation medium for a predefined time interval, according to the following formula:

$$\%w_{t_{loss}} = \frac{w_0 - w_t}{w_0} \cdot 100 \tag{3.1}$$

Results are reported as average value and standard deviation.
SEC analysis were also carried out on dried samples to estimate the change of the average molecular weigth during degradation:

$$\%M_{n_{loss}} = \frac{M_n(t_0) - M_n(t)}{M_n(t_0)} \cdot 100 \tag{3.2}$$

Finally, the modification of the surface morphology during the degradation was assessed through SEM analysis.

3.6 Scaffolds Fabrication

Bioglass®-based scaffolds were fabricated using the foam-replication method described in [82]. The idea is to use a polyurethane foam with the desired pore structure as a sacrificial template. This template is immersed in a slurry containing Bioglass® and, after heat treatments, a Bioglass®-scaffold is obtained.The foam was cut into cylindrical shape with 10 mm diameter and 10 mm thickness for mechanical test, meanwhile a thickness of 7 mm was chosen for other tests. The templates were cleaned with acetone in ultrasonic bath, squeezed and dried in the oven at 60°C before use.

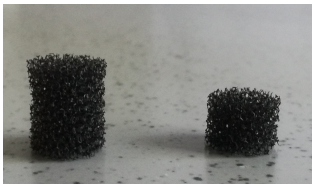

Figure 3.3: Images of PU foams

The slurry was prepared with the following composition: 50 wt% Bioglass® powders, 49.7 wt% deionised water (DI-water) and 0.3 wt% poly(vinyl alcohol) (PVA), added as a binder to control slurry viscosity and to enhance the adhesion of the Bioglass® particles to the polymeric sponge [85]. Briefly, PVA was dissolved in DI-water at 80°C under stirring for 1 hour. After that the solution was cooled down at room temperature and Bioglass® powder was added slowly under stirring for 1 h. The polymeric template was immersed in the slurry for around 1 minute and manually retrieved, the excess slurry was squeezed by hand, and the sample was dried in the oven at 60°C for 1 hour. The coating procedure was repeated twice for each sample in order to increase the thickness of the green body. The samples were then dried at 60°C for at least 12 h.

Then, the green bodies were put in the oven for the heat treatment (Figure 3.4): first, they were heated at 400°C for 1h to burn the polyurethane foams. After that the samples were sintered by heating at 1050°C for two hours. The heating rate must be slow enough to avoid damages to the glass coating; hence a heating rate of 2°C/min was set for both steps [82]. Finally, the samples were cooled down until room temperature with no control on the cooling rate.

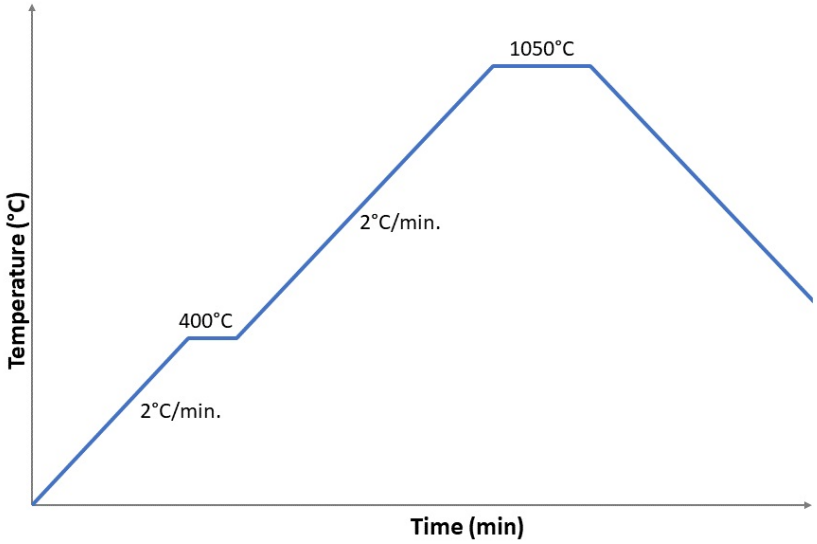

Figure 3.4: *Heat treatment*

3.7 Scaffold Coating

The dip coating procedure was used to coat 45S5 Bioglass® with the biodegradable PUs and PCL.
The control scaffolds were coated with PCL (M_n=80000 g/mol, Sigma Aldrich, UK) according to the protocol reported by Fereshteh et al. [86]. Briefly, PCL was dissolved in chloroform (VWR Chemicals, France) at 1% w/v and the scaffolds were completely immersed for 2.5 minutes.
The polyurethanes were dissolved in chloroform, at room temperature, under stirring for at least 4-5 hours. The coating conditions were optimized in previous works [87, 101]: 0.5% w/v for KHC2000 and 1% w/v for KHC2000E2000.
The samples were immersed in the solution for 1 minute and then put in a glass Petri dish and frequently moved from one spot to another and dried using compressed air, in order to avoid the presence of clogges pores. The scaffolds were then dried under the fume hood for 24 hours before the application of the next coating layer. The dip coating procedure was repeated three times on each scaffold.

3.8 Pellets Production and Coating

Bioglass® coated pellets were produced in order to analyse closely the effect of polimeric coating on the bioactivity of Bioglass® scaffold. 0.3 g of 45S5 Bioglass® powders were filled into a pressing tool (previously lubrificated with glycerin) and then the powdres were compressed using an uniaxial pression ($\sim$ 4 Tons). A compact disk with 13 mm diameter and 1 mm height was obtained. After that the scaffolds were sintered using the same heat treatment used for the scaffolds (1050°C for 2 hours with a heating rate of 2°C/min). Finally, they were coated following the same procedure described for the scaffolds.

3.9 Scaffold Characterisation

3.9.1 Scaffold Morphology

The morphology of the pure BG and polymer coated scaffolds was observed under a light microscope (Stemi 505, Zeiss) with attached camera (Axiocam 105 color) and Scanning Electron Microscopy (SEM) (Carl Zeiss Microscopy, software SmartSEM). SEM images were analysed with ImageJ software to asses the average pore size.
SEM is an imaging technique that creates images of a sample by scanning its surface with a focused beam of electrons and reveals information about the sample, like external morphology, chemical composition and crystalline structure.
The primary beam (max 15 KeV) is not fixed, but it is controlled in sequence, point by point and row by row, on a small rectangular area of the sample.

When the electrons beam interacts with the volume of the sample different phenomena occur (Fig 3.5):

1. Emission of secondary electrons with low energy (0-200 eV)
2. Emission of back-scattered electrons with high energy (1-50 KeV)
3. Emission of characteristic X-ray, due to the energy released from the secondary electron expulsion.

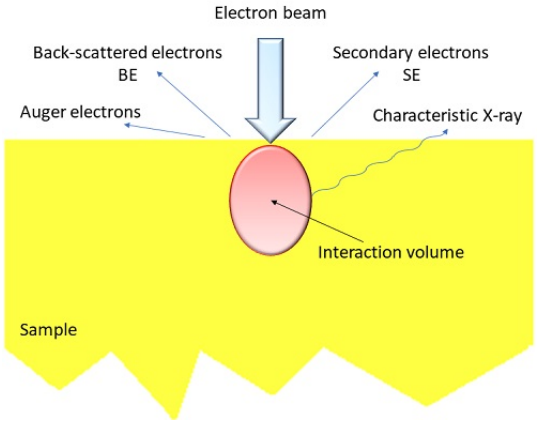

Figure 3.5: *Schematic representation of the working principles of SEM*

SEM provides detailed high resolution ($\sim$ 5 nm) B&W images of the sample by detecting the secondary and back-scattered electron signal.
In this work the scaffolds were fixed with silver conductive paste on the sample holder and covered with a gold layer to enhance their conductivity.

3.9.2 Scaffold porosity

The average porosity of the scaffolds was calculated before (p_1) and after (p_2) the coating, using the following formulae [88]:

$$\begin{cases} p_1 = \left(1 - \dfrac{w_1}{\rho_{BG} V_1}\right) \cdot 100 & (3.3) \\ \\ p_2 = \left[1 - \left(\dfrac{w_1}{\rho_{BG}} + \dfrac{w_2 - w_1}{\rho_{coat}}\right)/V_2\right] \cdot 100 & (3.4) \end{cases}$$

where ρ_{BG}= 2.7 g/cm^3 is the density of solid 45S5 Bioglass® [84] and ρ_{coat} is the density of the polymer used for the coating. The estimated density of homemade poly(urethane-urea)s and PCL (Sigma Aldrich, UK) are given in Table 3.3. PUs density were calculated by measuring the dimensions and the weigth of dense films prepared by solvent casting. V_1 and V_2 stand for the volume of the samples before and after coating, meanwhile w_1 and w_2 are the weights of the samples before and after coating respectively. The dimension of the scaffolds were mesured using a digital caliper.

Table 3.3: *Density of the polymers, ρ_{coat}*

PCL	1.145 g/cm^3
KHC2000	1.1 $\pm$ 0.04 g/cm^3
KHC2000E2000	1.07 $\pm$ 0.03 g/cm^3

3.9.3 Bioactivity Tests

Bioactivity tests were carried out according to the standard in vitro procedure described by Kokubo. Three samples of each type of scaffold were immersed in 35 ml of Simulated Body fluid (SBF) and incubated under slow tangential agitation at 37°C. After 1, 3, 7, 14 and 21 days, the samples were extracted from the SBF solution, rinsed gently with deionised water and left to dry at 37°C. SBF was changed twice a week. After soaking, SEM and ATR-FT-IR were performed in orderassess the deposition of a hydroxyapatite layer. Moreover, the crystallinity of the formed HA was assessed through X-ray diffraction (XRD) analysis. ATR-FT-IR and XRD (MiniFlex, Rigaku) were performed with samples in the form of powder.
XRD is a technique used to measure the crystal structure of material; it is based on Bragg's low that relates the wavelength of the electromagnetic radiation to the diffraction angle and the lattice spacing in the sample.

$$n\lambda = 2d\sin\theta \tag{3.5}$$

X-rays are produced by a vacuum tube similar to a cathode ray tube, filtered to produce a monochromatic radiation, collimated to concentrate, directed toward the sample and then, the incident rays are diffracted into a detector. If the conditions satisfy the Bragg's law, the interaction between the sample and the X-ray is a constructive interference and a signal spike is generated (Fig. 3.6). The XRD result is a diffractogram that shows the intensity as a function of the diffraction angles. Data were collected over the range of 2ϑ= 20-70° using 0.01°/step and 4°/min (radiation at 40kV and 15mA).

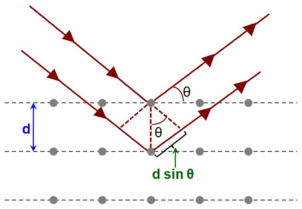

Figure 3.6: Illustration of Bragg's law [89]

Preparation of SBF

Simulated Body Fluid was prepared following the protocol developed by Kokubo *et al.* [90]. In this procedure pH and temperature condition should be finely monitored to avoid precipitation of apatite in the solution. Initially, a plastic bottle must be prepared by labelling the volume at 700 ml, 900 ml and 1 l (with the magnetic stirrer inside). The bottle should be smooth and without scratches. The first step consisted in heating 700 ml of DI-water at 36.5 ± 1.5°C under stirring. Then, the reagents are added in order one by one (Table 3.4):

1. Sodium chloride (NaCl)
2. Sodium hydrogen carbonate ($NaHCO_3$)
3. Potassium chloride (KCl)
4. Di-potassium hydrogen phosphate trihydrate ($K_2PO_4{\cdot}3H_2O$)
5. Magnesium chloride hexahydrate ($MgCl_2{\cdot}6H_2O$)
6. Calcium chloride dihydrate ($CaCl_2{\cdot}2H_2O$)

7. Sodium sulfate (Na_2SO_4)
8. Tris-hydroxymethyl aminomethane: ($(HOCH_2)3CNH_2$) (Tris)
9. 1.0M (mol/l) Hydrochloric Acid, 1M-HCl

Table 3.4: *Reagents for preparing 1 l of SBF*

Order	**Chemical**	**Amount**	**Purity (%)**	**Supplier**
1	NaCl	7.9948 g	100	VWR Chemicals, Germany
2	$NaHCO_3$	0.3532 g	100	Sigma Aldrich, Germany
3	KCl	0.225 g	99.5	Merck KGaA, Germany
4	$K_2PO_4 \cdot 3H_2O$	0.231 g	99.0	Sigma Aldrich, Japan
5	$MgCl_2 \cdot 6H_2O$	0.3048 g	100	Sigma Aldrich, Japan
6	1.0 M - HCl	39 ml		VWR Chemicals, France
7	$CaCl_2 \cdot 2H_2O$	0.3638 g	100	VWR Chemicals, France
8	Na_2SO_4	0.0719 g	99.2	VWR Chemicals, France
9	Tris	6.0568 g	100	VWR Chemicals, Belgium
10	1.0M - HCl			VWR Chemicals, France

Then, DI-water is added up to the marked 900 ml and the electrode of the pH-meter is inserted in the solution to control the pH. In this step the pH must be lower than 2 and the temperature in the range of 36-37°C. Subsequently, Tris is dissolved slowly spoon to spoon because the pH increases very fast and it is important that its value does not increase over 7.45. When the pH rises to 7.45, 1.0M – HCl is added to the solution by pipette to lower the pH to 7.42 ± 0.01. Tris and 1.0M – HCl were added alternately to control the pH until the total amount of Tris is dissolved. The pH is finally adjusted at the final value of 7.40 at 36.5°C. Finally, DI-water is added up to the marked 1 l and the solution is cooled down until room temperature. The final solution must be colourless and transparent and without precipitate. SBF should be stored in the fridge and before the test it is important to control the pH value (pH changes with the temperature in according to the Fig. 3.7), and heat it at 37°C.

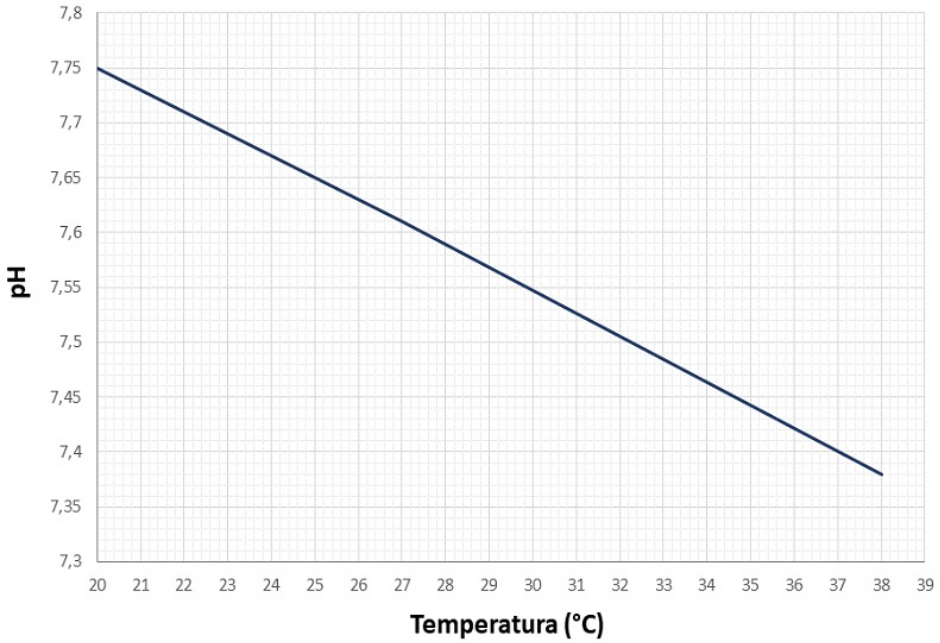

Figure 3.7: *Relationship between pH and temeprature*

3.9.4 Mechanical Tests

The compressive strength for uncoated and coated scaffolds was measured using a Zwick-/Roell Z050 mechanical tester at a crosshead speed of 5 mm/min and 1 kN cell load. The samples were analysed before and after immersion in SBF for 3, 7, 14 and 21 days. During the test, an increasing load was applied on the scaffold until the compressive strain reached 75%. The compressive stress was calculated with the following formula:

$$\mathrm{P} = \frac{\mathrm{F_{max}}}{\pi \frac{\mathrm{d}^2}{4}} \tag{3.6}$$

where P rapresent the compressive strength in MPa, d is the diameter of the samples and $\mathrm{F_{max}}$ is the maximum load determined according to the results already reported by Chen et al. [82] for the uncoated scaffolds, meanwhile for the coated scaffolds it was defined as the maximum load before the densification of the samples.
The work of fracture W is related to the energy required to deform a sample up to a certain deformation and it is considered proporzional to the area under the stress-strain curve; in the present work, W it was calculated by using Eq. 3.7

$$\mathrm{W}(\varepsilon) = \int \sigma(\varepsilon)\mathrm{d}\varepsilon \tag{3.7}$$

where $\sigma(\epsilon)$ is the stress and ϵ the strain.
Five samples for each condition were tested and the results were presented as the average value and standard deviation. In order to better simulate the *in-vivo* environment, five scaffolds were

also tested in wet conditions [91]. To this aim, the samples were soaked in PBS for 30 minutes before compressive strength test.

3.9.5 Degradation Tests

Hydrolytic degradation was performed by dipping each scaffold (with an initial weight w_0), in 50 ml of Phosphate Buffered Saline solution. The samples were incubated under slow tangential agitation at 37°C (Inkubator 1000, Heidolph). Three samples were removed from the solution after 1, 3, 7, 14 and 21 days and abundantly rinsed with DI-water in order to remove the soluble inorganic salts and to stop degradation. Afterwards the scaffolds were dried at 37 °C to avoid damages to the polymers. The pH of PBS was measured before the immersion of the scaffolds and after their removal. The dried samples were finally weighted (w_t), and the percentage of weight loss was calculated following the formula previously used for the degradation of polyurethanes 3.1.

3.9.6 Biological Tests

Cell culture

In order to assess the biocompatibility of the scaffolds, MG-63 (Sigma Aldrich, Germany), a human osteosarcoma cell line, was used for cell experiments. The cells were cultured in DMEM (Dulbecco's modified Eagle's medium, Thermo Fisher, Germany) containing 10% v/v fetal bovine serum (FBS, Sigma Aldrich, Germany) and 1% v/v penicillin/streptomycin (Gibco, Germany) in an incubator at 37 °C, 5% CO_2 and 95% humidity (Galaxy 170 R, New Brunswick). When the confluency in the cell culture flask was at 80-100%, cells were washed with sterile DPBS (Dulbecco's Phosphate-Buffered Saline, Thermo Fisher, Germany) and collected using Trypsin/EDTA (Thermo Fisher, Germany). After trypsinization the cells were re-suspended in fresh medium and counted by trypan blue exclusion method (Sigma Aldrich, Germany) in a Neubauer chamber.

Scaffold preparation

Before cell seeding the scaffolds were cleaned by soaking in a solution of 2% SDS (Sodium Dodecyl Sulfate, Carl Roth GmbH) and then in another solution at 5% Extran (Merck, Germany). Afterwards, they were left to dry in the sterile bench. Subsequently, the uncoated scaffolds were sterilized at 160°C for two hours in the furnace (B 180, Nabertherm), meanwhile coated scaffolds were put under UV light for 3 hours.
It is well known that the burst release of Bioglass® scaffold in aqueous environment causes the quick increasing of the pH (it could reach values higher than 8) and this can affect cell viability. In order to overcome this drawback, the literature suggests to adopt some form of scaffold preconditioning [93]; for this reason, the scaffolds were soaked in medium until the stabilization of the pH around 7 ± 1. During the preconditioning the scaffolds were incubated (Galaxy 48 R, New Brunswick) at 37°C, 2% O_2 and 10% CO_2 to enhance ion release and accelerate the

stabilization of pH around the desired value. DMEM without phenol red was used to exclude a change in colour due to pH fluctuation during absorbance measurements.

Cell seeding and cultivation

After the preconditioning period six replicates of each type of sample were placed in a 24-well plate and the required amount of cells was re-suspended in fresh medium at the final concentration of 100000 cells/µl.
In order to avoid cell sticking on the bottom of the well plate and to facilitate cell adhesion on the scaffold, MG-63 were seeded directly on the surface using a drop-on method. Briefly, 50 µl of solution with cells were gently deposited onto the scaffold surface and the samples were incubated at 5% CO_2 for 40 minutes to allow cell homing and adhesion. Afterwards the scaffolds were turned to induce their homogeneous distribution in the 3D scaffold, then 50 µl of cell suspension were added and they were incubated again for 40 minutes. At the end 1 ml of medium was added in each well and incubated for 2 days. In order to better control contamination and growing rate of cells, 6 well plates were filled with 1 ml of medium and 100 µl of cell suspension. The medium was changed every day in order to better mimic the in vivo condition and to avoid pH increase.

Cell Viability

To assess cell viability a cell counting kit was used (Cell Counting Kit - 8, Sigma-Aldrich) after 2 days of incubation. To avoid the influence of cells attached on the bottom of the well plate and to be ensure that only adherent cells were measured, samples were moved into a new 24-well plate and new fresh medium containing 3 % v/v WST (a water-soluble tetrazolium salt) was added. One well was filled only with WST-solution as blank, since a slight absorbance occurs even in the solution without cells.
The samples were incubated for 3 hours to give time to the WST to interact with cells. During the incubation, viable cells with active metabolism convert WST into formazan which is soluble in the medium (Fig. 3.8) [94]. When cells die, they lose the ability to give this yellow colored product; hence, formazan is a marker of viable cells since the absorbance at 450 nm is proportional to the number of viable cells in the medium [95].

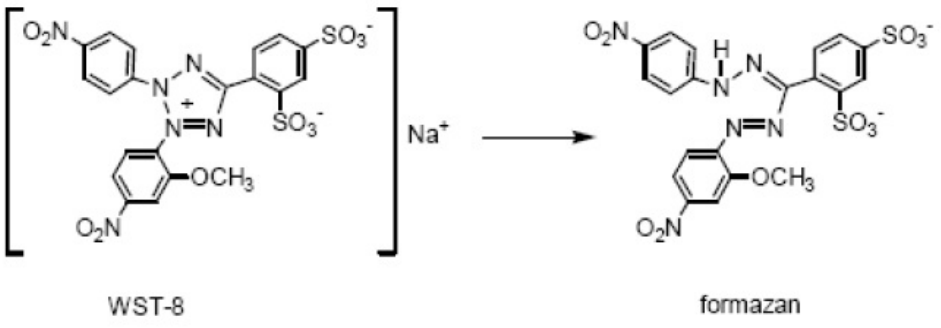

Figure 3.8: *Structure of WST-8 and WST-8 formazan (created by Sigma-Aldrich)*

Afterwards 100 µl of medium was transferred in a 96 well plate, four time from each well (6 well for each type of samples) and the absorbance at 450 nm was measured with a microplate reader (PHOmo, autobio labtec instruments co. Ltd. China).

Cell Staining

Rhodamine Phalloidin (Thermo Fisher, Germany) was used to stain cells to assess their viability. By fluorescence analysis, Phalloidin (red) allows to see the cytoskeleton, since it is a highly selective bicyclic peptide that interact with actin filaments. Cell nuclei were stained using DAPI (4',6-diamidino-2-phenylindole, dilactate, Invitrogen, USA) (blue) which preferentially bind to adenine and thymine regions of DNA.
In order to prepare the samples for the fluorescence analysis, they were washed with PBS and the cells were fixed using a Fluorescence Fixing solution (Tabl. 3.5) for 15 min. The samples were washed 3 times with PBS (5 minutes each) and then a Permeabilization Buffer (Tabl. 3.5) was added for 5 min. Then the scaffolds were covered with Phalloidin solution for 1 hour in the dark. Afterwards the samples were washed 2 times with PBS and DAPI solution was added for 5 minutes in the incubator. At the end the samples were washed with PBS and the images of the stained cells were taken through a fluorescence microscope (Axio Scope A.1, Carl Zeiss Microimaging GmbH, Germany).

Table 3.5: *Composition of Fluorescence Fixer and Permeabilization Buffer*

Chemical	**Fluorescence Fixer**	**Permeabilization Buffer**
PIPES	3.024 g	–
EGTA	0.038 g	–
PEG	4 g	–
Formaldehyde	3.7 g	–
NaOH-Pellets	ca. 0.4 g	–
Triton X-100	–	0.1 ml
Sucrose	–	5 g
DPBS	100 ml	100 ml

Cell Morphology

The morphology of the seeded MG-63 into the scaffolds was investigated by SEM analysis. After 2 days of incubation two samples of each type were washed with PBS, the SEM I fixing solution was added for 1 hour and then replaced by SEM II solution again for 1 h. The composition of the two fixing solutions is reported in Table 3.6. To rehydrate the scaffolds the usual protocol uses a graded ethanol series (30, 50, 70, 80, 90, 95 and 100 vol.%) for 30 minutes each. Since KHC2000E2000 polyurethane contains PEG, the coating could be partially solubilized and detached. To analyse how ethanol affects the coating, KHC2000- and KHC2000E2000-coated scaffolds were immersed in 100% ethanol for 4 hours and then analysed

with SEM.
Based on the identied results after SEM analysis the samples were immersed in the ethanol series only for 10 minutes for each step. Moreover, critical point dryer was avoid to prevent damage to the polymeric coating.
The samples were stuck on the holder with silver paste and sputtered with gold before SEM examination.

Table 3.6: *Composition of fixing solutions SEM I and SEM II*

Chemical	**SEM I**	**SEM II**
50% Glutaraldehyde-Solution	1 ml	3 ml
Formaldehyde	10 g	15 g
Sucrose	25 g	–
Sodium Cacodylate Trhydrate	21.403 g	21.403 g
DPBS	500 ml	500 ml

3.9.7 Statistical Analysis

All the obtained results are reported as a mean ± standard deviation. For mechanical test and cell viability tests, statistical analysis was performed using Origin for windows (OriginLab Corporation, Massachusetts, USA). One-way ANOVA followed by Bonferroni post hoc analysis were used to establish the differences among the results. A p value of less than 0.05 was considered as statistically significant [78].

4 . Results

4.1 Polyurethanes Characterisation

4.1.1 Chemical Characterisation

The two PUs were successfully synthesised as showed in ATR-FT-IR Spectra in Fig. 4.1. In fact, the peak in the region 1640-1620 cm^{-1} is ascribed to the C=O stretching (amide I) and the peak near 1560 cm^{-1} represents the simultaneous N-H bending vibration and C-N stretching (amide II). The other characteristic points of the urethane-urea groups are: N-H stretching in the region 3340-3360 cm^{-1} (due to urethane-urea group and amide group), N-H bending + C=O stretching near 1290 cm^{-1} and N-C-O asymmetrical stretching near 1240 cm^{-1} [96]. The highest peak in the spectra, at ca. 1723 cm^{-1}, represents C=O stretching, and it is due to the PCL-diol. Ester group also shows absorption at 1160 cm^{-1} due to C-O-C linkage, while CH_2 asymmetric and symmetric stretching vibrations are located at 2938 and 2865, respectlively [78]. Moreover, KHC2000E2000 polyurethane contains PEG, in fact its spectrum presents a peak at 1099 cm^{-1} due to the vibration of CH_2-O-CH_2 linkage of polyether.
The absence of absorbance at ca. 2260 cm^{-1} indicates that no unreacted isocyanate groups are still present in the PUs [97]. Also, it should be noted the absence of peaks due to DMF near 1673 cm^{-1} [98], suggesting a successful and complete drying of the materials. However, a not completely purification of L-lysine ethyl ester dihydrochloride, was obtained for the mixed polyurethane, in fact it possible to notice the peaks in the region 2600-2496 cm^{-1}. The residual lysine it is not a problem for the further investigation since it is perfectly biocompatible.
KHC2000 possesses a number average molecular weight (M_n) of 68600 g/mol and a polydispersity index (D = M_w/ M_n) of 1.8; KHC2000E2000 presents M_n=48400 g/mol and a polydispersity index of 2.1. The polydispersity index indicates the distribution of polymeric chain in terms of molecular weight, the more the chains were similar to each other, the less is the index (near 1 for natural monodisperse polymers). Synthetic polymers usually show a polydispersity index up to 1, since is not possible to have completely control on the polymerization process. Thus, the obtained values are in the expected range, suggesting that the polymer chains molecular weight are well distributed.

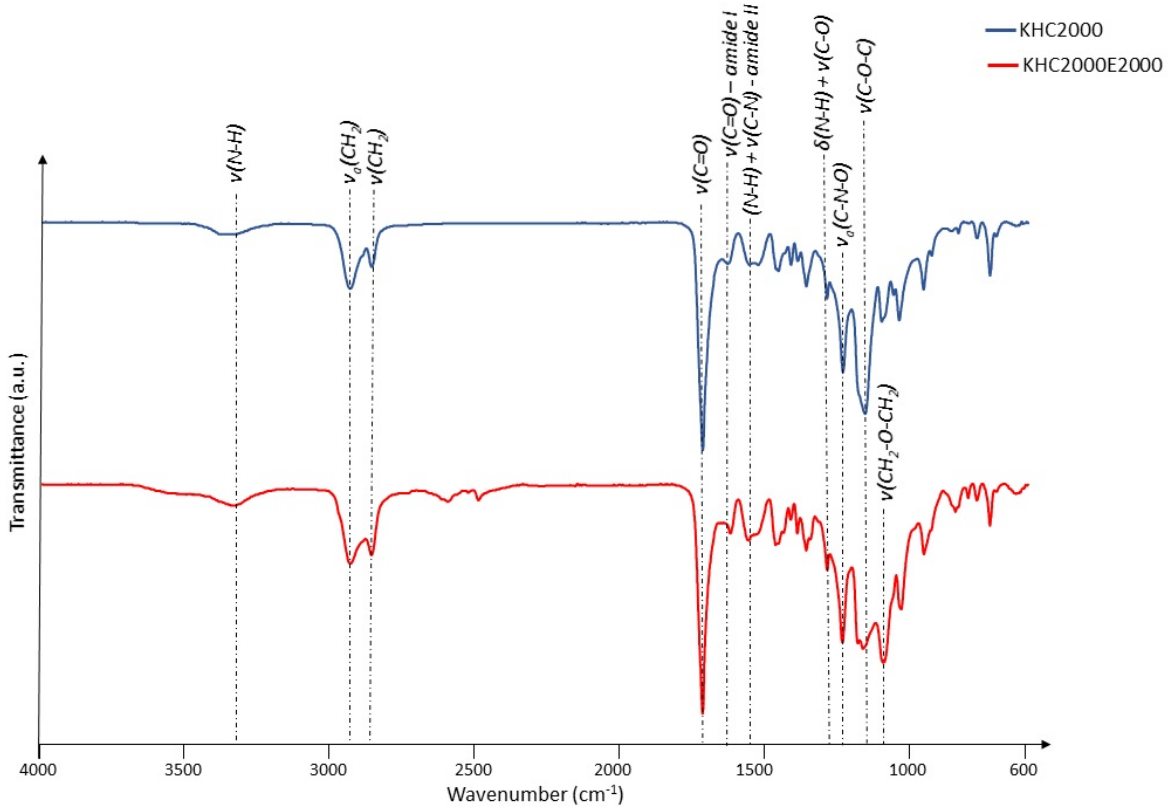

Figure 4.1: *ATR-FT-IR spectra of KHC2000 and KHC2000E2000*

4.1.2 Degradation/Dissolution Tests

The percentage of weight loss during hydrolytic degradation of PCL and PUs films in PBS is presented in Fig. 4.2.

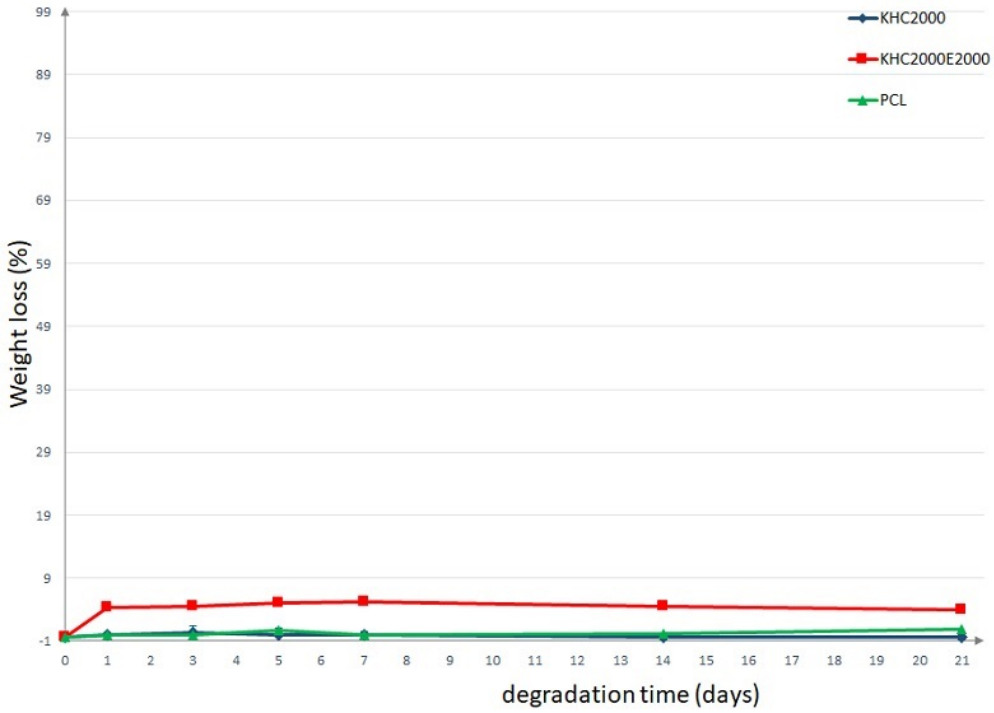

Figure 4.2: *Weight loss profile of PCL, KHC2000, KHC2000E2000 during hydrolytic degradation in PBS*

Insofar as PCL film degradation is concerned, after 21 days of incubation the percentage of weight loss was 1.27 ± 0.1%. The absence of evident changes in PCL mass can be ascribed to its high hydrophobicity and semi-crystalline nature. Hence, degradation is very slow according to literature data [99, 100].
Similarly, as shown in a previous work [101], KHC2000 polyurethane-urea exhibited almost no degradation after immersion in PBS for 21 days.
As the soft segment of the polyurethanes (macrodiol) determines the degradation type and kinetics, the polyurethane KHC2000E2000 was degraded (or solubilized) much faster than the other investigated materials. In fact, the presence of PEG increased polymer wettability as already reported [87, 101], thus allowing a higher hydration of the samples which resulted in a partial dissolution of the PEG's blocks, and, as a consequence, a faster formation of soluble fragments. Indeed, KHC2000E2000 films showed 4.19 ± 0.7% of weight loss after 21 days of incubation.
Furthermore, the rate of degradation is related to the initial molecular weight of the polymer [77], the broader is the molecular weight, the lower is the degradation. Hence, the lower molecular weight of KHC2000E2000 with respect to the ther investigated materials further accounted for its faster and enhanced degradation.

To better understand the degradation mechanism, the residual polymeric films after hydrolytic degradation were analysed through SEC and the loss in number average molecular weight (expressed as a percentage with respect to the initial M_n)has been reported as a function of time in Fig. 4.3

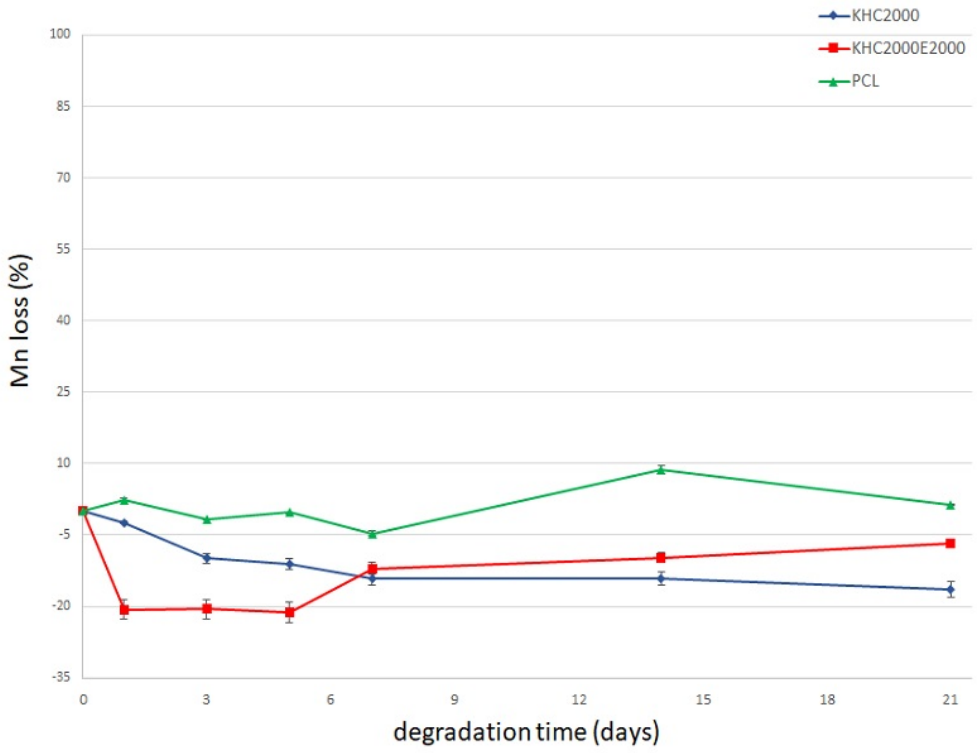

Figure 4.3: *Number average molecular weight loss profile of PCL, KHC2000, KHC2000E2000 during hydrolytic degradation in PBS*

As expected, no evident changes in molecular weight were observed in the samples; in fact, as discussed for weight loss, Pthe characterized materials are expected to show a slow hydrolytic degradation with no significant changes in molecular weight within the first weeks of incubation in aqueous media. Meanwhile, a slighly higher variation of the molecular weight was found in KHC2000E2000, since the presence of PEG arranged randomly in the polymeric chains, promoted the progressive solubilization of the polymer starting from shorter chains.
It is important to point out that the negative numbers obtained do not mean that new species or longer chains have been produced during the immersion in PBS. As M_n is based on the number of chains present in the investigated polymer, the negative slope suggests that in total the residual chains in the samples are those with a higher molecular weight, as well as that during the hydrolytic degradation only shorter chains are able to dissolve in the medium.
Furthermore, Fig. 4.4 collected the curves obtained by SEC analysis in which the response of the detector (RID signal) was plotted against retention time. Based on the working principle of SEC, longer polymeric chains are eluted earlier by the columns, while shorter molecules are eluted at the end; hence, the latter are reported in the right side of the graph. These curves

changed with increasing immersion time in PBS and they are essential to explain the variation of molecular weight loss.

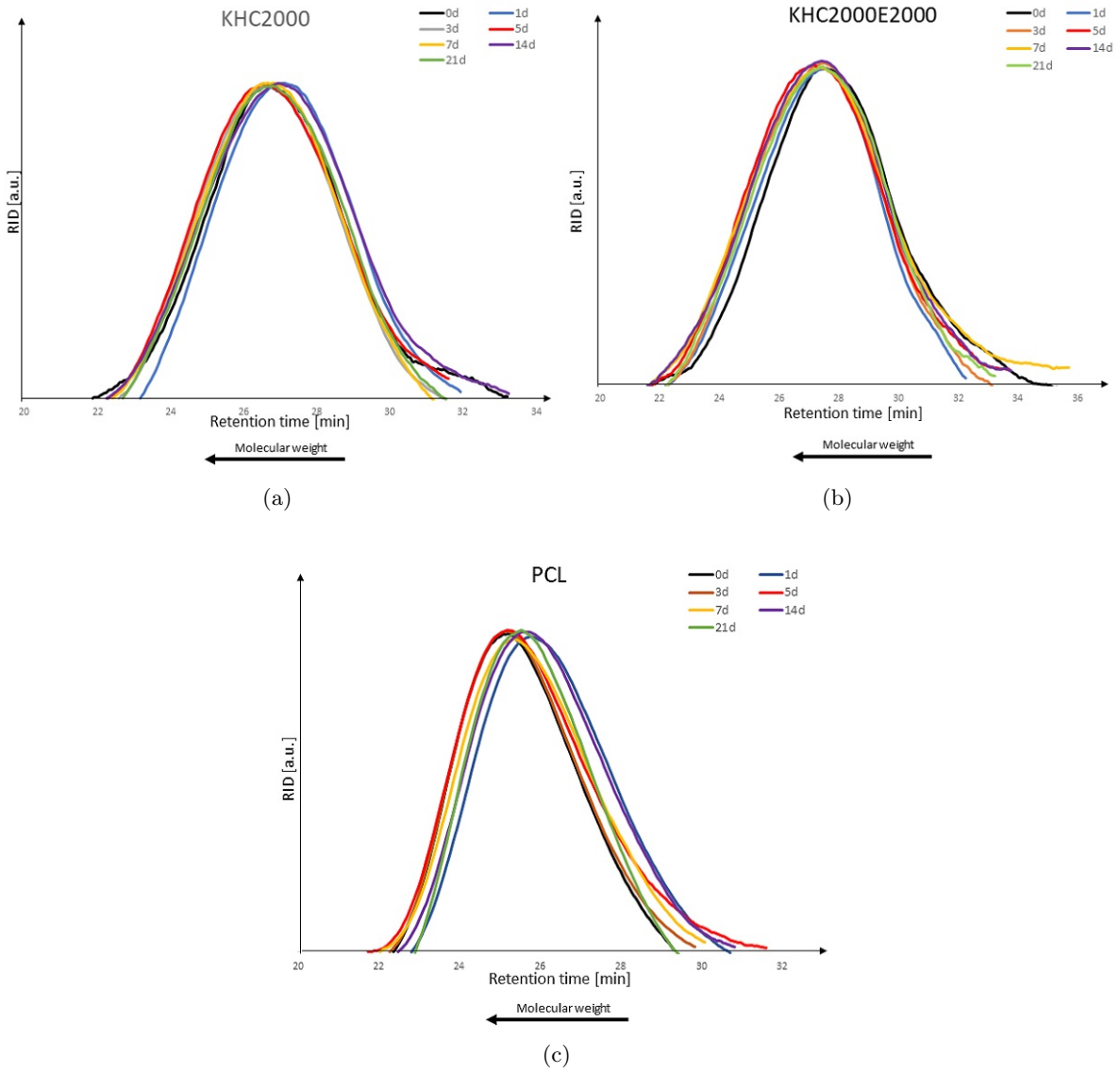

Figure 4.4: RID curves of a) KHC2000, b) KHC2000E200 and c) PCL after hydrolytic degradation

Regarding PCL, RID curves seem to slightly shift randomly around a central value probably as a consequence of the high intrinsic variation of SEC analysis.
However, a more evident change can be detected on KHC2000 films in fact, after 21 days in PBS the molecular weight increased by 16%. The curve of the samples after synthesis (in black) presented a large distribution containing a lot of short chains, while after 21 days of degradation (green) the curve became narrower and it lost the queues in the right part, meaning that shorter chains were preferentially dissolved in aqueous environment. Furthermore, the polydispersity index D slightly decrease after immersion in PBS from 1.8 to 1.6, proving that the increasing of molecular weight is just due to the narrower curves on a higher molecular weight.

The hydrolytic degradation of KHC2000E2000 is more complex compared to the other polymers and seems to occur in three stages. After only one day, the molecular weight increased due to dissolution of short chains as reported before. Then, an equilibrium situation was achieved was observed up to 7 days incubation, probably resulting from the balance between two concurrent phenomena, i.e. dissolution of shorter chains and progressive polymer degradation (due to hydrolysis of ester or urethane bonds and/or oxidation of ethylene oxide moities). Finally, degradation phenomena prevailed, and the curve had a positive slope, demonstrating that PU KHC2000E2000 is more responsive in aqueousenvironment with respect to the other polymers.

The enzymatic degradation of the samples is showed in Fig. 4.5b. In this analysis lipase was used because it works selectively on ester bonds and it breaks up the polymer into a series of monomers and shorter chains.

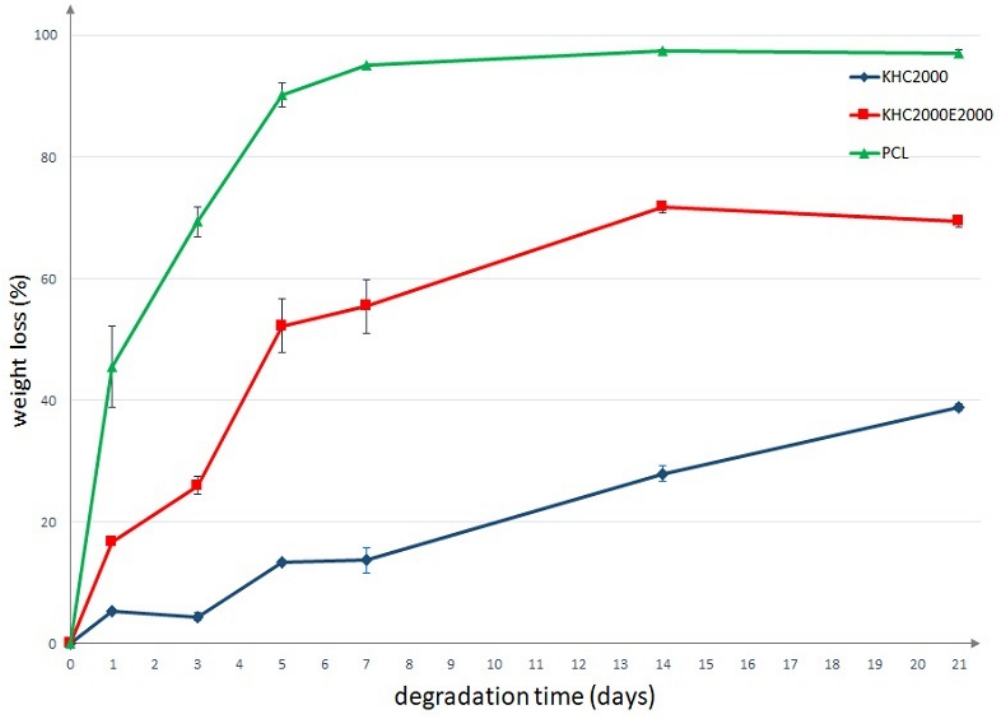

Figure 4.5: *Weight loss profile of PCL, KHC2000, KHC2000E2000 during enzymatic degradation in PBS containing an excess of Lipase from Pseudomonas cepacia*

The fastest degradation was observed in PCL samples; in fact, after 21 days the percentage of weight loss was 97.08 ± 0.4% and the films were completely destroyed. This behaviour is confirmed by literature data [99, 103, 104] and might be ascribed to the presence of a high number of ester groups which are subjected to lipase-mediated hydrolysis. Indeed, the number of ester bonds (ES) in the PCL used in this work was estimated to be approx. 700 per polymer chain, as calculated with the following formula:

$$ES_{PCL} = \frac{M_n}{M_{n_{CL}}} = 700 \text{ units} \tag{4.1}$$

Where is the number average molecular weight of PCL and $M_{n_{CL}}$ is the molar mass of the repeating unit ε-caprolactone (114.14 g/mol).
The same equation can be adapted to estimate the mean number of ester moities of each PUR chain, as follows:

$$\begin{cases} ES_{KHC2000} = \dfrac{M_n}{M_{n_{diol}} + 2M_{n_{HDI}} + M_{n_{lys}}} = 27 \text{ units} & (4.2) \\ \\ ES_{KHC2000E2000} = \dfrac{M_n}{M_{n_{diol}} + 2M_{n_{HDI}} + M_{n_{lys}}} \cdot 70\% = 13 \text{ units} & (4.3) \end{cases}$$

Where M_{ndiol}, M_{nHDI} and M_{nlys} are the number average molecular weight of the diol, the diisocyanate and the chain extender used during the synthesis, respectively. M_n is the number average molecular weight of the PU estimated by SEC. The sum of M_{ndiol}, $2M_{nHDI}$ and M_{nlys} defines the molecular weight of the repeating unit of the poly(urethane). The number of ester groups was calculated assuming that 70% of the synthesized prepolymers contain PCL and the remaind 30% contain PEG, in accordance with the weight ratio used for the synthesis.
As showed, the weight loss of KHC2000 samples after 21 days was 38.73 ± 0.6%, while for the KHC2000E2000 was 69.30 ± 0.8%.

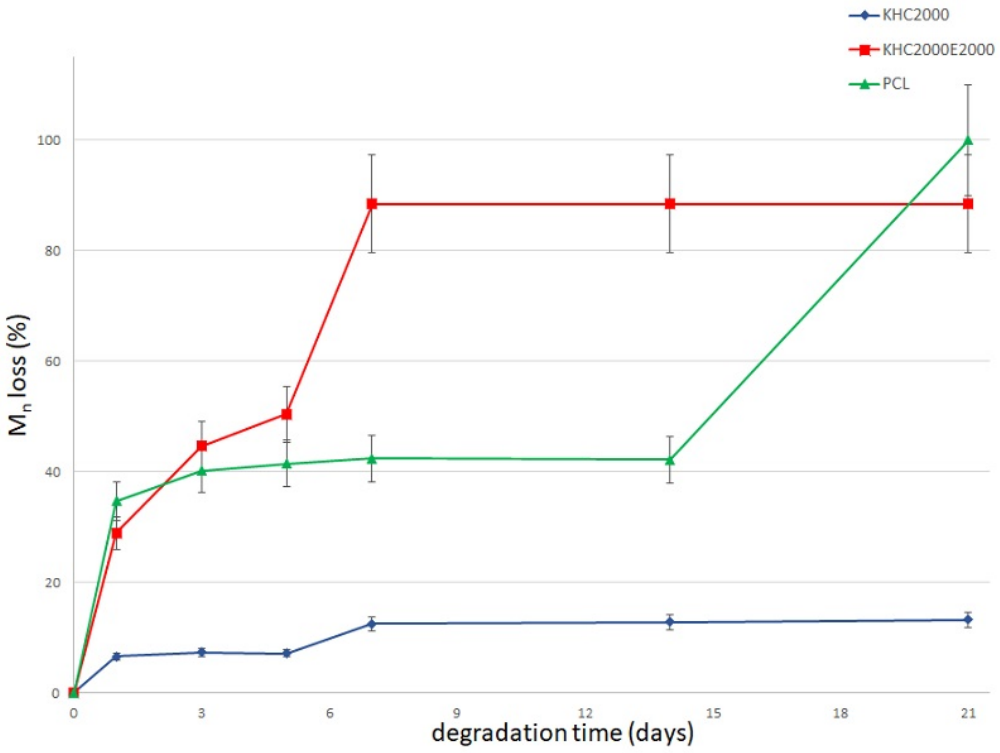

Figure 4.6: *Number average molecular weight loss profile of PCL, KHC2000, KHC2000E2000 during enzymatic degradation in PBS containing an excess of Lipase from Pseudomonas cepacia*

Concerning molecular weight loss, during enzymatic degradation all the samples showed aprogressive decrease in molecular weight, as reported in Fig. 4.6, meaning that soaking the samples

in PBS with lipase leads to a faster and more pronounced degradation.
PCL films presented almost 40% of molecular weight loss after 1 day incubation in PBS added with lipase, due to the high presence of ester groups that are selectively degraded by lipase. As a matter of fact, RID curves (Fig. 4.7c) after 1 day of immersion resulted clearly shifted on the right side, i.e. towards lower molecular weight [105].

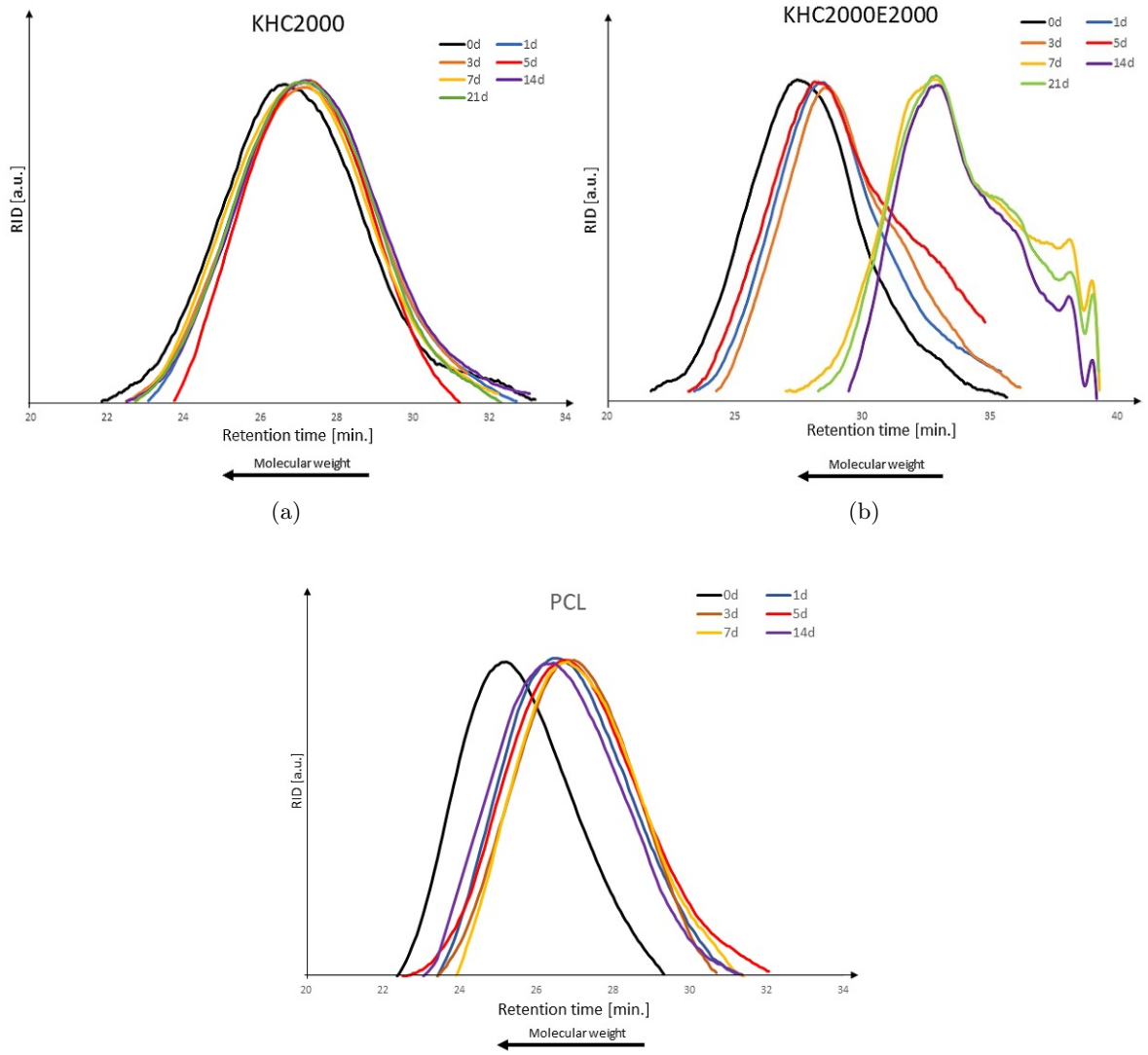

Figure 4.7: RID curves of a) KHC2000, b) KHC2000E200 and c) PCL after enzymatic degradation

Afterwards the percentage of molecular weight lost remained almost the same, probably because of the steady-state condition between the enzymatic activity that provides the breakage of the polymeric network (decreasing of the molecular weight) and the loss of chains small enough to be dissolved in the medium (increasing of the overall molecular weight). Moreover, it was not possible to perform SEC analysis on the samples after 21 days of degradation since the polymeric films were completely disappeared.

The maximum weight loss measured for KHC2000 films was almost 13% after 7 days in PBS and remained constant with the increasing of soaking time, reaching a final M_n of 60700 g/mol. Also in this case the RID curves after one day were slightly shifted on the right side, however no more changes were observed with increasing incubation time. Thus, the enzymatic degradation seems to have a fewer effect on PCL-based polyurethane with respect PCL homopolymer, probably due to the less presence of ester groups.
In contrast with KHC2000, KHC2000E2000 polyurethane presented a higher variation in terms of molecular weight, as can be been also in the trend of RID signal as a function of time which is reported in Fig. 4.7b. KHC2000E2000 lost almost 40% of its initial molecular weight after 5 days of immersion and reached a plateau after 7 days,with a final M_n of 5600 g/mol. This behaviour was confirmed by the trend of RID curves, which moved to higher elution time. Moreover, a unique behaviour was observed in KHC2000E2000: multimodal distributions of RID signal, and as a consequence of molecular weight, were obtained after 7 days of immersion in PBS, suggesting the formation of new species with lower molecular weight [105]. This drastic change in RID signal trend is probably due to the complex degradation mechanism of KHC2000E2000, as discussed before.

SEM images of the surface and the cross section of the three types of films before and after hydrolytic and enzymatic degradation.
In accordance with data previously reported, no changing of surface or cross section morphologies were observed in PCL-based samples after 21 days of immersion in PBS (Fig. 4.8). On the contrary, enzymatic degradation, carried out using an excess of Lipase, led to drastic changes in sample surface. After 7 days immersion in PBS added with lipase, the film was wearing thin due to the progressive surface erosion, in accordance with the fact that enzymatic degradation takes place on the surface [106] without affecting the bulk structure.

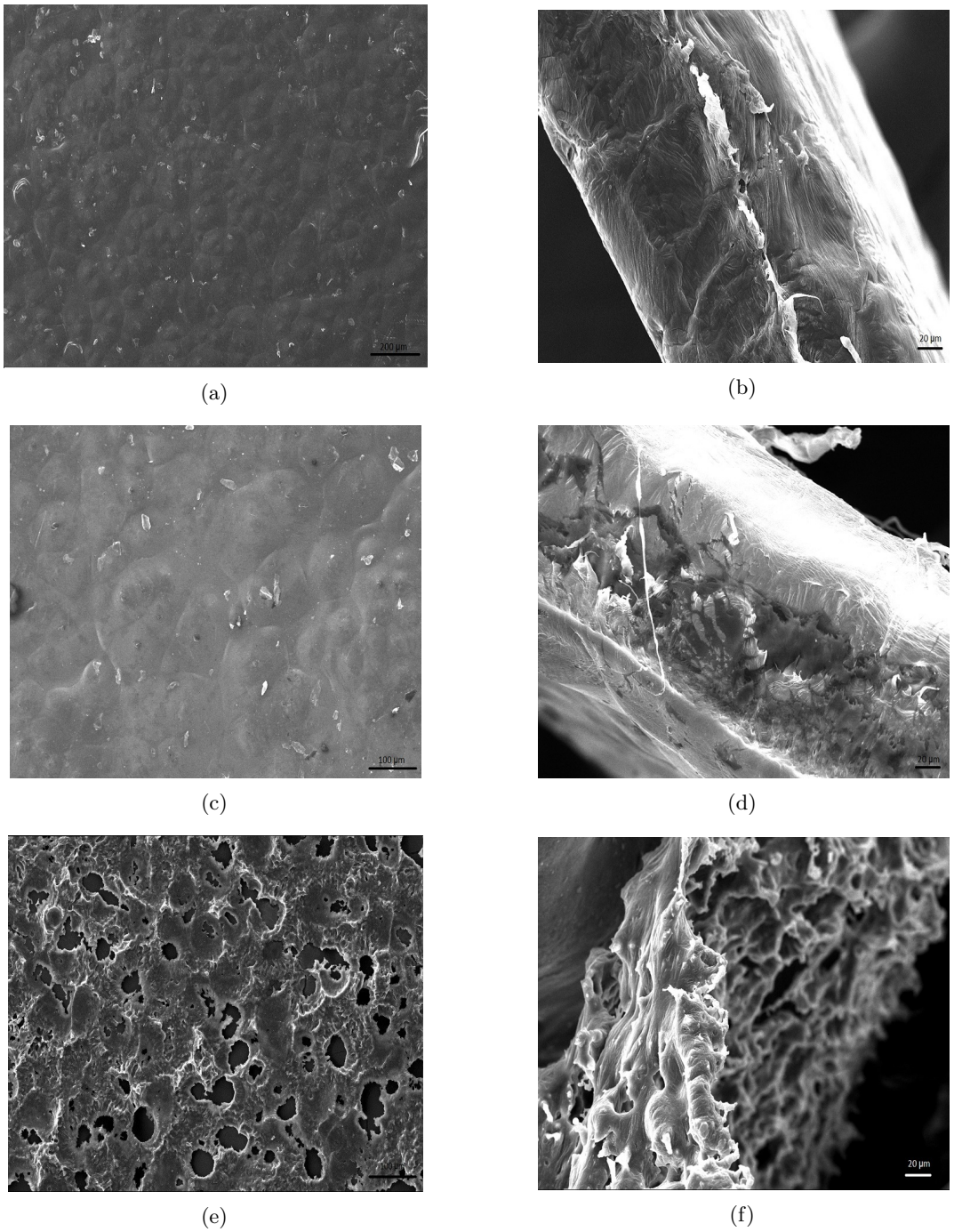

Figure 4.8: SEM micrographs of a) surface and b) cross section of a PCL film before degradation onset, c) surface and d) cross section of hydrolytic degadation after 21 days immersion and e) surface and f) cross section of an enzymatically-degraded PCL film (7 days immersion in PBS added with lipase)

SEM images of KHC2000 (Fig. 4.9) films after degradation confirmed its higher resistance to this process with respect to the other investigated materials; indeed, it showed almost the same surface after 21 days of hydrolytic degradation, while it presented some cracks on the surface after immersion in PBS containing Lipase.

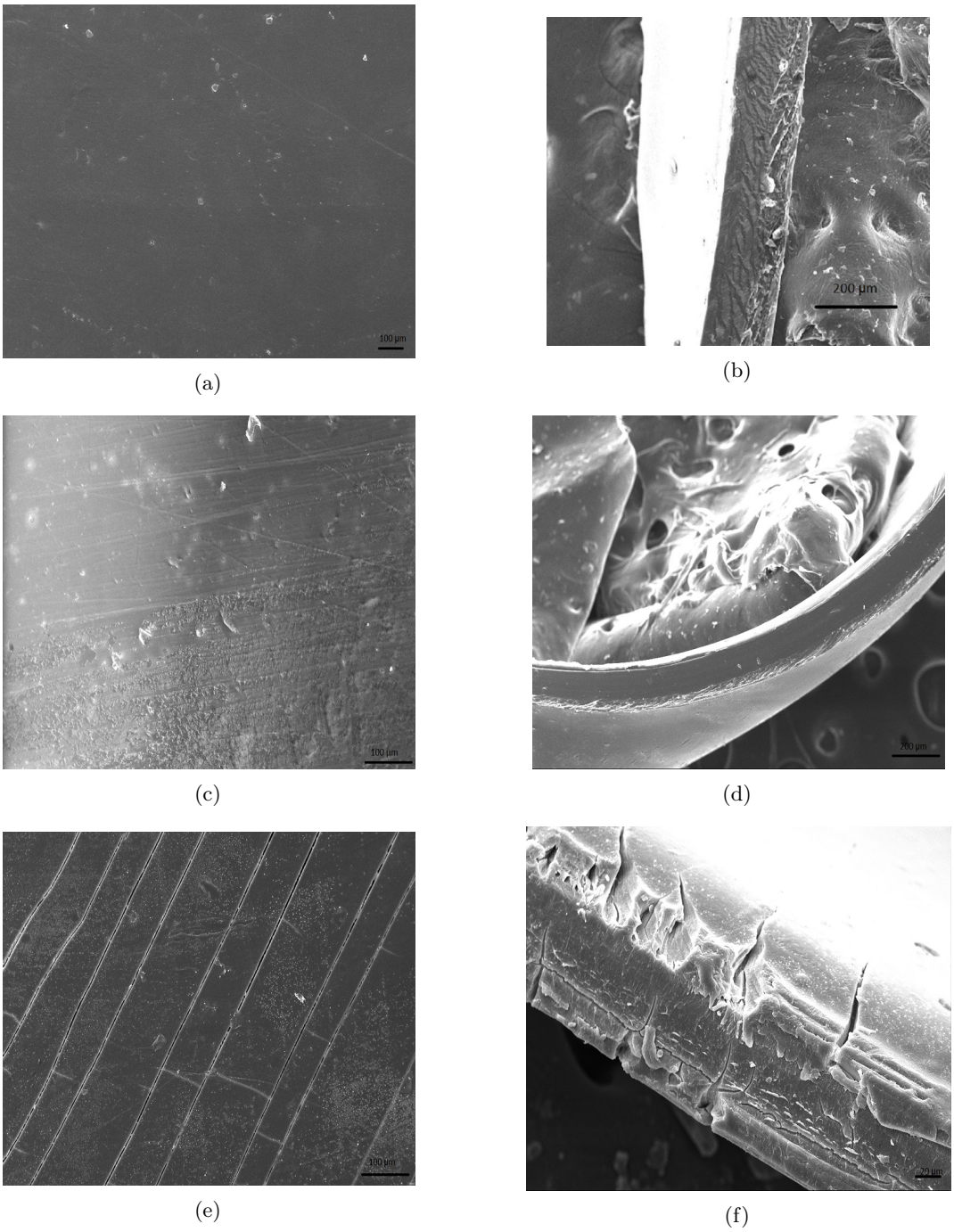

(a) (b) (c) (d) (e) (f)

Figure 4.9: SEM micrographs of a) surface and b) cross section of a KHC2000 film before degradation onset, c) surface and d) cross section of hydrolytic degadation after 21 days immersion and e) surface and f) cross section of an enzymatically-degraded KHC2000 film (21 days immersion in PBS added with lipase)

For what concerns KHC2000E2000 (Fig. 4.10), in addition to surface erosion, a form of bulk degradation can be observed in SEM images, probably due to the presence of PEG moities that favor the permeation of the degradation medium through sample thickness (Fig. 4.10f). However, in accordance with previous considerations, the enzymatic degradation of KHC2000E2000 is

less pronounced with respect to PCL because of the less amount of ester grousp present in its chains.

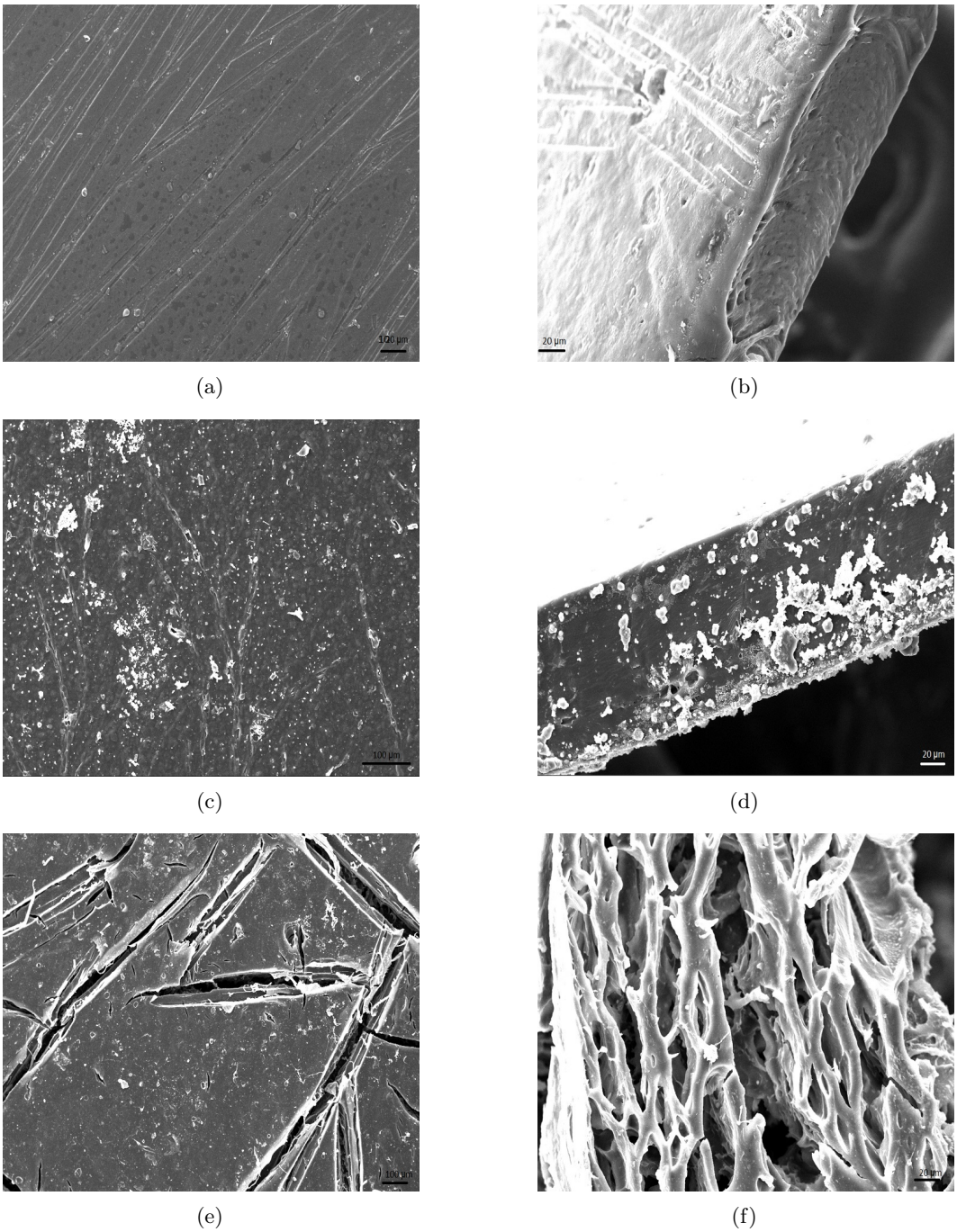

(a) (b) (c) (d) (e) (f)

Figure 4.10: SEM micrographs of a) surface and b) cross section of a KHC2000E2000 film before degradation onset, c) surface and d) cross section of hydrolytic degadation after 21 days immersion and e) surface and f) cross section of an enzymatically-degraded KHC2000E2000 film (21 days immersion in PBS added with lipase)

4.2 Scaffold Characterisation

4.2.1 Morphology of Pure BG Scaffolds

The weight, diameter, height, porosity and pore size of pure BG scaffolds produced with the foam replica technique are given in Table 4.1. The results are expressed as average value and standard deviations.

Table 4.1: *Average dimensions of pure BG scaffolds*

Weight	0.052 ± 0.01 g
Diameter	7.8 ± 0.2 mm
Height	5.1 ± 0.1 mm
Porosity	92.1 ± 1.6 %
Pore size	408.0 ± 186.1 µm

The obtained values are typical for BG scaffold produced using the foam replication method. Moreover the average pore size is in the range 200 - 500 µm, suitable for tissue engineering applications, in fact many in vitro studies reported that a pore size greater than 200 µm is necessary to allow osteoconduction [108]. A macroscopic view of the structure of the sintered scaffolds is given in Fig. 4.11a

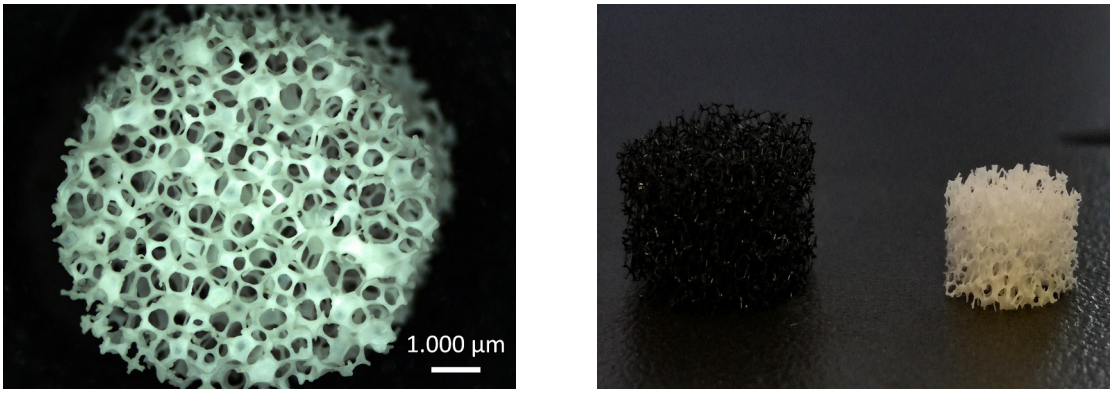

(a) (b)

Figure 4.11: *a) Light microscope images of top-view of 45S5 BG-based scaffolds after the sintering process and b) Shrinkage of the scaffold after the sintering process*

Moreover, the macro and microstructure of the pure Bioglass® scaffold are show in Fig. 4.12 at different magnifications; similar morphologies have been reported elsewhere [82, 83].
The hollow nature of the struts showed in Fig. 4.12(c) can be associated with the burning out of the sacrificial PU foam.
It is possible to notice the highly interconnected pore structure of the scaffold and the sintered particles in Fig. 4.12(d).
Indeed during the heating at 1050°C sintering occurs and the original particles were melted and partially crystallized [83], causing a normal shrinkage of the foam, reported in Fig. 4.11b.

This densification of compact 45S5 Bioglass® was better investigated in detail through hot-stage microscopy (HSM) images at diferrent temperatures, by Baino et al. [109]. In details, during the sintering, samples undergo densification in two steps: the first one between 530°C and 620°C and the second at temperature up to 850°C, where the shrinkage phenomenon is more evident [110]. Among the two phases crystallization of the powders occours leading the formation of a glass-ceramic as extensively reported elsewhere [54, 82, 83, 112]. Moreover, looking at the obtained value of diameter and high, with respect the initial value (H_0=7 mm and D_0=10 mm), it is possible to notice that the shrinkage in the axial direction (S_H) is slightly higher than the diametral shrinkage (S_D), as reported by Bretcanau et al. [110].

$$\begin{cases} S_H = \dfrac{H_0 - H_f}{H_0} = 0.27 & (4.4) \\ S_D = \dfrac{D_0 - D_f}{D_0} = 0.22 & (4.5) \end{cases}$$

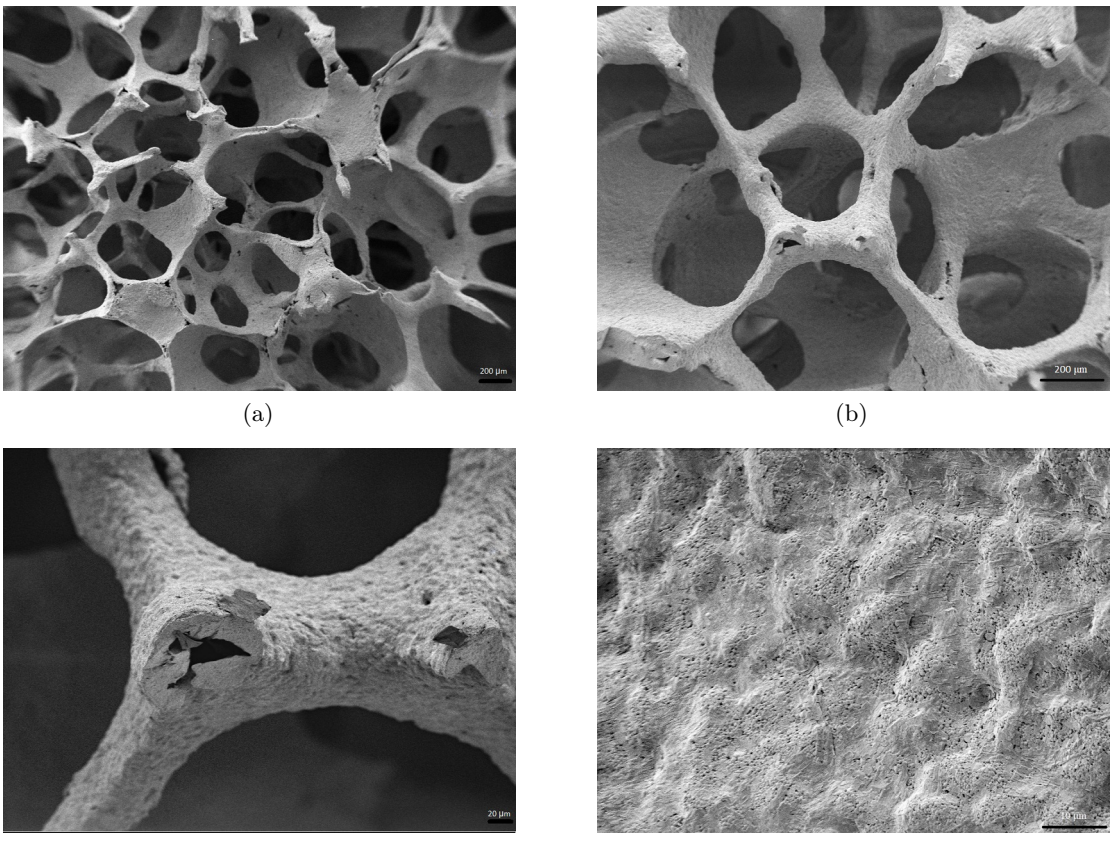

(a) (b)

(c) (d)

Figure 4.12: *SEM micrographs at a) 70X, b) 150X, c) 500X and d) 3.5KX of Bioglass® scaffolds*

4.2.2 Morphology of Coated BG Scaffolds

The morpholgy of polymer coated Bioglass® scaffols was assessed by SEM analisys and through light microscope. The morphology of PCL-coated scaffolds is reported in Fig. 4.13.

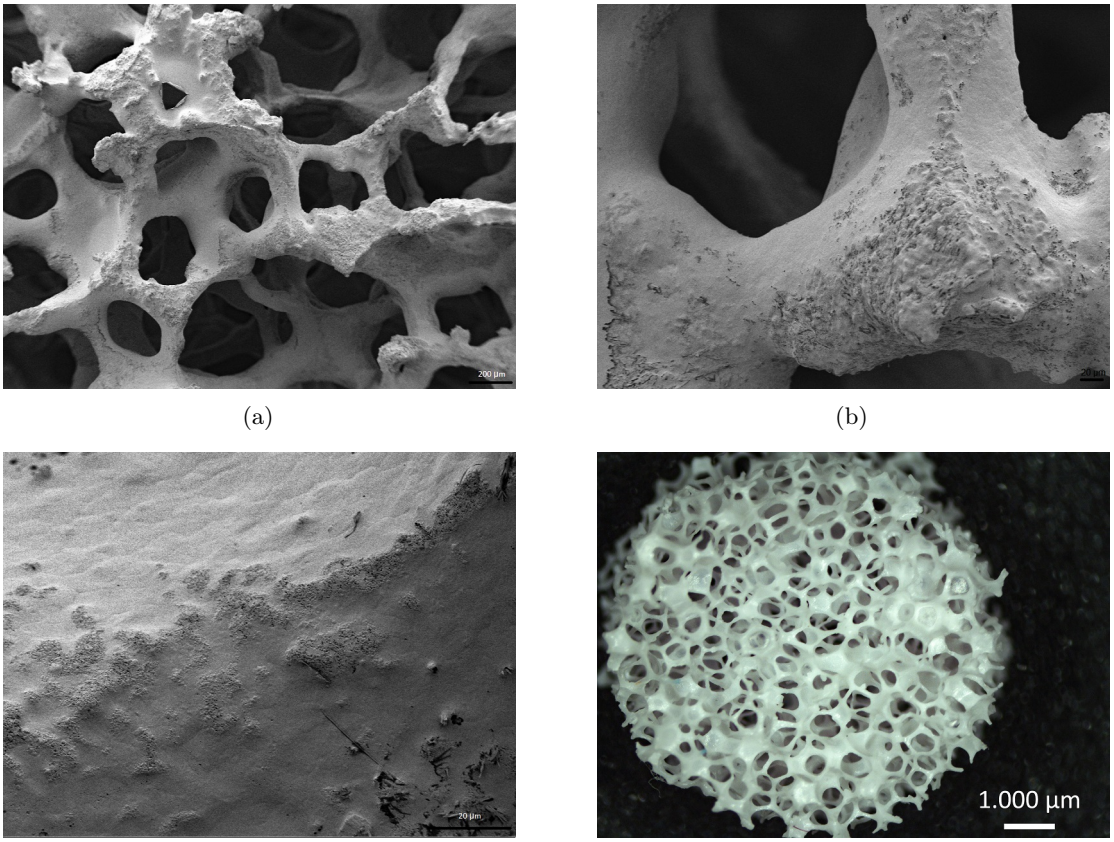

(a) (b)

(c) (d)

Figure 4.13: SEM micrographs at a) 100X, b) 500X, c) 2KX and d) light microscope images of top-view of PCL coated Bioglass®-scaffolds

Scaffolds produced with 2.5-minutes dip-coating technique in a PCL solution in chloroform, with a concentration of 1% w/v present some clogged pores, as showed in Fig. 4.13(a)-(d). Furthermore the scaffold is only partially covered by PCL and it is easy to distinguish the rough surface of the bioactive glass. Similar results have been reported in previous works [86, 87]. In particular Fereshteh et al. [86] speculated that this might not be a drawback since to cover completelly the surface with the non-bioactive polymer could retard or even suppres the bioacity of the glass-ceramic. Finally, after the coating the porosity slightly decreased from 92% to 90%.

Composite scaffold obtained with 1-minute dip coating procedure in a KHC2000 solution in chloroform with a concentration of 0.5% w/v is reported in Fig. 4.14.

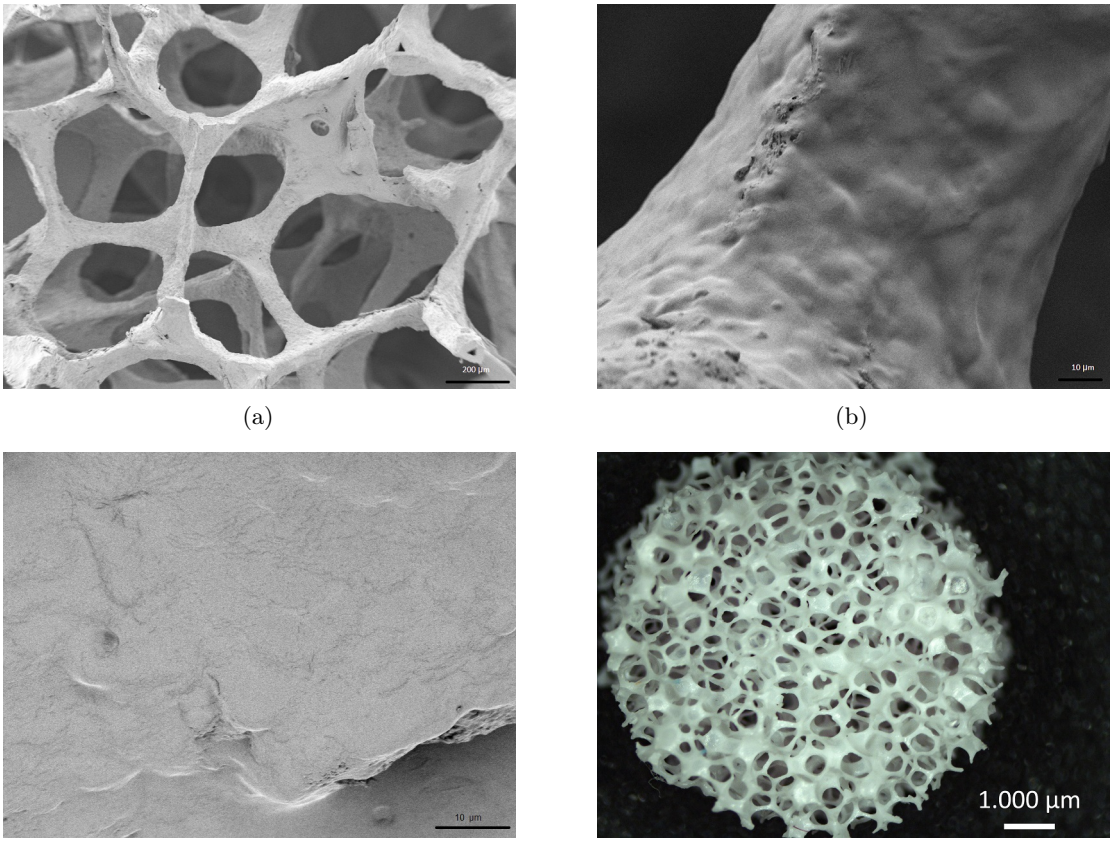

(a) (b)

(c) (d)

Figure 4.14: SEM micrographs at a) 150X, b) 2KX, c) 3.5KX and d) light microscope images of top-view of KHC2000 coated Bioglass®-scaffolds

It possible to notice the homogeneous coating of the bioactive scaffold, in fact the polymer penetrates in the cracks, leading to a more resistant structure. In particular, Fig. 4.14(c) shows a film of polyurethane that covers completely the surface. Therefore, compared to PCL, KHC2000 leads a much homogeneous and well distributed coating, although the concentration and the consequent amount of polyurethane into the scaffold, is less than in PCL/BG-based scaffold. Moreover, KHC2000 coated scaffolds present a porosity around 91%.

The images of the last type of samples, that were produced performig 1-minute dip coating in chloroform solution containing 1%w/v KHC2000E2000, are collected in Fig. 4.15.
Also in this case the polyurethane leads a more homogeneous coating than PCL, hence most of the glass-ceramic struts is covered by a thin layer of KHC2000E2000.

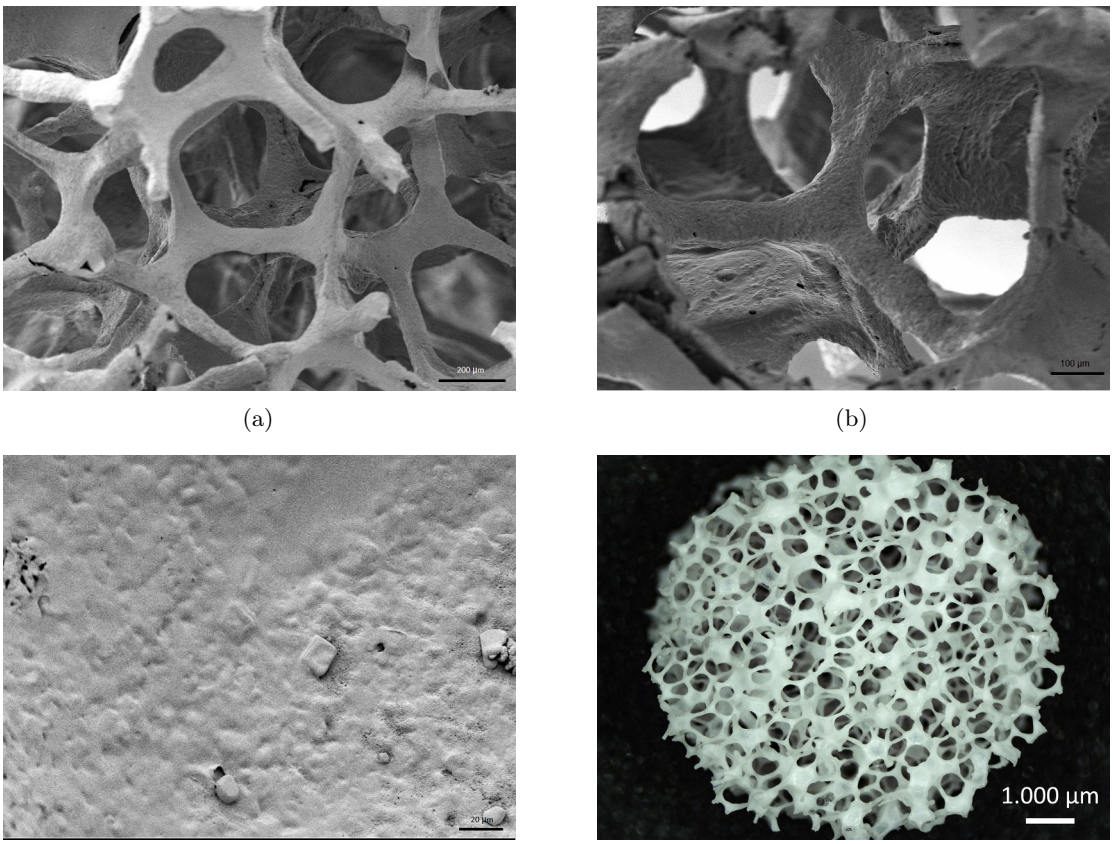

(a) (b)

(c) (d)

Figure 4.15: SEM micrographs at a) 150X, b) 250X, c) 1KX and d) light microscope images of top-view of KHC2000E2000 coated Bioglass®-scaffolds

It has to be pointed out that even if few pores were blocked, due to the fact that the procedure was repeated three times, the open porosity of the uncoated scaffold was well manteined in the samples coated with both polyurethanes, while slightly decreased for PCL-coated scaffolds. Thus, concerning the morphology, both polyurethanes seem to provide better features than PCL.
The average amount of each type of polymers bonded to the scaffolds and the final porosity of composites are reported in Tab. 4.2

Table 4.2: *Average amount of polymer and porosity after coating*

	Amount of polymer (mg)	Porosity (%)
PCL/BG	1.5 ± 0.3	90.7 ± 1.6
KHC2000/BG	0.9 ± 0.2	91.1 ± 1.7
KHC2000E2000/BG	1.5 ± 0.5	91.7 ± 1.5

4.2.3 Bioactivity Tests

The *in-vitro* bioactivity of the composite scaffolds was investigated at different time points after immersion in SBF through SEM, FTIR and XRD.
SEM images after 3 days in SBF are showed in Fig. 4.16. Meanwhile the typical cauliflower shape of hydroxyapatite was present on the unocated scaffold surface, it was sligthtly retarded in coated ones.

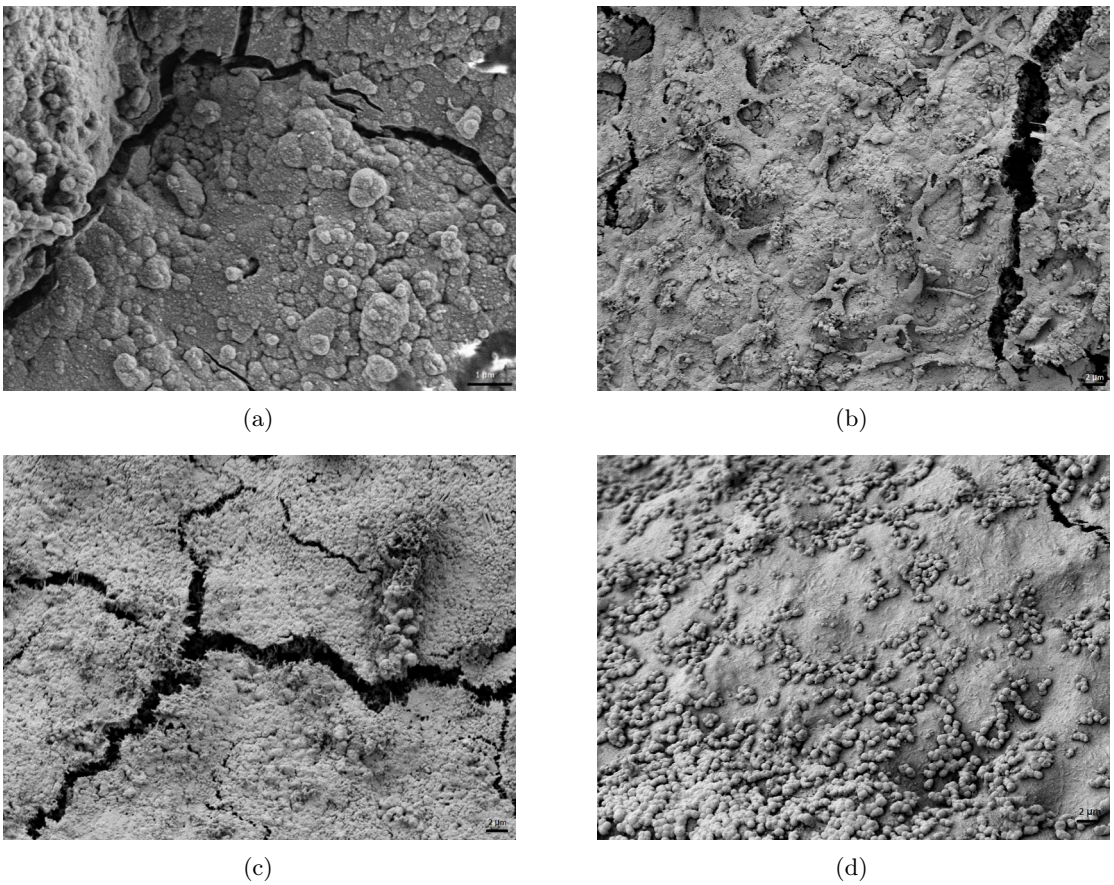

(a) (b)

(c) (d)

Figure 4.16: SEM micrographs of a) BG (20KX) b) BG/PCL (5KX) c) BG/KHC2000 (5KX) and d) BG/KHC2000E2000 (5KX) scaffolds after 3 days immersion in SBF

However, after 21 days of immersion also the surface of coated samples was covered with HCA layer as showed in Fig. 4.17. The well-maintained bioactivity is probably due to some small uncoated regions on the composites surface, present after the coating and also caused by the

degradation in aqueous solution. In these regions occurs the ions exchange between SBF and Bioglass, that are directly in contact, by which begins the bioactive mechanism leading the nucleation of HA crystals [70].

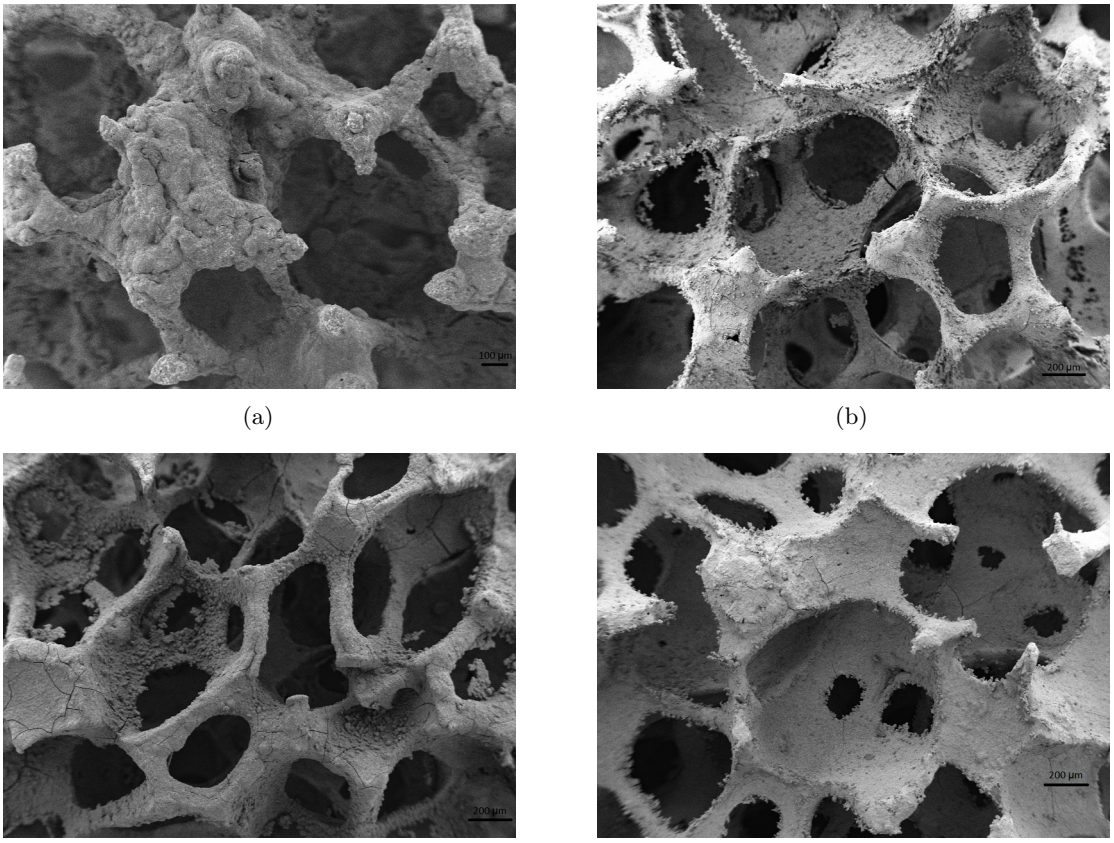

(a) (b)

(c) (d)

Figure 4.17: SEM micrographs of a) BG (120X) b) BG/PCL (100X) c) BG/KHC2000 (100X) and d) BG/KHC2000E2000 (100X) scaffolds after 21 days immersion in SBF

ATR-FT-IR analysis was performed on all types of samples for a preliminary confirmation of their bioactive behaviour. Fig. 4.18 showed an overall view of the modification of the surface of uncoated 45S5 Bioglass® scaffold due the growth of hydroxyapatite-like phase within immersion in SBF. Concerning the spectra of control samples (0d), the peak in the range 1100-1000 is due to the concomitantly P=O and Si-O-Si asymmetric stretching [111], meanwhile Si-O (non-brinding oxygen) shows absorption at 915 cm^{-1}. The other characteristic points are: 438 cm^{-1} due to the Si-O-Si bending vibration; 619, 575 and 521 cm^{-1} ascribed to P-O bending that suggest the presence of calcium phosphate phase [112]. Soaking the samples in SBF led the formation of new peaks related to the growing of HCA layer, in fact after only 3 days it is possible to notice the peak at ca. 800 cm^{-1}, that becomes more clear with the increasing of time, and it is an indication of the formation of a silica rich layer [113]. Furthermore, CO_3^{2-} groups in the carbonate HA layer generate a peak at 1418 cm^{-1} due to C=O stretching. The double peak at ca. 570 cm^{-1} is ascribed to P-O bending vibration (showed better in Fig. 4.19 a)

indicating the crystallization of the calcium phosphate into HCA [114].
Apart the shaping of these peaks it is interesting to consider that the peak due to Si-O stretching disappear and the peak at 1100 cm^{-1} is due only to the P=O stretching. Moreover also the peaks at 619, 575 cm^{-1} due to P-O bending gradually disappear proving the dynamical transformation of the surface and its degradation. Finally, the peak at 438 cm^{-1} is slightly shifted probably because of the variation of ionic concentration [113].

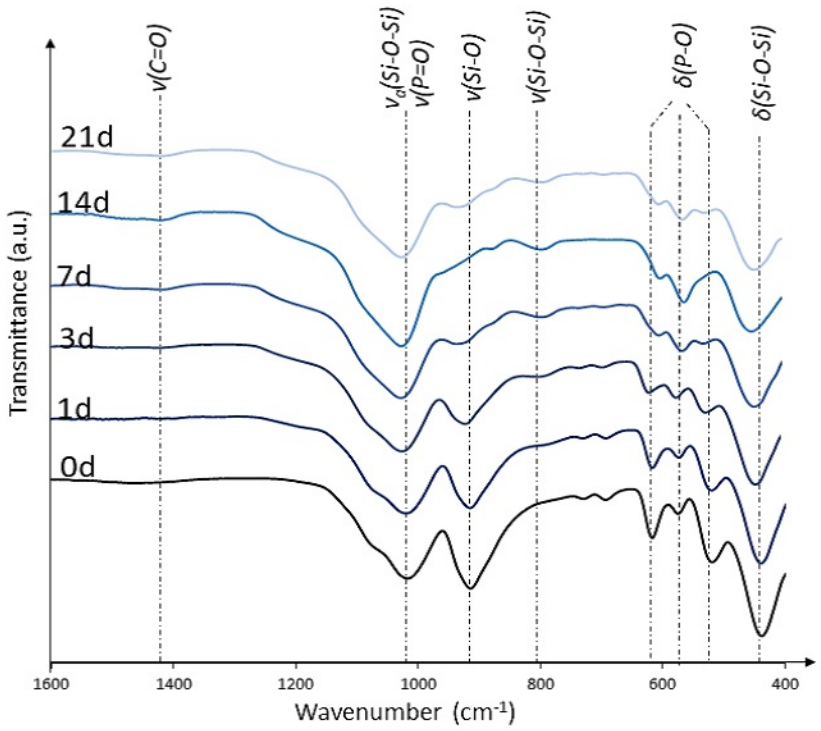

Figure 4.18: *ATR-FT-IR spectrum of 45S5 Bioglass®-based scaffold after immersion in SBF*

Fig. 4.19 collects the ATR-FT-IR spectra of uncoated and coated scaffolds before and after 21 days of immersion in SBF. Concerning the spectra referred to 0 day they result quite similar between each other and the more evident peaks are those of pure scaffolds. The reason of that could be the low amount of polymer with respect the Bioglass®. However, in all coated scaffolds it is still evident the peak at ca. 1700 cm^{-1} due to the stretching vibration of C=O belonging to PCL diol. Additionally, the small peak present in the coated scaffolds it is relate to symmetric and asymmetric vibration of CH_2 of the ester group.
Hypothesis discussed before for uncoated scaffolds remain true also for the coated ones, the only difference regards the double peak at ca. 570 cm^{-1} ascribed to P-O bending vibration due to the crystallization. Indeed, this peak is less evident in the spectra of coated scaffolds, meaning that the polymeric coating slight retards but did not inhibits the bioactivity, as confirmed by SEM images.

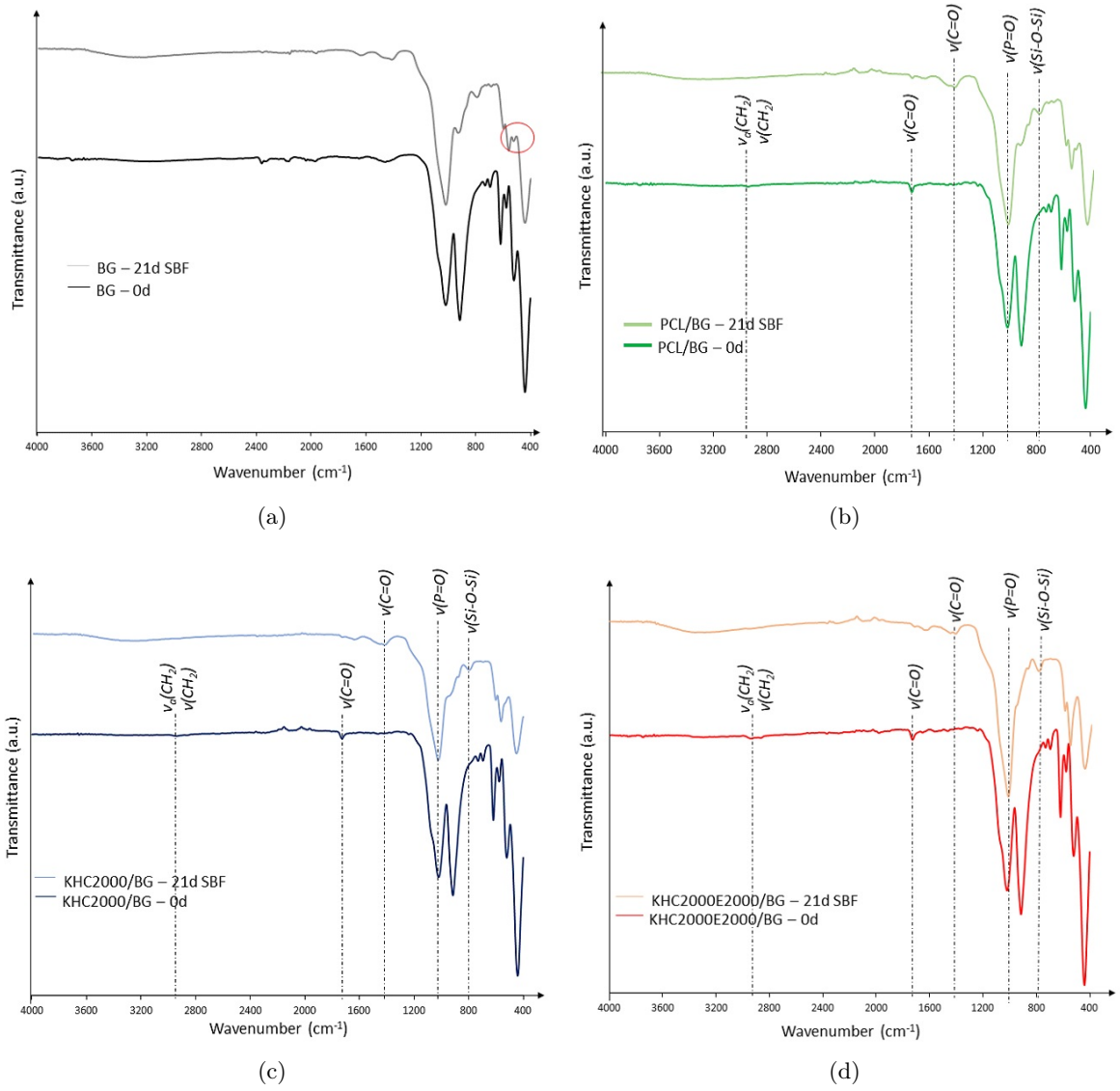

Figure 4.19: FTIR spectra of a) BG b) PCL/BG c) KHC2000/BG and d) KHC2000E2000/BG scaffolds at 0 day and after 21 days immersion in SBF

However, to assess the presence of crystalline hydroxyapatite XRD analysis were carried out. In Fig. 4.20 were presented the XRD spectra of uncoated and coated scaffolds after thermal treatment, and were marked the major peaks identified at 20°, 24°, 27°, 34°, 49° and 60°. As expected, sintering process of 45S5 Bioglass® scaffolds leads the formation of $Na_2Ca_2Si_3O_9$, called combeite, as main crystalline phase [82]. However, to give a completely overview on what reported in the literature, it must be pointed out that there is no accordance about the nature of the crystalline phase, in fact Lefebvre and co-worker [112] suggested that the crystalline phase $Na_2CaSi_2O_6$ is more realistic than combeite, due to its similarity with Bioglass® composition. Moreover, they found that after sintering at higher temperature (800–950°C) a second minor crystalline phase is formed and could be identified as ($Na_2Ca_4(PO_4)_2SiO_4$) [112].
Finally, the XRD spectra of composite scaffolds present similar shape to the uncoated one, since

the polymers added were amorphous and they did not contribute to the crystallinity.

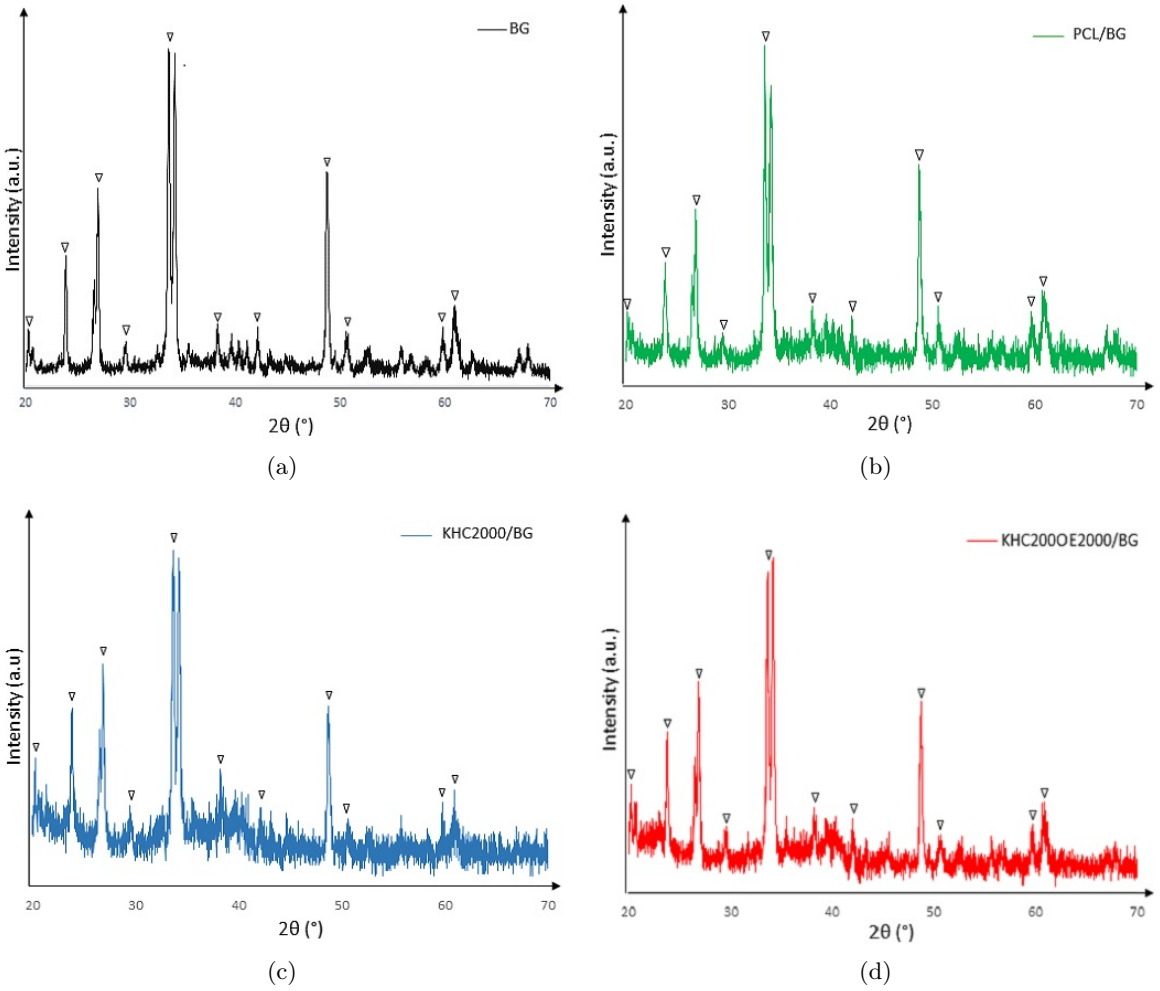

Figure 4.20: XRD spectra of a) BG b) PCL/BG c) KHC2000/BG and d) KHC2000E2000/BG scaffolds

Fig. 4.21 reports XRD analysis of pure 45S5 Bioglass® scaffolds soaked for 1-21 days in SBF to assess the changing of the surface and to confirm that the layer visible in SEM images is not only composed of amorphous calcium phosphate, but also of crystalline hydroxyapatite. During the immersion in SBF the peaks of the crystalline phase gradually disappear, meanwhile a new peak at 2ϑ=32° becames narrow. Finally, after 21 days of immersion in SBF the XRD spectra presents the typical shape produced by amorphous phase, with the addition of the two peaks at 26° and 32° that are related to the deposition of crystalline hydroxyapatite [116]. Thus, other than the formation of crystalline HCA, a decreasing of the crystallinity occurs, meaning that during the time in SBF this phase is preferentially degraded and transformed into an amorphous phase [82].

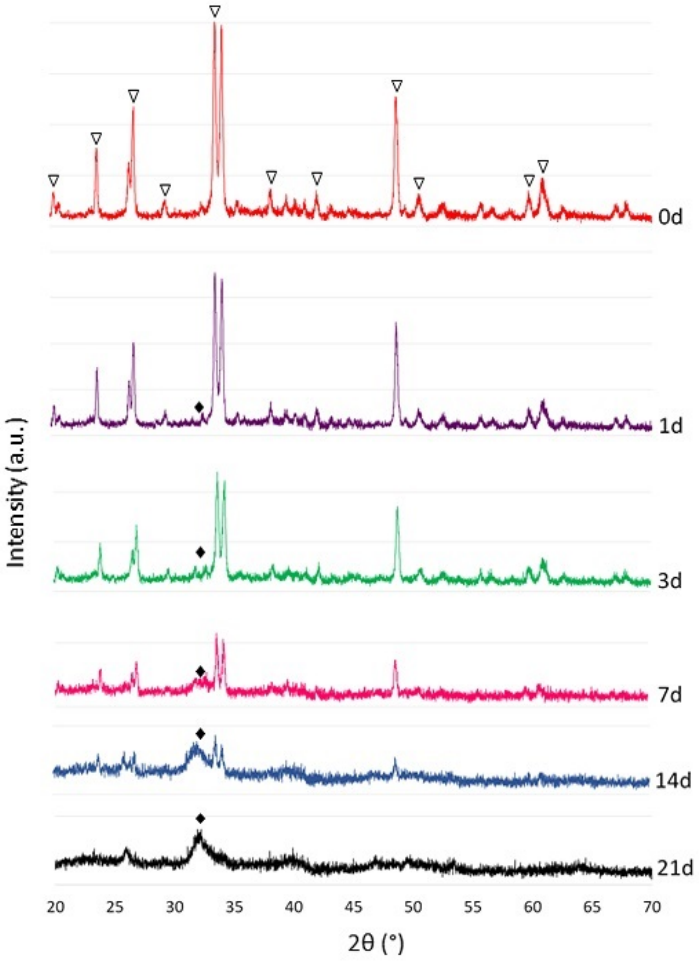

Figure 4.21: *XRD spectrum of 45S5 Bioglass®-based scaffold after immersion in SBF*

Furthermore Fig. 4.22 shows XRD spectra of coated scaffolds in comparison with the pure BG scaffold after 21 days in SBF, to evaluate how the presence of the coating affects the crystallization of hydroxyapatite. As discussed before, the coating slight decreases the transformation kinetics of the crystalline phase into amorphous one, characteristic of Bioglass®. In fact, in the spectra of coated scaffolds the major peak at 34° is still evident. However the polymeric coating did not inhibit the bioactivity, confirmed by the presence of the typical peaks of hydroxyapatite (marked in black) [88].

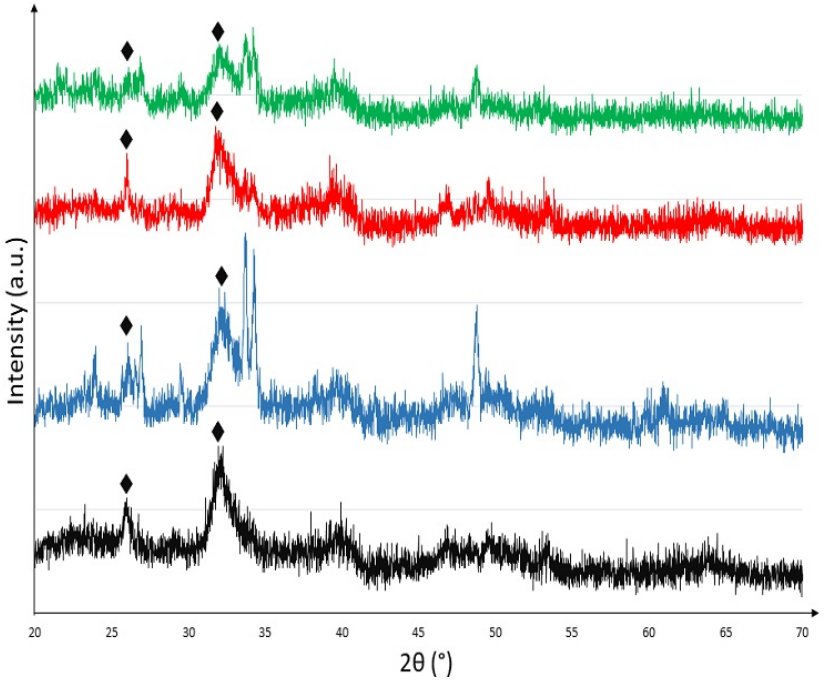

Figure 4.22: *XRD spectra of uncoated and coated 45S5 Bioglass®-based scaffold after 21 days immersion in SBF*

Moreover, to clarify the effect of polyurethanes coating on bioactive behaviour of 45S5 Bioglass®, the coated pellets were immersed in SBF for 7 days, to analyse directly the surface through FTIR analysis without crash the scaffolds. In fact, using powders it is possible to mix and confuse the signal from the glass with those derived from hydroxyapatite. In particular, germanium crystal was used for its less penetration power, that allows a superficial analysis of the coating.
Fig. 4.23 collects the ATR-FT-IR spectra of coated pellets, each graph reports three overlapped spectra: BG pellet (control at day 0), coated-pellet before immersion in SBF and the spectra of the specific polymer. This representation should show better the variations of the spectra due to the presence of the coating, that was impossible to asses in the coated scaffolds because of the low amount of polymer with respect the Bioglass® powders.

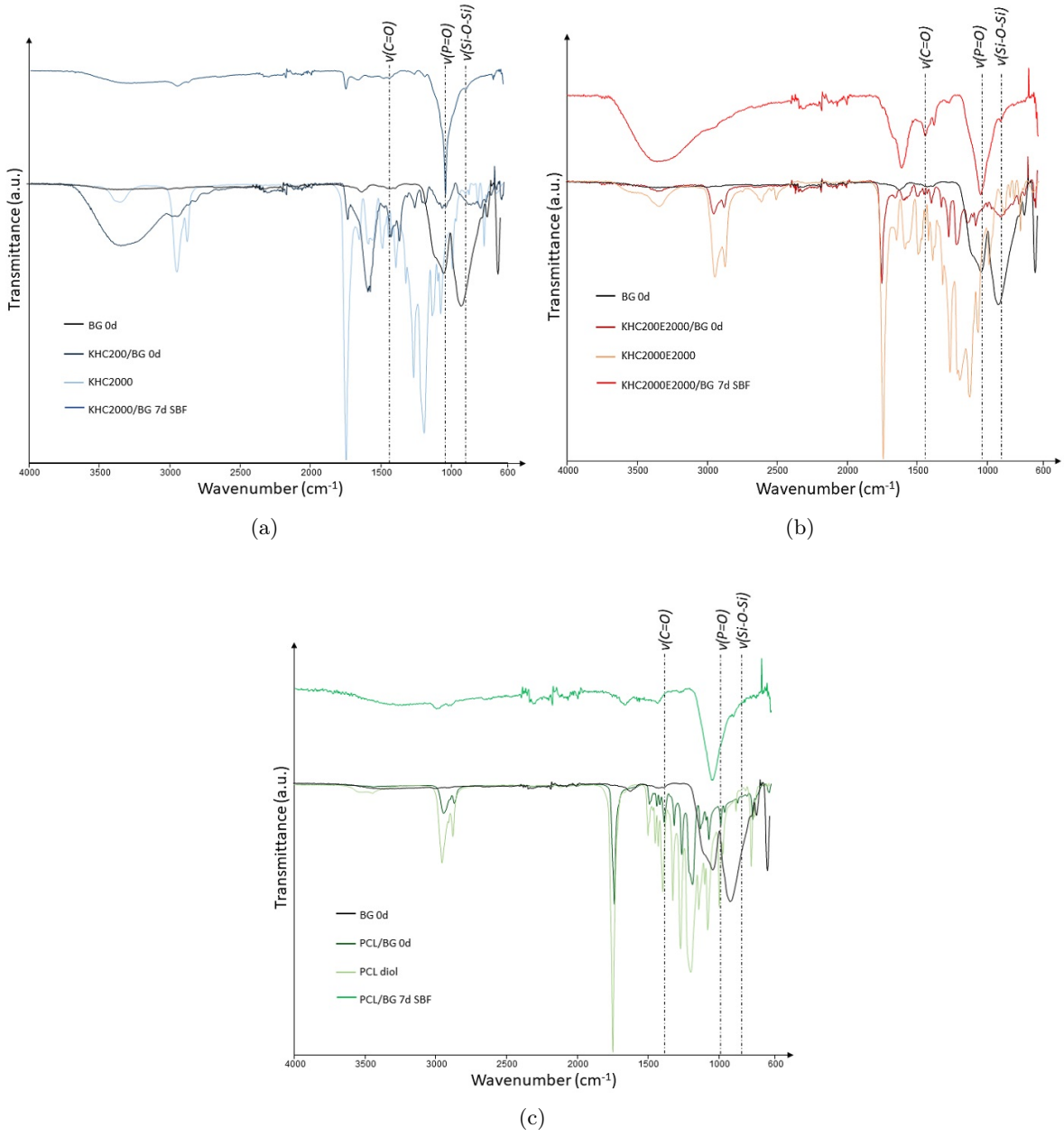

Figure 4.23: ATR-FT-IR spectra of a) KHC2000/BG and b) KHC2000E2000/BG c) PCL/BG pellets after 7 days immersion in SBF

In contrast with ATR-FT-IR spectra of coated scaffolds that showed mainly the peaks ascribed to the glass-ceramic, coated pellets revealed peaks of both polymer and Bioglass®.
In all the spectra of coated pellets are present the characteristic peaks of PCL diol: two peaks in the region 2850 – 2950 cm^{-1} ascribed to CH_2 asymmetric and symmetric stretching vibrations; highest peak at ca. 1723 cm^{-1} due to C=O stretching. However, this peak is less evident in the spectra of KHC2000/BG pellet probably to the interference of the glass. The highest peak in KHC2000/BG spectra is at ca. 1560 cm^{-1} due to the simultaneous C-N stretching and N-H bending, less visible in the spectra of mixed polyurethane. The peak at 3360 cm^{-1} is ascribed

to N-H stretching, due to urethane-urea and amide groups, in fact this peak is not present in PCL/BG spectrum. Finally, it is possible to notice in the coated pellets, two small peaks derived from the glass, one at 1020 cm^{-1} ascribed to asymmetric Si-O-Si and P=O vibration, the second one at 930 cm^{-1} that is due to vibration of non-binding oxygen Si-O. Moreover, the large peak at ca. 3500 cm^{-1} is due to the presence of water.
Concerning the spectra after immersion in Simulated Body Fluid they present the characteristic peaks already analysed for coated scaffolds. As showed in Fig. 4.23 the spectra present three main peaks ascribed to hydroxyapatite formation: C-O symmetric vibration at ca. 1400 cm^{-1} that provse the formation of HCA layer, P-O vibration at ca. 1000 cm^{-1} and Si-O-Si- stretching at 800 cm^{-1}. However, using germanium crystal it is not possible to see the peaks below 600 cm^{-1} such as the peaks ascribed to P-O bending vibration.
In addition, the presence of hydroxyapatite on the coated pellets was confirmed through SEM analysis (Fig. 4.24). The surface was covered with hydroxyapatite layer and the typical cauliflower structure is reported at higher magnification in Fig. 4.24d.

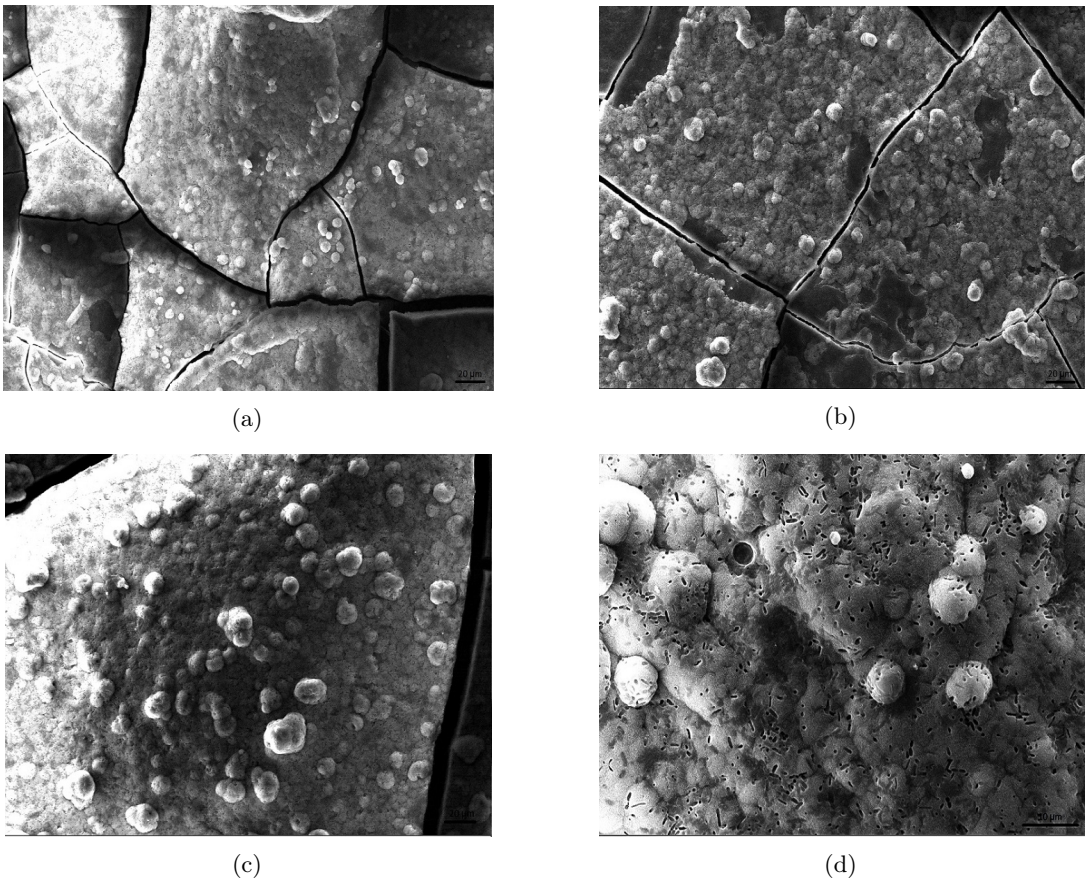

(a) (b)

(c) (d)

Figure 4.24: SEM Images of a)KHC2000/BG, b) KHC2000E2000/BG, c) PCL/BG pellets after 7 days in SBF and d)typical cauliflower structure of hidroxyapatite at higher magnification

Altogether SEM, ATR-FT-IR and XRD results proved the well-known bioactivity of 45S5 Bioglass® scaffolds as well as its retention in the composite samples. It has to be pointed out

that the bioactivity of the composites was due to bioactive glass; in fact, the polyurethanes were not designed to be bioactive as confirmed in previous work [101]. In fact, as discussed before the deposition of hydroxyapatite layer could be due to the thin polymeric layer and to the small uncoated region in the surface of composite scaffolds that allow a direct contact between bioactive glass and SBF.

4.2.4 Mechanical Tests

In order to investigate the potential of polyurethane-urea-coated 45S5 Bioglass® scaffolds for application in bone tissue engineering, the compressive strength (σ) and the work of fracture of the scaffolds were determined.
The compressive stress-strain curves for the different tested scaffolds are shown in Fig. 4.25.

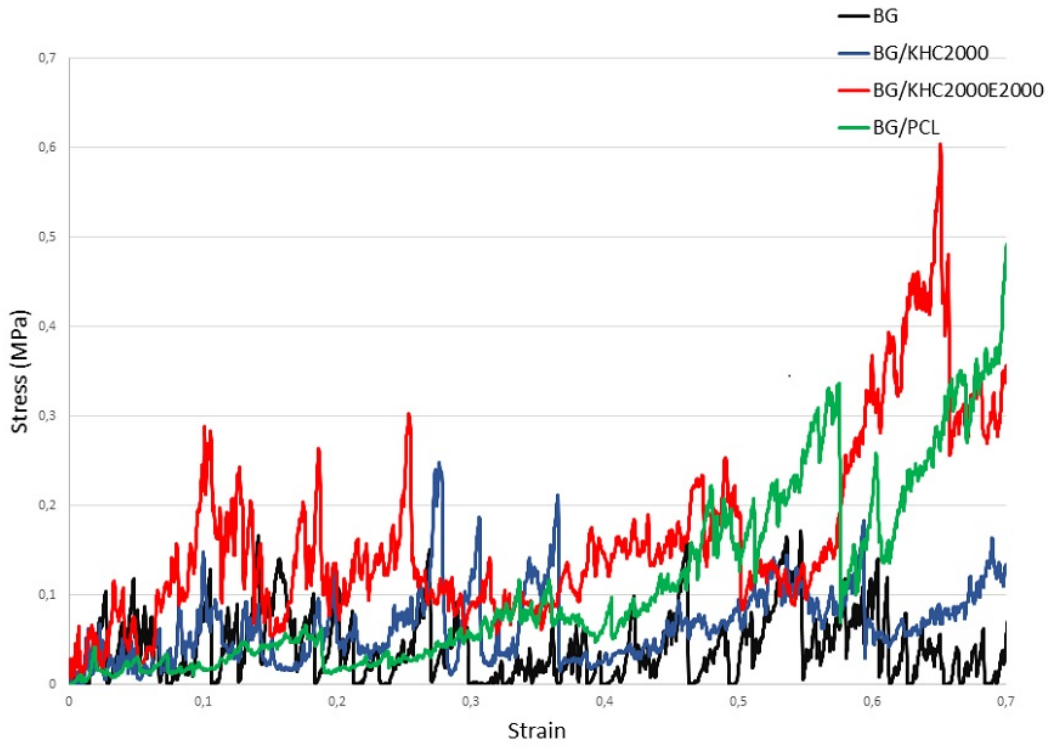

Figure 4.25: *Stress-strain curves of coated and uncoated scaffolds*

Due to the hollow nature of the struts and the presence of microcracks on the surfaces, under compression all the samples exhibited the typical jagged curve characteristic for BG scaffolds, obtained with the foam replication technique [82]. Moreover, while BG scaffolds showed a catastrophic failure, in the coated scaffolds densification occurred at strain around 60% which induced a quick increase in strength. But, it has to be pointed out that it is not the real maximum compressive strength, since the structures had different porosity grade (very low) with respect to the original shape. Therefore, coated scaffolds showed a completely different shape after compression; in fact, meanwhile the pure Bioglass® scaffolds appeared completely destroyed due to their very brittle nature, the polymeric coating allowed the maintenance of

the integrity of the shape, as showed in Fig. 4.26

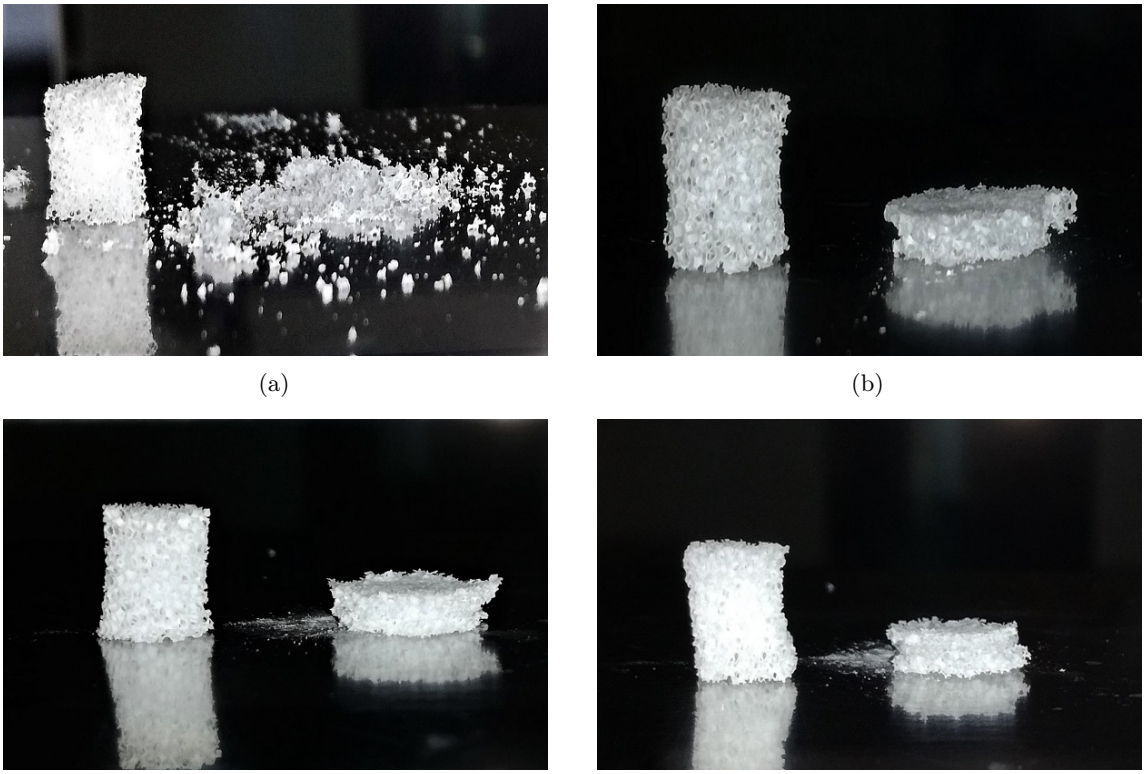

(a) (b)

(c) (d)

Figure 4.26: Images of a) 45S5 BG scaffold, b) KHC2000/BG, c) KHC2000E2000/BG and d) PCL/BG before and after compression

The compressive strength and the work of fracture were measured in dry e wet conditions to better simulate the *in-vivo* environment; the obtained values are presented in Fig. 4.27.

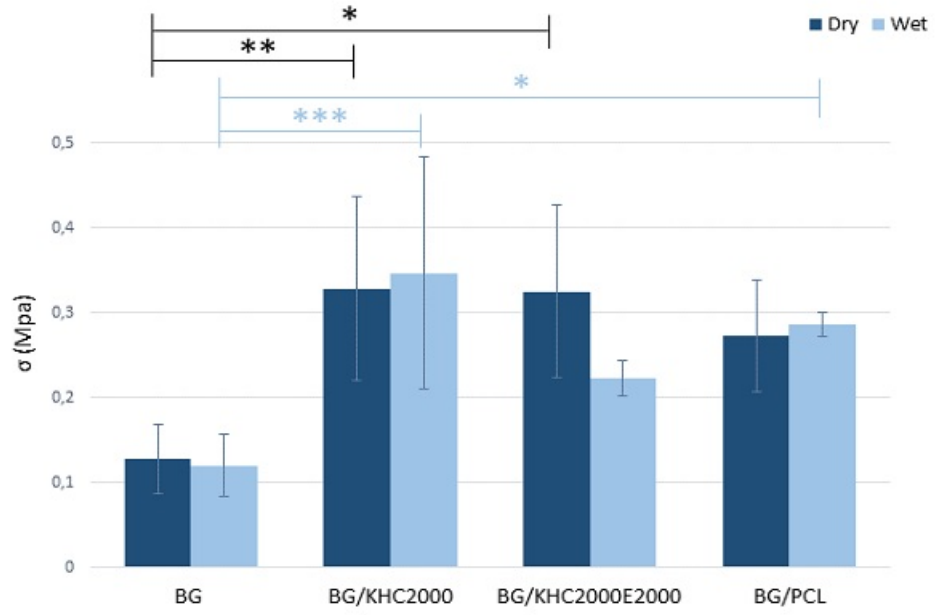

(a)

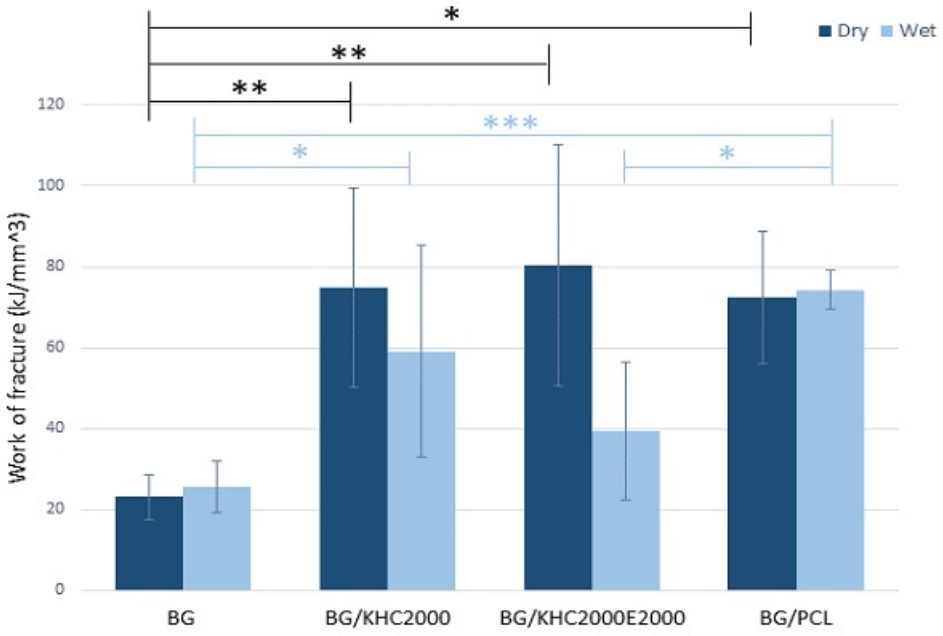

(b)

Figure 4.27: *Mean values and standard deviation of a) compressive strength and b) work of fracture of the different type of scaffolds. Asterisks denote significant differences, * $p<0.05$, ** $p<0.01$ and *** $p<0.001$ (Bonferroni's post-hoc test)*

The compressive strength of BG scaffolds was significantly increased by coating them with the investigated polyurethanes. Since the overall porosity of the samples is not considerably decreased after the coating (from 92.1% to around 91%) this improvement can be ascribed to the polyurethane layer and not to the presence of clogged pores. Moreover,although coating

polymer content was lower in KHC2000/BG scaffolds with respect to KHC2000E2000/BG samples, a higher value of significance compared to bare BG scaffolds was obtained incase of KHC2000-coated scaffolds. This could be due to the intrinsic higher mechanical properties of KHC2000 (stress at break of 20.30 ± 3.13 MPa and 11.96 ± 0.70 MPa for KHC2000 and KHC2000E2000, respectively) [87]. Also the work of fracture was considerably increased with the polymeric coatings.

It has been speculated in several works that the improvement of mechanical properties in coated Bioglass® scaffolds is due to the fact that the polymer fills micropores and microcracks on the surface[88]. Furthermore, the strengthening and toughening effects exhibited by coated scaffolds could be explained by a mechanism of crack-bridging at the microscale [126, 87], typical of the fracture behaviour of human bones to a certain extent.

The values of compressive strength, lie closer to the lower extreme of the compressive strength of spongy bone (0.2 - 4 MPa), in accordance with results reported in the literature for similar constructs [82, 70, 88]. This is not a great disadvantage because it has been speculated, that it is not mandatory to produce a scaffold with the exact properties of the native bone, since the growing of hydroxyapatite and the formation of new tissue increase the mechanical properties of the scaffolds [82]. In particular, Chen et al. [117] reported that cell-cultured scaffolds for 6 days retain better the mechanical properties with respect to the scaffolds after immersion in SBF. This behaviour is probably due to cell adhesion and proliferation, as well as to the progressive deposition of collagen that fill the microcracks. However, a sufficient mechanical strength is required to allow the adequate manipulation of scaffolds for tissue engineering applications.

Testing the scaffolds in wet conditions (30 minutes immersion in PBS before the test) did nothighlight significant changes in scaffold behavior with the exception of KHC2000E2000 coated scaffolds, probably due to the presence of PEG and its natural instability in aqueous environment.

Mechanical tests were performed on all the samples after 3, 7, 14 and 21 days of immersion in SBF, in order to assess their behaviour after the partial degradation and the modifications that occur with the deposition of HA.

The stress-strain curves of the tested samples after 21 days in SBF are collected in Fig. 4.28.

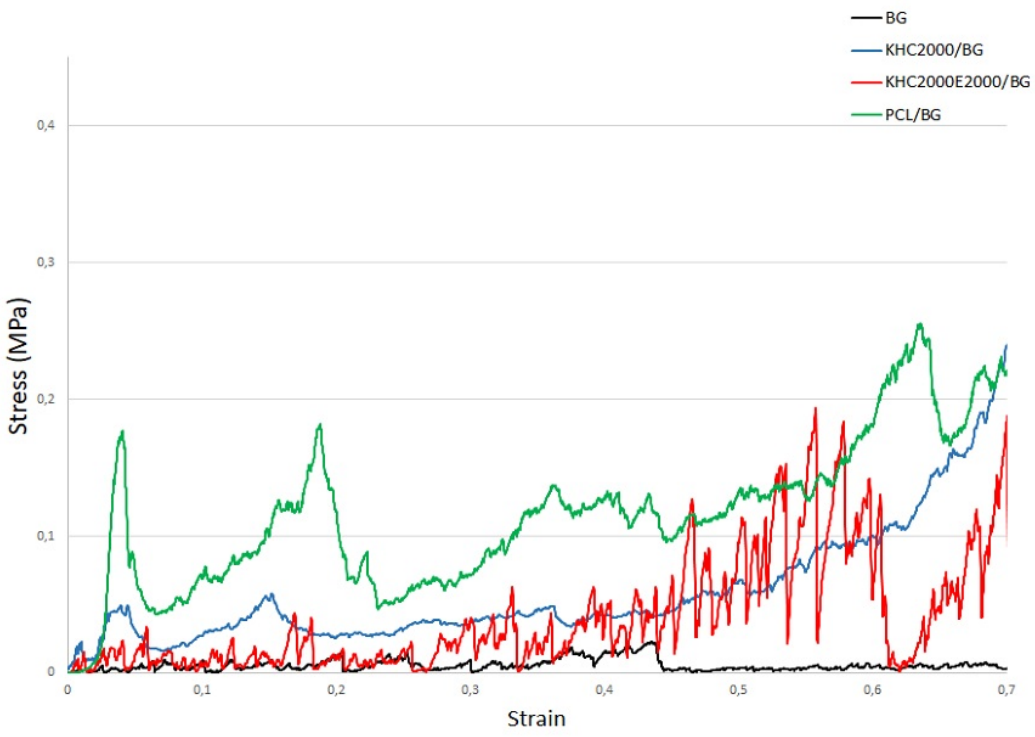

Figure 4.28: *Stress-strain curves of coated and uncoated scaffolds after 21 days in SBF*

All the samples showed the typical jagged curves as described before; however densification phenomena in composite samples occurred earlier, especially for PCL coated scaffolds. In fact, the fast increase of the stress was registered at a strain in the range 20%-30% for PCL/BG composites and 50%-60% for polyurethane/BG scaffolds.
For a better comparison, Fig. 4.29 shows the compressive stress and the work of fracture of the all types of scaffolds analysed after 21 days of immersion in SBF.

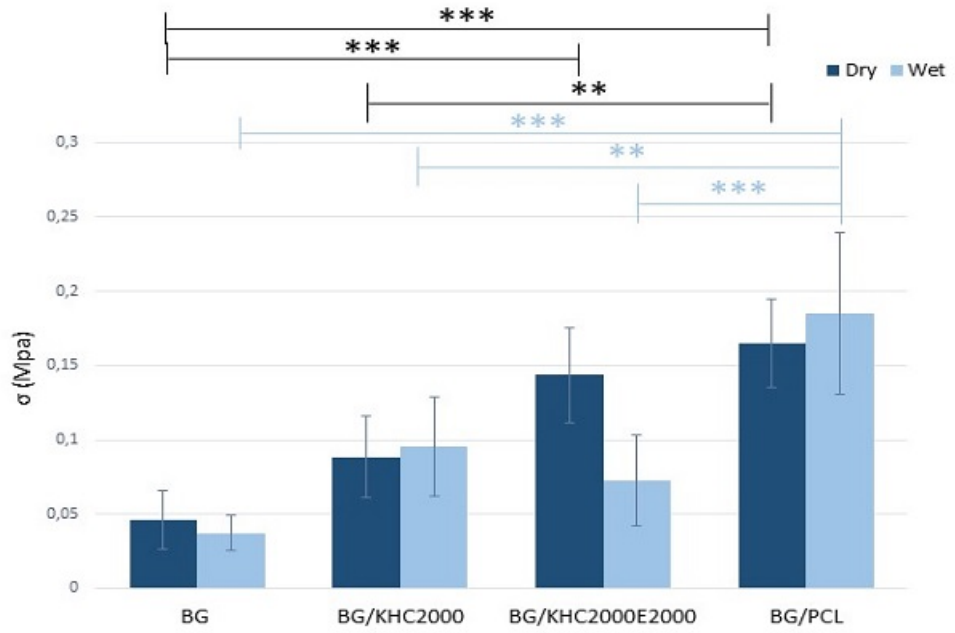

(a)

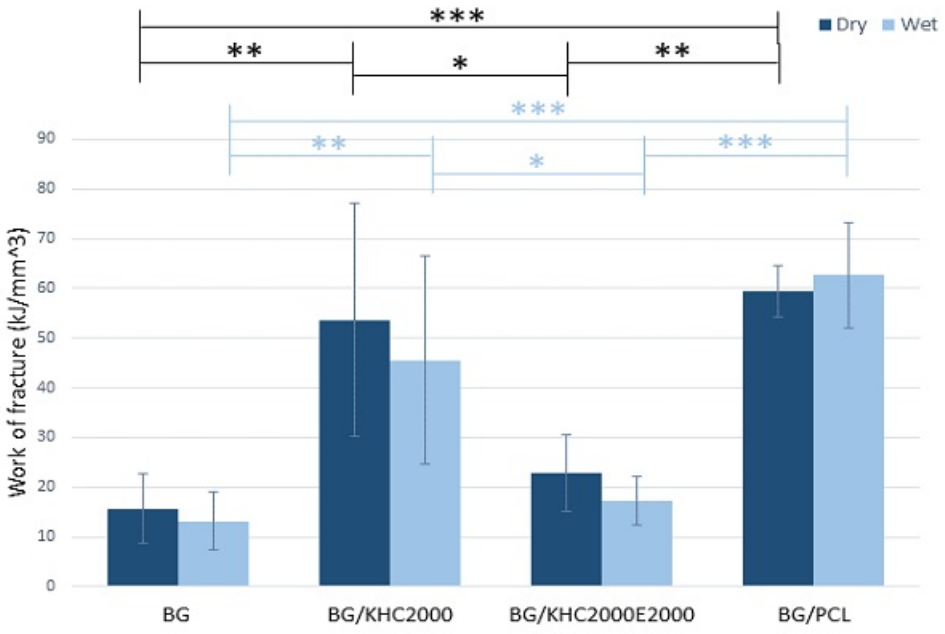

(b)

Figure 4.29: *Mean values and standard deviation of a) compressive strength and b) work of fracture of the different type of scaffolds after 21 days immersion in SBF. Asterisks denote significant differences, * $p<0.05$, ** $p<0.01$ and *** $p<0.001$ (Bonferroni's post-hoc test)*

As expected, after immersion in Simulated Body Fluid both the compressive strength and work of fracture of the samples decreased due to the dissolution of the crystalline phase and its conversion to amorphous calcium phosphate [88]. Although crystalline hydroxyapatite was formed on the Bioglass® surface , as assessed by XRD and SEM, it was still not enough to

ensure the maintenance of the started mechanical properties.
Moreover, composite scaffolds showed significant higher mechanical properties with respect to the uncoated ones, meaning that the polymeric coating not only induces an increase in the starting compressive strength but it also slows down the rate of compressive strength decrease during the immersion in SBF.
Compressive strength was plotted against time in order to investigate more accurately the variation of mechanical properties by soaking the scaffolds in SBF (Fig. 4.30).

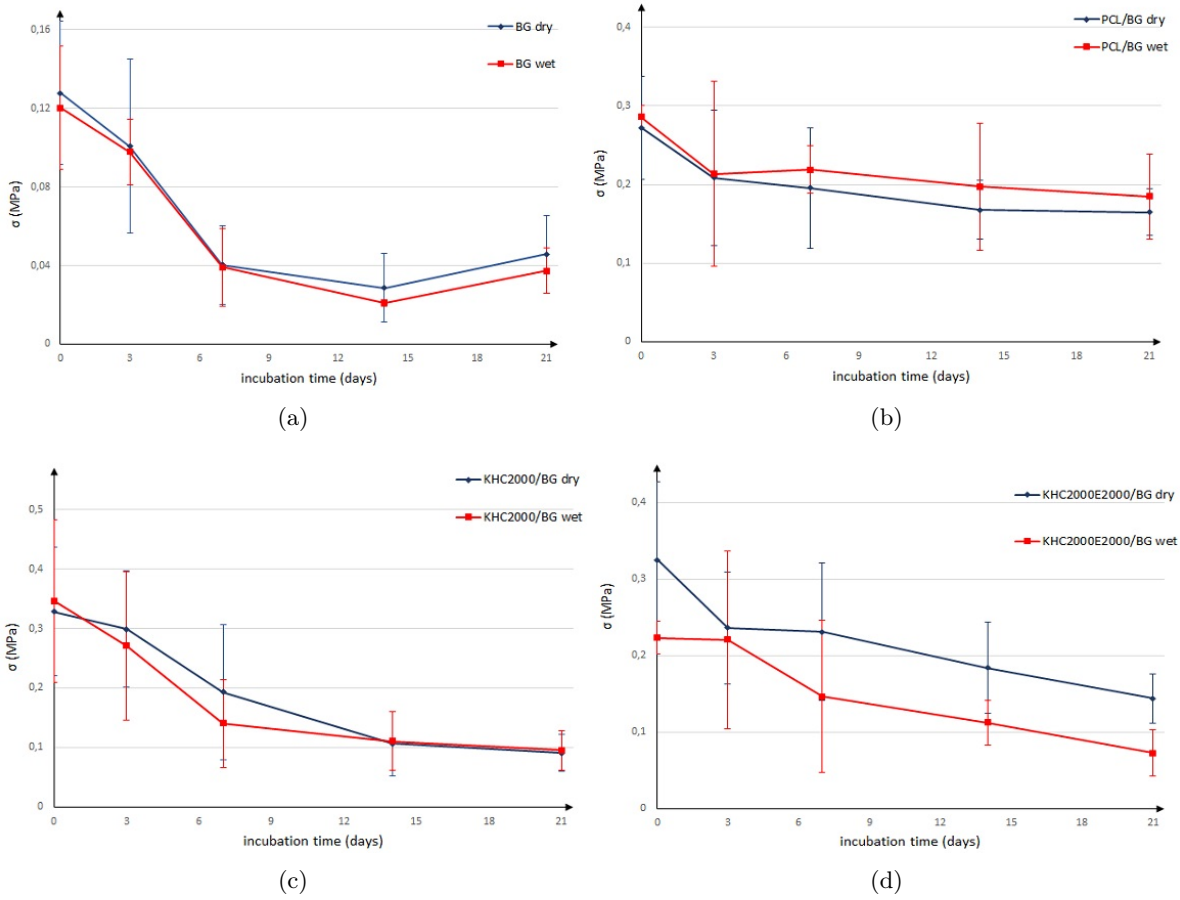

Figure 4.30: compressive strength of a) 45S5 BG b) PCL/BG c) KHC2000/BG and d) KHC2000E2000/BG scaffolds after immersion in SBF

As mentioned before the compressive strength decreased during the immersion in SBF due to the progressive dissolution of combeite, that is the main crystalline phase present after the sintering of 45S5 Bioglass® [88].
Also in this case the values calculated after wet condition tests showed the same trend to the dried samples and the values in the two different conditions are quite similar at each time point, with the exception of KHC2000E2000. In fact, the presence of PEG provides instability in aqueous environment, the curve for KHC2000E2000/BG evaluated in wet conditions showed almost the same trend as observed in dry conditions, but it was shifted to lower values.
For a better comparison and understanding of the variation in mechanical properties of the

different tested samples, the change in compressive strength was calculated as a function of incubation time in SBF according to the following equation: (Fig. 4.31)

$$\%\sigma_{\text{remaining}} = \frac{\sigma_t}{\sigma_0} \cdot 100 \tag{4.6}$$

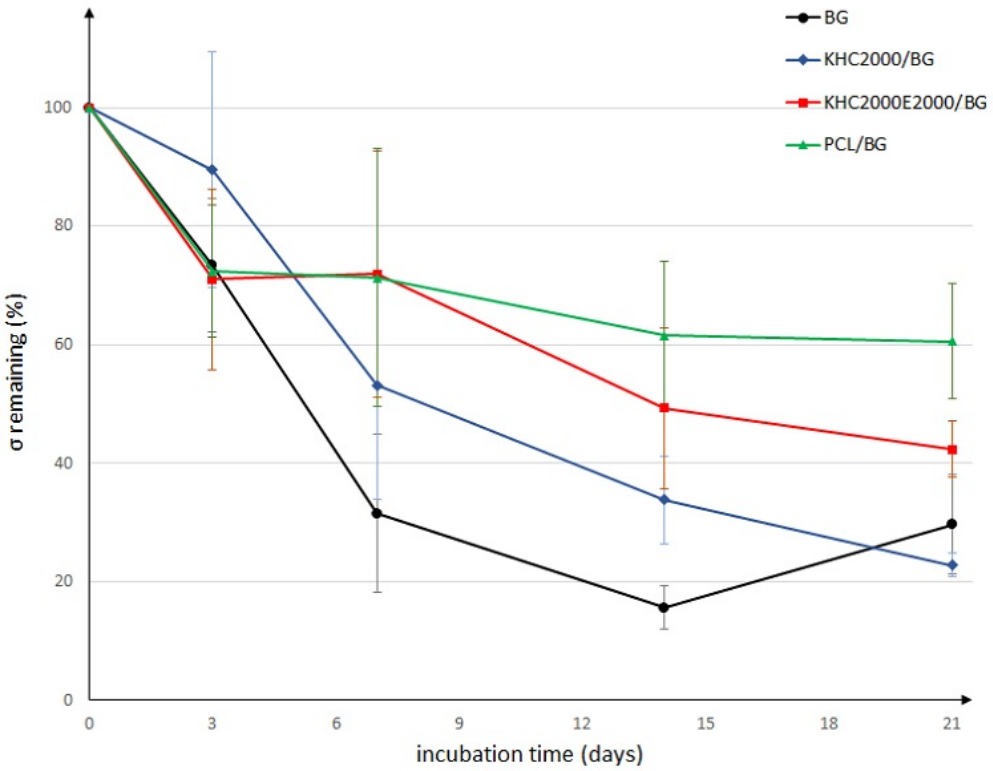

Figure 4.31: *Percentage of compressive strngth remaining after immersion in SBF*

The compressive strength of uncoated scaffolds decreased drastically in the first 7 days of immersion, with a decrease in compressive strength of approax. 70%. After that the deterioration rate became much slower and inverted its trend compared to the other samples,probably as a consequence of the progressive crystallization of the hydroxyapatite layer that started on the dissolution of the main crystalline phase.
Furthermore, PCL coated scaffolds seemed to retain better the mechanical strength, and even after 21 days in SBF they lost only 40% of the initial value (0.16 ± 0.03 MPa). Similar behaviour was observed in a previous work [87] and it is probably due to the major presence of clogged pores and to the intrinsic higher mechanical properties of PCL with respect to the polyurethanes.
KHC2000/BG scaffolds initially showed the lowest decrease of compressive strength compared to the other samples (compressive strength was 0.30 ± 0.09 MPa, almost 90% of the initial value) thank to its slower degradation (as reported in next section). However, starting from 1 week incubation in SBF, KHC2000/BG scaffolds started to behave similarly to the other

investigated samples.
KHC2000E20000/BG scaffolds showed a decreasing of the mechanical strength comparable to PCL coated scaffolds.
Summarizing, coated scaffolds showed well-maintained mechanical properties thanks to the slower rate of dissolution of the crystalline phase, as demonstrated in previous section through XRD analysis, nevertheless for all the three coated samples the compressive strength after 21 days in SBF was found to be within 0.09 – 0.16 MPa which was in the same range of the compressive strength of as-sintered scaffolds without immersion in SBF [88].

4.2.5 Degradation Tests

One of the required features for an ideal scaffold is to match the degradation kinetics of the host tissue in order to provide a temporarily support during tissue repair. In bone tissue engineering the scaffold should degrade in three-six months, depending on the anatomic site and mechanical load [118]. Thus, it is extremely important to understand the degradation behaviour of the coated scaffolds.
Degradation tests were carried out soaking the samples in PBS for 1, 3, 7, 14 and 21 days, percentage of weight loss and pH at each time point were measured.

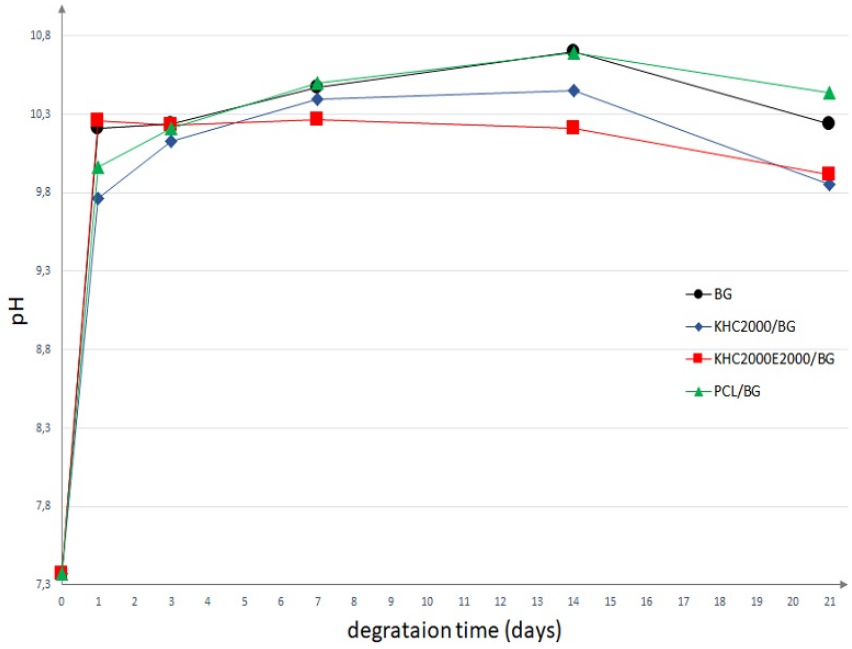

Figure 4.32: *pH variation of pure BG, PCL/BG, KHC2000/BG, KHC2000E2000/BG scaffolds during hydrolytic degradation in PBS*

Concerning the pH, showed in Fig. 4.32 , it is possible to notice the fast increasing after only 1 day, when the measured values for all type of scaffolds were in the range 9.7 – 10.2, due to the well-known burst release of 45S5 Bioglass®.

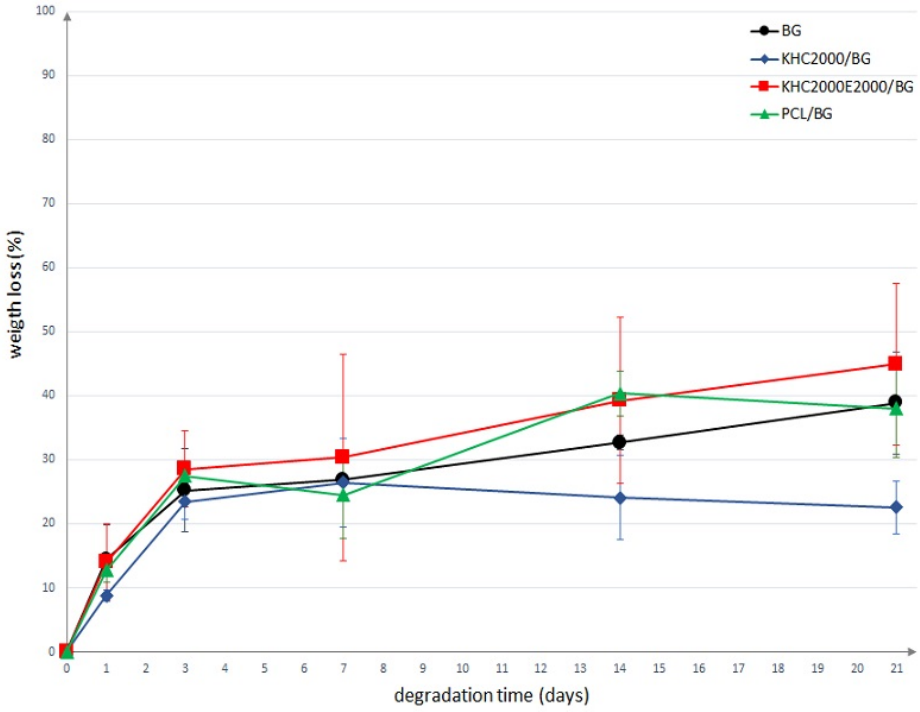

Figure 4.33: *Weight loss profile of pure BG, PCL/BG, KHC2000/BG, KHC2000E2000/BG scaffolds during hydrolytic degradation in PBS*

Pure BG scaffolds showed a gradually increasing of weight loss as well as of the pH, and after 21 days of immersion in PBS they presented a weight loss of 38.86 ± 8.02% and pH of 10.24 ± 0.14. As reported extensively in literature the mechanism of degradation in Bioglass® scaffolds is the dissolution of the main crystalline phase and its transformation into an amorphous calcium-phosphate layer [119]. This dissolution is dependent on many factors, such us composition, chemical and morphological characteristics of the surface, composition of the solution in which the scaffold is immersed, and crystallinity [120].

As already proved in previous work [101], PCL coated scaffolds presented almost the same behaviour, with some little fluctuation, of uncoated samples, probably due to the not homogeneous coating that leaves exposed the Bioglass® struts. Thus, coating with PCL do not lead a controlled degradation kinetics of degradation.

On the contrary, KHC2000/BG scaffolds exhibited different and in somewhat improved behaviour compared to the Bioglasss® dissolution. This phenomenon is due to the aforementioned high stability of KHC2000 films in aqueous environment, that do not affect so much the weight loss and the number molecular weight of the starting polymeric films. While in the early days of degradation until day 7, KHC2000/BG and pure BG scaffolds had the same degradation rate, after 14 days of immersion the coated samples seem much stronger against degradation. Indeed, at the end of the test KHC2000/BG presented the lower value of weight loss (22.54 ± 4.11%) as well as the pH (9.85 ± 0.16) with respect to uncoated scaffolds and to the other composites. KHC2000E2000 coated Bioglasss® scaffolds showed the higher percentage of weight loss (44.96 ± 12.64% after 21 days of immersion) as well as the higher variability, in particular the longer the

samples were soaked in PBS, the higher was the standard deviation. This behaviour, as found in previous work [87], is due to the intrinsic instability of the mixed polyurethanes. Because of the presence of PEG in fact, water-uptake tendency occurs, leading a high variability of the results. However, opposite tendency could be notice on the pH curves, where KHC2000E2000/BG showed the lower values specially after 14 day of immersion. Therefore, the interpretation of data is difficult due to the high variability. For this reason, an optimised procedure of drying could be useful to completely clarify the degradation process of KHC2000E2000.
Furthermore, the dissolution of pure BG leads the creation of a basic environment that could accelerate the degradation of PCL based polymers, as proved by Loh [107], who has found that in basic solution (pH=9.5) the PCL-PEG copolymer was degraded faster. He speculated that the basic pH enhances the cleavage of ester bond accelerating the degradation.
This could be a further reason to understand why the polymeric coating did not help to decrease the degradation rate of Bioglass®.
Furthermore, to investigate the variation of the morphology, SEM analysis were carried out on coated and uncoated scaffolds. The images of the samples after 21 days of immersion in PBS are collected in Fig. 4.34. It is possible to notice the cracks propagation on uncoated scaffolds, while coated scaffolds with KHC2000 and PCL allowed to avoid these phenomena. However, KHC2000E2000/BG exhibited several cracks into the surface due to its faster degradation and instability in aqueous solution.
Moreover, all the samples exhibited deposition of spherical particles. These salts were likely amorphous calcium phosphate, formed due to the interaction between the phosphate solution and the ions released from the glass-ceramic. Probably with longer time of immersion these particles could undergo transformation into crystalline hydroxyapatite, but as reported by Fu. et al. [121], the assessment of bioactivity in PBS required more time than SBF. In fact, they investigated the bioactivity of the glass 13-93, that is a glass ceramic similar to 45S5 Bioglass®, but with higher content of SiO_2. They reported that immersing the scaffold in PBS, spherical particles were visible only after 6 weeks, while in previous study [122] they found deposition of crystalline hydroxyapatite into the 13-93- based scaffolds even after 7 days in SBF.

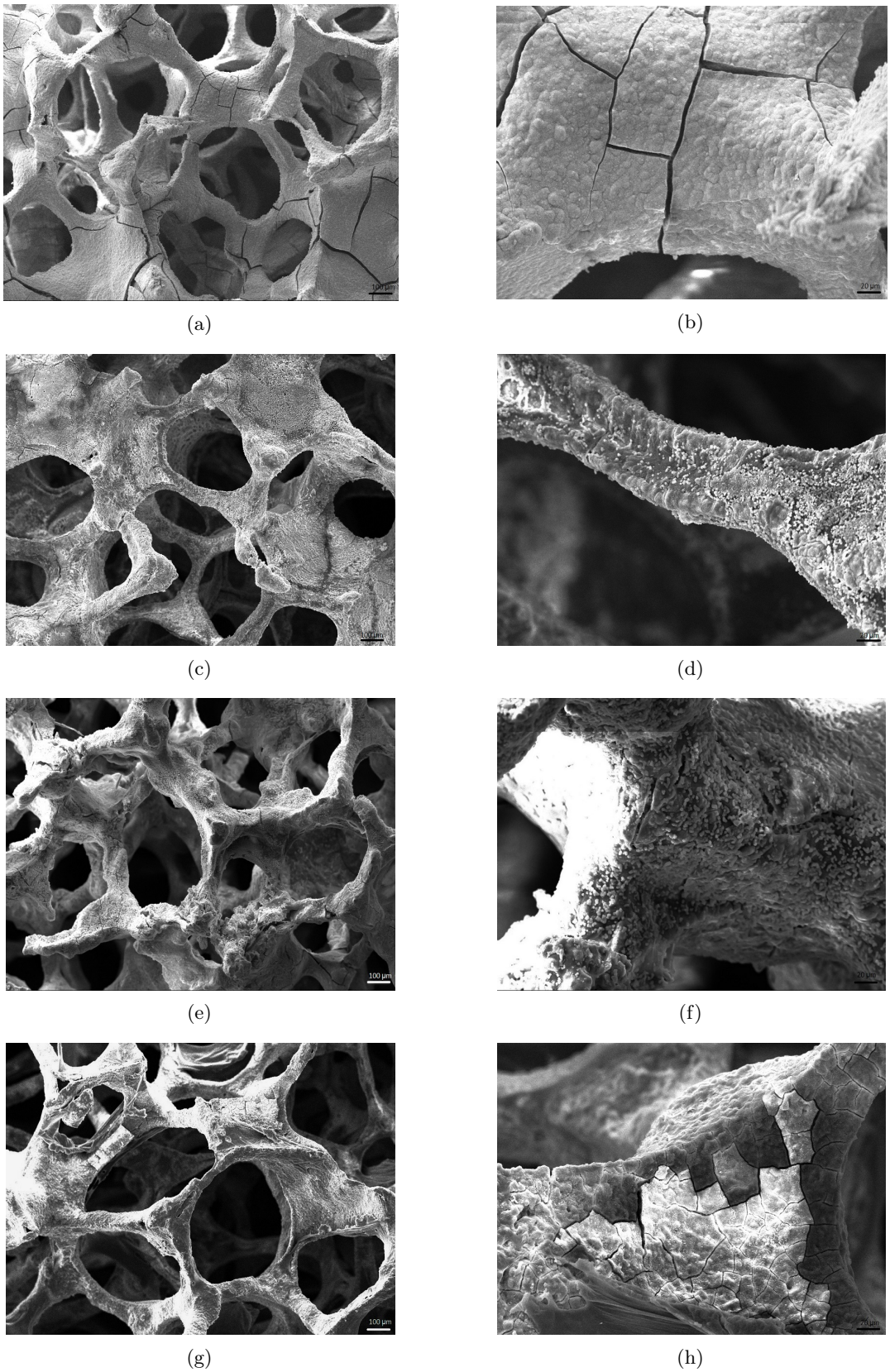

Figure 4.34: SEM micrographs of a) - b) BG, c) - d) PCL/BG, e) - f) KHC2000/BG anf g) - h) KHC2000E2000/BG scaffolds after 21 days immersion in PBS

In conclusion, PCL/BG showed the same degradation rate of pure Bioglass® scaffold due to the not homogeneous coating and to the higher presence of hydrolysable groups that can be faster degraded in the presence of basic pH.
On the contrary, the more homogenous coating and its higher stability in acqueous envirmnemnt shall ensure that KHC2000 coating provide an improvement of the degradation rate, especially for long time period.
Instead it is not possible drawing conclusion about the degradation behaviour of KHC2000E2000 coated scaffolds due to the high variability, because of the many concomitantly phenomena: dissolution of crystalline phase of Bioglass®, accelerated degradation and subsequent dissolution of the polymer in basic conditions.
However, it has to be pointed out that *in-vitro* condition of the tested scaffolds are extremely more aggressive than in body environment, where the continuous blood flow ensures the maintenance of physiological pH. Thus, further degradation studies on the coated scaffolds are required to better understand their degradation behaviour, using dynamic conditions in a bioreactor or, at least, static-dynamic conditions changing the PBS solution more frequently.

4.2.6 Biological Tests

MG-63 osteoblast-like cells were seeded on BG, PCL/BG, KHC2000/BG and KHC2000E2000/BG and cultivated for 2 days to conduct a primary investigation of the cytocompatibility of synthesized polyurethanes and their potential application for BTE.
As mentioned before, due to the burst release of 45S5 Bioglass®, before to apply cell tests it is necessary some form of preconditioning to stabilize the pH at more suitable value for cells. This solution creates a good environment for cells, but on the other hand, it is a great limit for static cultivation *in-vitro*, since the scaffold starts changing due to the dissolution of the glass in medium during the preconditioning period. A more realistic test would be with shorter preconditioning times considering that in a real application this is not performed. Anyways in *in-vivo* tests the system is dynamic and this pH change might not affect too much the surrounding cells. Therefore, in *in-vitro* tests cells are under more extreme conditions even though more parameters could be controlled compared to the *in-vivo*.
However, the polymeric coatings applied did not act as a barrier against this burst release, as is possible to notice in Fig. 4.35, where is presented how the pH was changing during the preconditioning period. No significant differences with respect the pure Bioglass were observed. Thus, the idea to use a shorter precondition it is not applicable in this work, since after only one day the pH value for all the sample was near 8.5, that is unsuitable to perform cell culture.

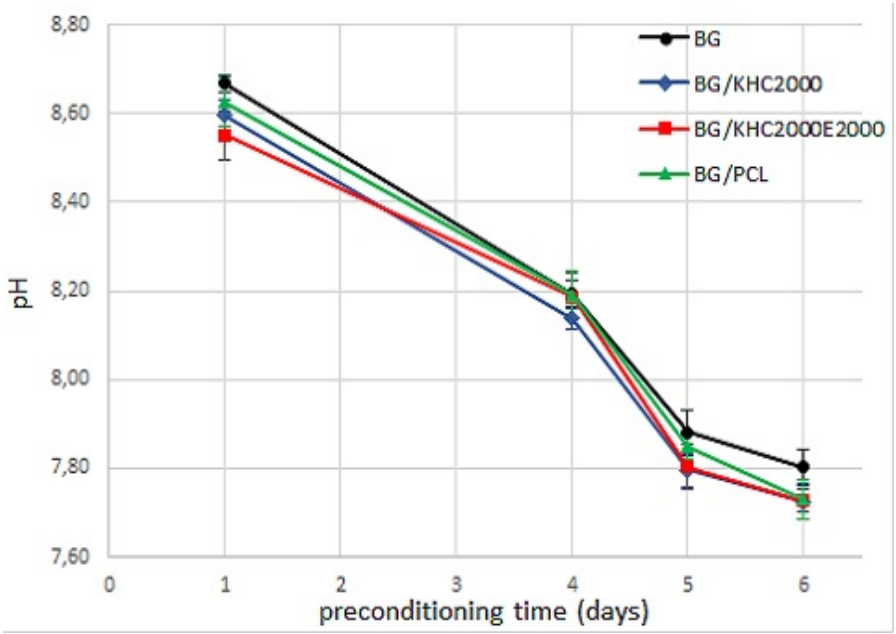

Figure 4.35: *pH change in uncolorless DMEM of coated an uncoated scaffolds during preconditioning period*

Cell viability was investigated through WST-8 assay, by which is obtained a quantitative analysis of mitochondrial activity of the alive cells seeded into the scaffolds.
Fig 4.36 shows the cell viability after two days of incubation. Pure BG scaffolds were considered as control since large documentations have been reported in the literature about their ability to

enhance adhesion, growth and differentiation of osteoblasts [123].

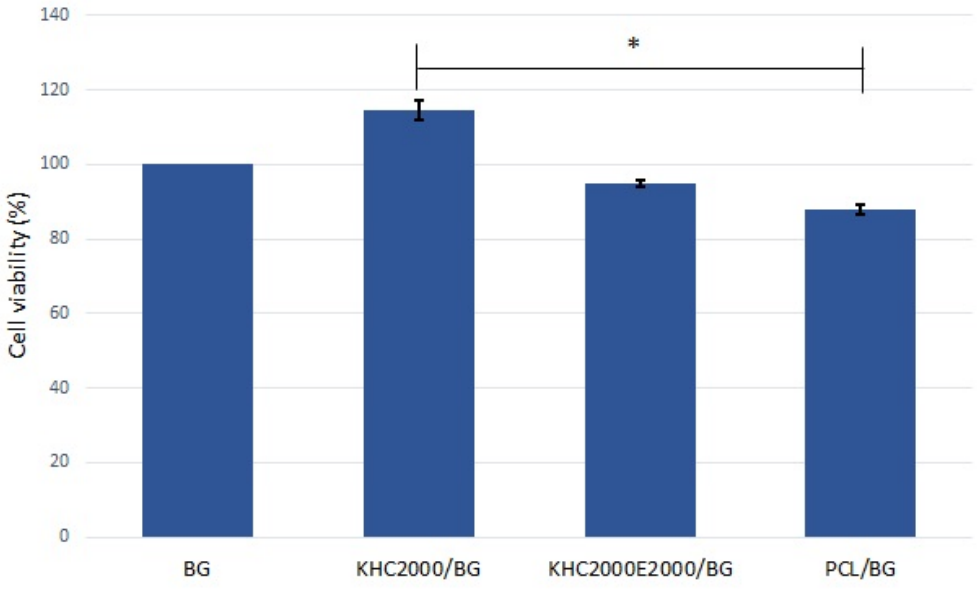

Figure 4.36: *Evaluation of cells viability of MG-63 on the samples: the values obtained on the composites are expressed as percentage with respect to pure BG scaffolds. Asterisks denote significant differences, *p<0.05, **p<0.01 and ***p<0.001 (Bonferroni's post-hoc test)*

All the composites result to be cytocompatible, indeed no significant differences in cell viability were found between coated and uncoated scaffolds. However, the relative mitochondrial activity of cells seeded into the KHC2000 coated BG scaffolds results significantly ($p>0.05$) higher than the PCL composite scaffolds, proving an improvement, through multi-block structure, of the properties derived from the commercial poly(ε-caprolactone).

In order to better investigate the cell viability and the morphology of the cells on the cultivated scaffolds, fluorescence analysis were carried out. In Fig. 4.37 are reported the fluorescence images of the scaffolds. Cytoskeleton was fixed using Phalloidin staining, thus it appear coloured in red, meanwhile the nuclei were stained through DAPI, that confer blue colour. However, at lower magnifications the two structure are not well defined. Nevertheless, the images reveal the high presence of attached cells after only two days of incubation. Moreover, all the scaffolds were highly colonized by cells even into the inner part, thanks to the high porous and interconnected structure [117]. It is important to notice that, despite the high number of cells added during the seeding, most of them are lost on the bottom of the well plate due to the high porous structure.

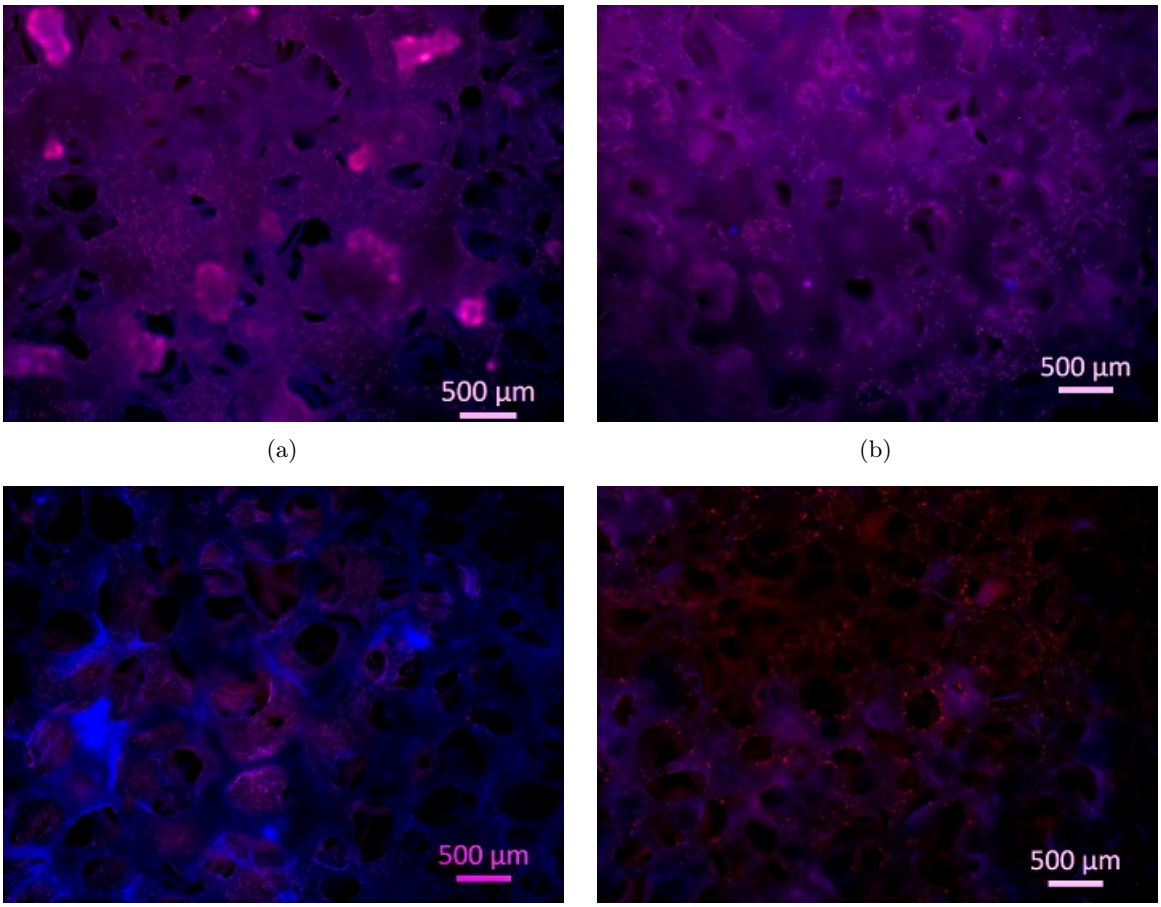

(a) (b)

(c) (d)

Figure 4.37: Fluorescent images of a) BG b) PCL/BG c) KHC2000/BG and d) KHC2000E2000/BG scaffolds at 2.5X

At bigger magnification (Fig. 4.38) it is possible to observe the cells morphology and their good spreading on the surface, meaning that they feel comfortable on the substrate. Furthermore, the shape of cells on the scaffolds is quite similar to those cells cultivated in the 2D well plate, showed in Fig. 4.39, where the cells are in the best environment possible during *in-vitro* tests. However, a further investigation through SEM images is necessary to confirm this hypothesis.

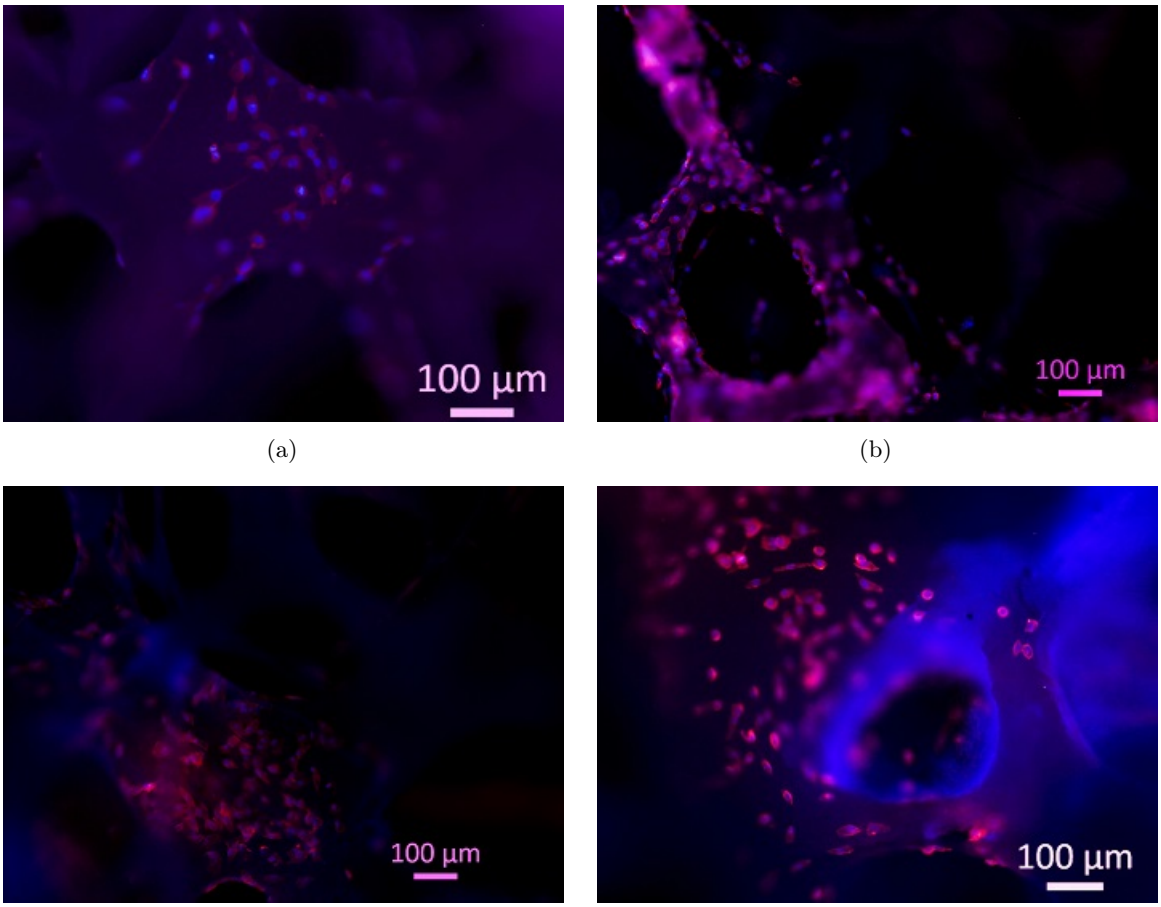

(a) (b)

(c) (d)

Figure 4.38: Fluorescent images of a) BG b) PCL/BG c) KHC2000/BG and d) KHC2000E2000/BG scaffolds at bigger magnifications 10X

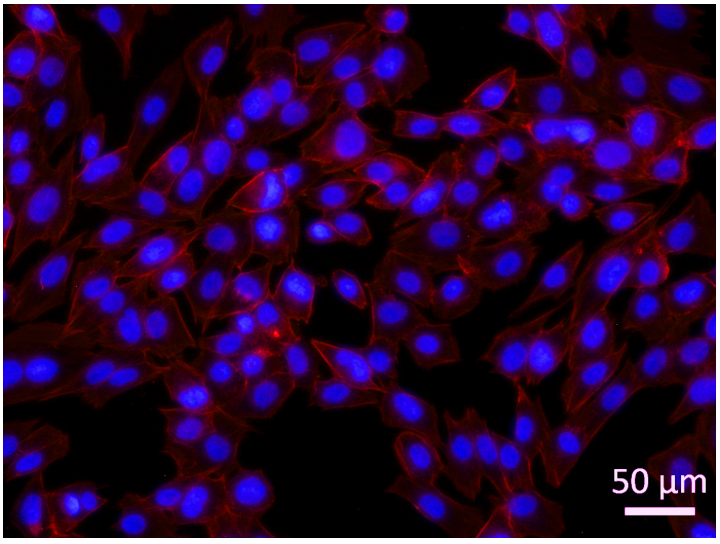

Figure 4.39: *Fluorescent images of MG-63 on the 2D control*

As discussed before, the protocol normally used to fix cells before SEM analysis provide to immerse the sample in an ethanol series to achive good images resolution. However, this series could be too aggressive for the synthesized PU. For this reason, two samples coated with polyurethanes were immersed in 100% ethanol for 4 hours. After drying, the samples were observed through SEM and the images are reported in Fig. 4.40.

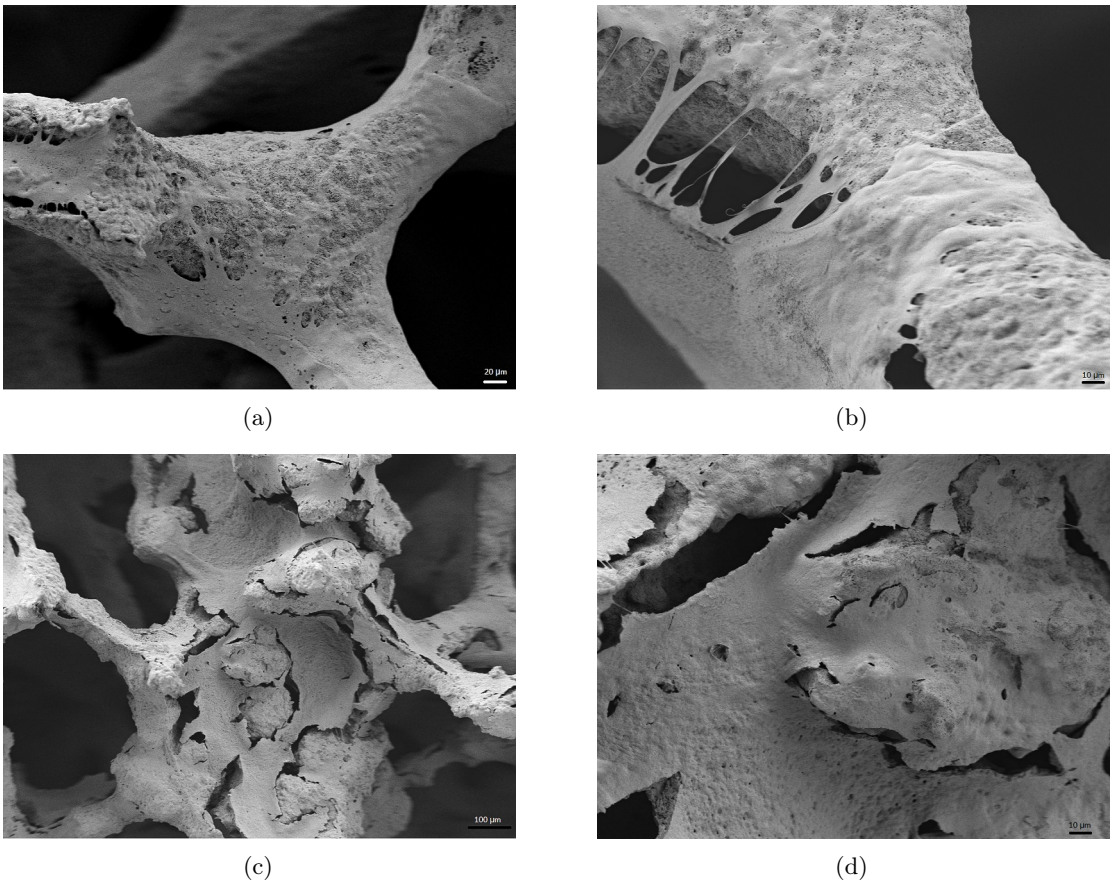

(a) (b)

(c) (d)

Figure 4.40: SEM images of a) - b)KHC2000/BG and c) - d) KHC2000E2000/BG scaffolds after 4 hours immersion in ethanol

As expected, the coating is extremely degraded after soaking in ethanol, especially the coating containing PEG results detached, making impossible to analyse the cells. Therefore, to avoid these damages to scaffolds and cells, the samples were prepared soaking only for ten minutes, instead of 30, in each solution of the ethanol series. Moreover, also the step in the critical point dryer was eliminated and the samples were dryed under the fume hood overnight.
It was impossible to asses the cell morphology by SEM analysis because all the cells were completely detached after the SEM preparation. Thus, an optimization of this preparation process is necessary to investigate cells, without destroyed the polymeric coatings.

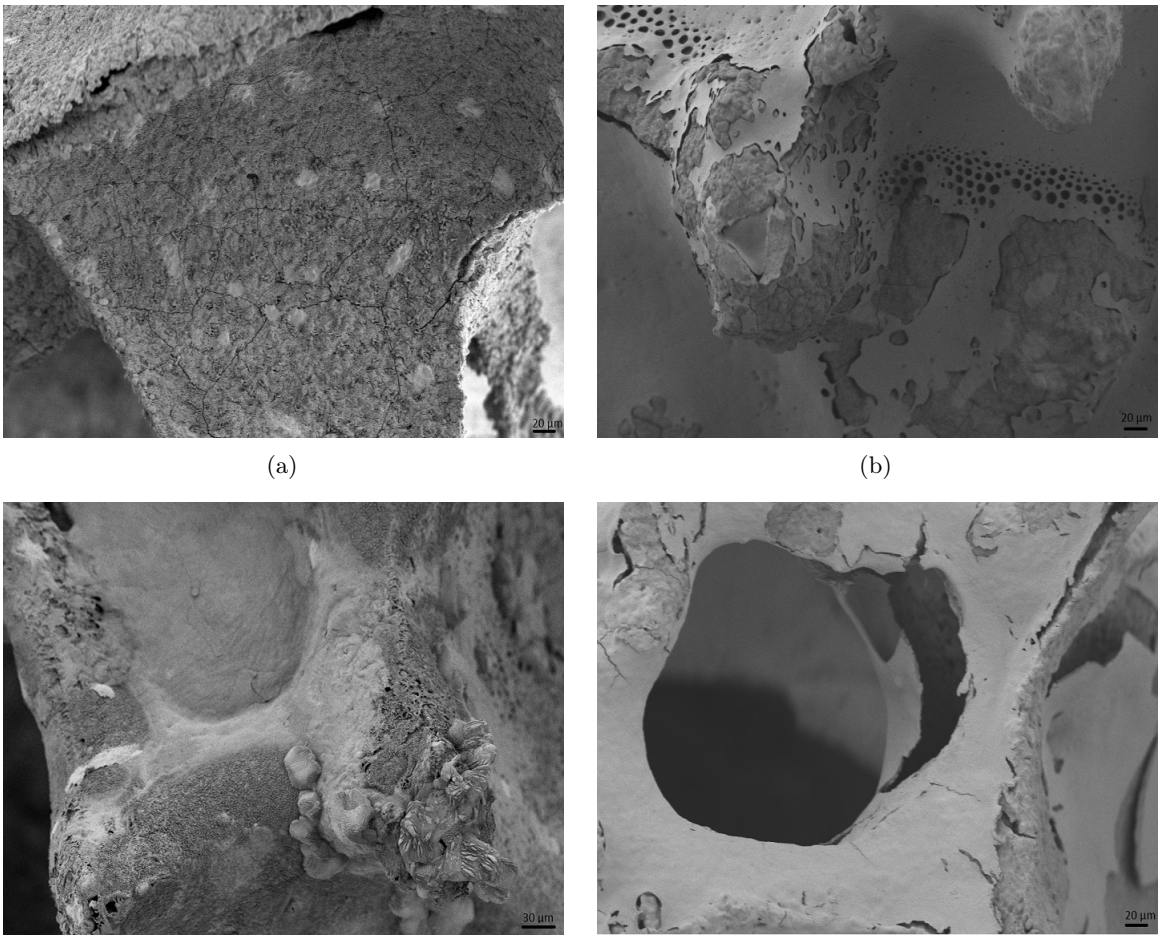

(a) (b)

(c) (d)

Figure 4.41: SEM images of a) BG b) PCL/BG c) KHC2000/BG and d) KHC2000E2000/BG scaffolds after 2 days of cell culture

In summary, it can be concluded that the coating layer did not influence the good biocompatibility of the parent 45S5 Bioglass® scaffolds that is well known to promote the adhesion ad proliferation of osteoblasts [124]. However, it has been pointed out that the presented results offer only a basic investigation of the interaction between cells and materials. To get a complete knowledge about the *in-vitro* behaviour of the polyurethanes, more cell biology studies are required. Different assays can be used, such as life-dead staining, enzyme-linked immunosorbent assay (ELISA) to assess the relative cells proliferation or ALP activity to investigate the osteogenic differentiation. Nevertheless a longer period cells cultivation should be performed using more specific cells to understand how the coating affect the bone formation [125].

5 . Conclusion and future works

The goal of this thesis was the improvement of the characteristic poor mechanical propertiesof 45S5 Bioglass® glass-ceramic scaffolds by coating them with two novel custom-made poly(urethane-urea)s. In addition, the polymeric coating is expected not to inhibit the typical good bioactive behavior of 45S5 Bioglass scaffolds.

The polyurethanes were synthesized following a two steps procedure to ensure better control on the molecular weight and mechanical properties [78]. 1,6-hexamethylene diisocyanate and L-lysine ethyl ester were selected as diisocyanate and chain extender, respectively, to form the hard segment of the typical multiblock structure of PU. The two polyurethanes only differed for their soft segments, KHC2000 contained PCL (M_n=2000 g/mol) as macrodiol, while KHC2000E2000 had a mixture of PCL and PEG (M_n=2000 g/mol) in 70/30 weight ratio. The addition of PEG as soft segment enhanced wettability and degradation/dissolution kinetics of PCL-based polyurethanes, and this composition was selected in a previous work [87] to ensure also adequate stability in aqueous environment.

The successfully synthesis of KHC2000 and KHC2000E2000 was demonstrated through ATR-FT-IR, presented all the peaks characteristics of urethane-urea groups.

Both polyurethanes presented a number molecular weight in the range 48000-70000 g/mol with relative low polydispersity index that proves a good polymerization with a well distributed molecular weight.

Detailed investigation of the hydrolytic and enzymatic degradation behaviour was carried out on both polyurethanes films and compared to commercial PCL homopolymer (80000 g/mol). After 1, 3, 5, 7, 14 and 21 days of immersion in the degradation medium, the samples were washed, dried and the percentage of weight loss was calculated. Moreover, SEC and SEM analysis were carried out on the residual polymeric films. PCL exhibited almost no degradation when soaked in PBS. On the contrary, enzymatic degradation, tested in PBS containing an excess of Lipase from Pseudomonas cepacia, drastically affected PCL films, with a weight loss of 95.06 ±0.06 % after 7 days incubation in the degradation medium and the films were completely dissolved after 21 days.

KHC2000 presented the higher stability in both enzymatic and hydrolytic degradation. The analysis of the RID signal showed that during immersion in PBS only shorter chains became soluble and were dissolved in the solution, thus leading to narrower RID curves.

KHC2000E2000 presented the more complex behaviour. During hydrolytic degradation, other

than very slow hydrolysis of ester groups, PEG promotes the penetration of water that can enhance the possibility to solubilise ester and urethane groups. However, the more evident variation was observed during enzymatic degradation especially on the RID profile. In fact, after 7 days of enzymatic degradation multimodal distributions were obtained, meaning that other than the prevalent presence of long molecular chains, also new species with lower molecular weight were formed during the degradation [105]. This drastic change is probably due to the complex degradation mechanism of KHC2000E2000which is characterized by concomitant degradation phenomena occuring at both the ester and ether bonds.

45S5 Bioglass® scaffolds were fabricated by foam replication method [82] that allows the fabrication of highly porous scaffolds (92.1 ± 1.6%) with well interconnected structure and pore size in the range 200 – 500 µm, suitable for bone tissue engineering applications.

Composites scaffolds were produced through dip coating procedure, by dipping the as-sintered scaffolds in a polymeric solution prepared in chloroform.

For comparative purposes BG scaffolds were also coated with commercial poly(ε-caprolactone), performing dip coating for 2.5 minutes in a polymeric solution at 1%w/v [86]. SEM images showed that PCL led to a non-homogenous coating and the resulting scaffolds presented some clogged pores and the porosity after the coating slightly decreased to 90.7 ± 1.6%.

KHC2000/BG scaffolds were produced by dipping the scaffolds in a solution at 0.5%w/v for 1 minute. On the contrary, coating the scaffolds with KHC2000 provided a more adherent and homogenous coating although the concentration and the consequent amount of polyurethane forming the coating was less than in PCL/BG-based scaffolds.

SEM analysis proved that KHC2000E2000/BG composites produced by dipping BG scaffolds in a solution of polymer in chloroform at 1% (w/v) for 1 minute exhibited a homogenous and adherent coating with a porosity of 91.7 ± 1.5%.

The in vitro bioactivity of the composites was investigated at different time points (1, 3, 7, 14 and 21 days) after immersion in SBF through SEM, FTIR and XRD. SEM images revealed the presence of the typical cauliflower structure of hydroxyapatite, while its deposition was slightly retarded in the coated scaffolds. However, after 21 days of immersion in SBF the surface of both coated and uncoated scaffolds was completely covered by HCA layer. Since the polymeric coating was not designed to be bioactive, the deposition of hydroxyapatite depended only of the glass. In particular, it has been speculated that the uncoated regions of the struts are responsible for the direct contact between the glass and SBF which is required to activate the mechanism of bioactivity [70]. FTIR analysis presented all the peaks related to the growing of hydroxyapatite layer, proving that coated scaffolds did not inhibit the deposition of HCA layer. Furthermore, XRD spectra after 21 days of immersion in SBF confirmed the presence of crystalline hydroxyapatite on both coated and uncoated scaffolds, as well as the dissolution of the main crystalline phase ($Na_2Ca_2Si_3O_9$) and its transformation into amorphous calcium phosphate [82].

To assess the improvement of mechanical reliability of Bioglass® scaffolds through the polymeric coating mechanical test were performed and the compressive strength and the work of fracture

were measured. All the samples showed the typical jagged curves due to the high porosity grade and to the hollow nature of the struts. However, while BG scaffolds appeared completely destroyed at the and of the test, coated samples underwent densification and maintained their shapes. Moreover, both polyurethanes significantly improved the compressive strength of BG scaffolds. Since the overall porosity of the foam is not considerably decreased after the coating (from 92.1% to around 91%) this improvement can be ascribed to the polyurethane and not to the presence of clogged pores. It was extensively reported in literature that the improvement of mechanical properties through polymeric coating is due to the fact that the polymer fills micropores and microcracks on the surface, thus it works as collagen in the bone [88, 70]. Furthermore, KHC2000 reported significantly higher compressive strength compared to the other composite scaffolds although the amount of KHC2000 forming the coating was much lower with respect to the other investigated samples. However, the obtained values are still in the lower boundary of the strength range of cancellous bone. The cause could be principally ascribed to the high porous structure and brittle nature of Bioglass® scaffolds.
Compressive strength and the work of fracture of coated and uncoated scaffolds were also measured after 3, 7, 14 and 21 days in SBF, to assess their behaviour after the partial degradation and the modifications that occur with the deposition of HA. As expected, compressive stress gradually decreased with increasing incubation time in SBF due to the preferential dissolution of the main crystalline phase that was replaced by the amorphous calcium phosphate layer. This amorphous layer is responsible of the bioactivity of the samples, but at the same time it causes theobserved decrease in mechanical properties. However, thanks to the presence of the polymeric coatings the mechanical properties deteriorated much slower compared to Bioglass® scaffolds. Nevertheless, for all the three coated samples the compressive strength after 21 days in SBF was found to be in the range 0.09 – 0.16 MPa which was in the same range of the compressive strength of as-sintered scaffolds without immersion in SBF.
Compressive tests were also carried out in wet conditions to better mimic the physiological environment; the samples showed the same trend observed by testing them in dy conditions and the values in two different conditions were quite similar at each time point, with the exception of KHC2000E2000, due to its instable nature in aqueous solutions.
It is possible to conclude that the polyurethane coating led to a significant improvement of the mechanical strength and toughness of the Bioglass® scaffolds, with a good maintenance of the strength even after several days of immersion in SBF. However, the data showed high variability due to the high porous structure and the small number of tested samples, thus mechanical test should be repeated on a higher number of samples to better clarify the differences among the different types of scaffolds.
Regarding degradation test, PCL coated scaffolds presented almost the same behaviour of Bioglass®, probably due to the non-homogenous coating. On the contrary KHC2000/BG, thanks to the high stability of the polymer in aqueous environment and the much more homogenous coating, showed a less pronounced destabilizati, in particular for long incubation times. Instead KHC2000E2000 exhibited complex behaviour with high variability, due to the presence of PEG.

Furthermore, the high burst release of Bioglass® produces a basic environment in which PCL-based polymers can be degraded faster due to the cleavage of ester bonds. This is probably one of the reasons why the polymeric layer did not act as a barrier to the fast dissolution of Bioglass®. To better understand the degradation behaviour, further degradation study on the coated scaffolds are required, using dynamic conditions in a bioreactor or at least, static-dynamic conditions changing the PBS solution more frequently.
Biological test proved the cytocompatibility of the coated scaffolds with no significant differences in cell viability between coated and uncoated scaffolds. However, the relative mitochondrial activity of cells seeded into the KHC2000 coated BG scaffolds turned out to be significantly ($p>0.05$) higher than that of PCL composite scaffolds. Moreover, the cells were infiltrated also in the inner part of the scaffold and they were well spreaded on the surface.
Summarizing, KHC2000/BG led to highly porous structures and the homogenous and adherent coating did not inhibit the bioactivy of the Bioglass®. Moreover, these scaffolds exhibited significantly improved compressive strength although the amount of polymer forming the coating was much lower compared to the other investigated samples. It provided well-maintained mechanical properties after several days in SBF, although the slight deterioration on the long period. However, it presented the slower degradation rate during immersion in PBS and significantly higher mitochondrial activity of MG-63 with respect the commercial PCL.
Also the scaffolds coated with KHC2000E2000 presented homogenous coating and bioactive behaviour as well as improved mechanical properties even after 21 days in SBF. However, the presence of PEG confers instability in aqueous environment and the mechanical reliability drastically decreases in wet conditions. Moreover, the degradation behaviour was difficult to assess due to the high variability.
Thus, the investigated polyurethanes revealedto be promising polymer coatings for BG scaffolds, with the potential to improve their mechanical properties, with no detrimental effects on bioactivity and cytocompatibility. However, further investigation is required to better clarify the degradation behaviour. Specially the direct interaction between polyurethanes and proteins should be investigated, since this is the first step before the cell attachment. Moreover, to get a complete knowledge about the in vitro behaviour of the polyurethanes, more advanced cell biology studies are required. In addition, long lasting cell culture should be performed using more specific cells to understand how the coating affects bone formation.
Altogether, the results of this work have proved the successful production of composite 45S5 Bioglass® coated with tailor-made poly(urethane-urea)s as promising candidates for bone tissue engineering application.

Acknowledgments

I would like to thank Prof. Gianluca Ciardelli and Prof. Aldo R. Boccaccini who gave me the opportunity to work in two different labs with two amazing teams.
My gratitude is dedicated to Dr. Monica Boffito for her great patience, precious support to achieve the best results and for her extremely dedication to work.
I would like to thank my supervisor in Germany, Marcela Arango Ospina that introduced me in a complete new experience and new environment as was the Erlangen lab, and gave me good ideas and suggestions.
I would like to thank Susanna, Rossella, Alessandro and Arianna from Biolab in Alessandria for the support they gave me.
Thanks to all Boccaccini's staff for their friendship and support. Special thanks to Francesca for sharing with me our "mai una gioia", it is always easier with a friend. Thanks to all student room's group, Alessandro, Ilenia, Steffen, Andy, Julius, Lan, Anne, James and Niklas, I spent with them amazing time also outside the lab with very good beer.
I want to express my deepest gratitude to my parents because nothing of this would be possible without their trust, unconditional love and great support in everything that I choose. Thanks to my sister for her patient with my mess in her room during the last two months, but especially to be a person that I can always trust.
I would like to thank all my family, my big family for their love and attention and for being always present in my life, I feel grateful to those people that are always with me in a special way.
A particular and big thank to all my friends who have become my second family in Turin.
Thanks to all the people that I met during my Erasmus in Erlangen, in particular I thank my "German friends" Marika and Alessia.
Last but not least, I'm very grateful to my boyfriend Rosario for his love and support during all these years together, and for pushing me to be always the best of whatever I am.

Bibliography

[1] Walsh, J. *" Normal bone physiology, remodelling and its hormonal regulation"*, Surgery (Oxford), 33(1), 1-6 (2015).

[2] Lopes, Martins-Cruz, Oliveira, & Mano, *"Bone physiology as inspiration for tissue regenerative therapies"*, Biomaterials, 185, 240-275, (2018).

[3] Adele L Boskey, *" Bone composition: Relationship to bone fragility and antiosteoporotic drug effects"*, BoneKEy Reports, 4, 710-710, (2015).

[4] Loi, Córdova, Pajarinen, Lin, Yao, & Goodman, *" Inflammation, fracture and bone repair"*, Bone, 86, 119-130, (2016).

[5] Kini U, Nandeesh B. *"Physiology of bone formation, remodeling, and metabolism"*, Radionuclide and Hybrid Bone Imaging: Springer; 2012. p. 29-57.

[6] Imai Y, Youn M-Y, Inoue K, Takada I, Kouzmenko A, Kato S. *"Nuclear receptors in bone physiology and diseases"*, Physiological Reviews. 2013;93:481-523

[7] *"Biomarkers in Bone Disease"*, Springer Nature, 2017

[8] A. Cacchioli et al. *"The critical sized bone defect: morphological study of bone healing"*, Ann. Fac. Medic. Vet. di Parma 26, 97–110 (2006).

[9] Schemitsch, Emil H. MD, FRCS(C), *"Size Matters: Defining Critical in Bone Defect Size!"*, Journal of Orthopaedic Trauma: October 2017 - Volume 31 - Issue - p S20–S22.

[10] Hsiong S., & Mooney D., *" Regeneration of vascularized bone"*, Periodontology 2000, 41, 109-22.

[11] Salgado A. J. Coutinho, O. P. & Reis, R. L., *"Bone tissue engineering: state of the art and future trends"*, Macromol. Biosci. 4, 743–65 (2004).

[12] Henkel J., Woodruff M., Epari D., Stec, R., Glatt V., Dickinson I.; Choong P., Schuetz M, Hutmacher D., *"Bone Regeneration Based on Tissue Engineering Conceptions - A 21st Century Perspective. Bone Research"*, 1(3), 216-48 (2013).

[13] Bergmann C.P., Stumpf A. *"Biomaterials. In: Dental Ceramics Topics in Mining, Metallurgy and Materials Engineering"*, Springer, Berlin, Heidelberg (2013).

[14] Hench, L. *"Biomaterials: A forecast for the future"* Biomaterials, 19(16), 1419-1423 (1998).

[15] L. L. Hench, *"Biomaterials"*, Science, vol. 208, no. 4446, pp. 826-831, 1980.

[16] Cao, & Hench, *"Bioactive materials"*, Ceramics International, 22(6), 493-507 (1996).

[17] L. L. Hench, R. J. Splinter, W. C. Allen, T. K. Jr Greenlee, *"Bonding mechanisms at the interface of ceramic prosthetic materials"*, J. Biomed. Mater. Res., vol. 2, pp. 117-141, 1972.

[18] Hench, L., & Thompson, I. *"Twenty-first century challenges for biomaterials"*. Journal of the Royal Society, Interface, 7 Suppl 4(4), S379-91 (2010).

[19] Hutmacher, D., Schantz, J., Lam, C., Tan, K., & Lim, T. *"State of the art and future directions of scaffold-based bone engineering from a biomaterials perspective"*, Journal of Tissue Engineering and Regenerative Medicine, 1(4), 245-60 (2007).

[20] G.P. Kothiyal, Arvind Ananthanarayanan and G.K, *"Glass ang Glass-Ceramic"* in Dey Functional Materials : Preparation, Processing and Applications, edited by S. Banerjee, and A. K. Tyagi, Elsevier, 2011.

[21] De Aza Moya, Piedad Nieves, Aza Moya, Antonio H. de, Pena, P., & Aza, S. de., *"Bioactive glasses and glass-ceramics"*, Boletín De La Sociedad Española De Cerámica Y Vidrio, 46(2), 45-55 (2007).

[22] L. L. Hench, *"The story of Bioglass®"*, J. Mater. Sci. Mater. Med., vol. 17, no. 10, pp. 967-978, 2006.

[23] F. Baino, *"Bioactive glasses-when glass science and technology meet regenerative medicine"*, Ceramics International (2018).

[24] L. C. Gerhardt, A. R. Boccaccini, *"Bioactive Glass and Glass-Ceramic Scaffolds for Bone Tissue Engineering"*

[25] J. Najdanović, J. Rajković, S. Najman, *"Bioactive Biomaterials: Potential for Application in Bone Regenerative Medicine"*, In: Zivic F., Affatato S., Trajanovic M., Schnabelrauch M., Grujovic N., Choy K. (eds) Biomaterials in Clinical Practice. Springer, Cham (2018).

[26] P.N. Gunawidjaja, R. Mathew, A.Y.H. Lo, et al. *"Local structures of mesoporous bioactive glasses and their surface alterations in vitro: inferences from solid-state nuclear magnetic resonance"*, Philos Trans R Soc A Math Phys Eng Sci 2012; 370: 1376–1399.

[27] Hench, L., & Polak, J. *"Third-generation biomedical materials"*, Science (New York, N.Y.), 295(5557), 1014-7 (2002).

[28] Rahaman, Day, Sonny Bal, Fu, Jung, Bonewald, Tomsia, *" Bioactive glass in tissue engineering"* Acta Biomaterialia, 7(6), 2355-2373, (2011).

[29] M. Islam, R. Felfel, E. Abou Neel, D. Grant, I. Ahmed, K. Hossain, *"Bioactive calcium phosphate–based glasses and ceramics and their biomedical applications: A review"*, Journal of Tissue Engineering, 8, 2041731417719170, (2017).

[30] S. Fagerlund, L. Hupa, M. Hupa, *"Comparison of reactions of bioactive glasses in different aqueous solutions"*, Ceram Trans 2010; 218: 101.

[31] D. Rohanová, A.R. Boccaccini, D.M. Yunos, et al. *"TRIS buffer in simulated body fluid distorts the assessment of glass-ceramic scaffold bioactivity"*, Acta Biomater 2011; 7:2623–2630.

[32] D. Rohanová D, A.R. Boccaccini, D. Horkavcová et al. *"Is non buffered DMEM solution a suitable medium for in vitro bioactivity tests?"*, J Mater Chem B Mater Biol Med 2014; 2: 5068–5076.

[33] A. Popa, G. Stan, M. Husanu et al. *"Bioglass implant coating interactions in synthetic physiological fluids with varying degrees of biomimicry"*, Int J Nanomedicine 2017; 12: 683–707.

[34] Z. Zhou, Q. Yi, X Liu et al. *"In vitro degradation behaviors of poly-L-lactide/bioactive glass composite materials in phosphate-buffered solution"* Polym Bull 2009; 63: 575–586.

[35] Hoppe, Güldal, & Boccaccini, *"A review of the biological response to ionic dissolution products from bioactive glasses and glass-ceramics"*, Biomaterials, 32(11), 2757-2774, (2011).

[36] Maeno S, Niki Y, Matsumoto H, Morioka H, Yatabe T, Funayama A, et al. *"The effect of calcium ion concentration on osteoblast viability, proliferation and differentiation in monolayer and 3D culture"*, Biomaterials 2005;26(23): 4847e55.

[37] Blaker JJ, Nazhat SN, Boccaccini AR.*"Development and characterisation of silver-doped bioactive glasscoated sutures for tissue engineering and wound healing applications"*, Biomaterials 2004;25(7e8):1319e29.

[38] Kawashita M, Tsuneyama S, Miyaji F, Kokubo T, Kozuka H, Yamamoto K.*"Antibacterial silver-containing silica glass prepared by sol-gel method"*, Biomaterials 2000;21(4):393e8.

[39] Verné E, Miola M, Vitale Brovarone C, Cannas M, Gatti S, Fucale G, et al. *"Surface silver-doping of biocompatible glass to induce antibacterial properties.Part I: massive glass"*, J Mater Sci Mater Med 2009;20(3):733e40.

[40] Bellantone, M.; Williams, H.D.; Hench, L.L. *"Broad-spectrum bactericidal activity of Ag2O-doped bioactive glass"* Antimicrob. Agents Chemother. 2002, 46, 1940-1945.

[41] Newby, P., El-Gendy, J., Kirkham, R., Yang, X., Thompson, B., & Boccaccini, I. *"Ag-doped 45S5 Bioglass®-based bone scaffolds by molten salt ion exchange: Processing and characterisation"*, Journal of Materials Science: Materials in Medicine, 22(3), 557-569, (2011).

[42] Zreiqat, H., Howlett, C., Zannettino, A., Evans, P., Schulze-Tanzil, G., Knabe, C., & Shakibaei, M. *"Mechanisms of magnesium-stimulated adhesion of osteoblastic cells to commonly used orthopaedic implants"*, Journal of Biomedical Materials Research, 62(2), 175-184, (2002).

[43] Balasubramanian, Büttner, Miguez Pacheco, & Boccaccini. *"Boron-containing bioactive glasses in bone and soft tissue engineering"*, Journal of the European Ceramic Society, 38(3), 855-869, (2018).

[44] Yao, A., Rahaman, M., Lin, N., & Huang, J. *"Structure and crystallization behavior of borate-based bioactive glass"*, Journal of Materials Science, 42(23), 9730-9735.

[45] Liu, Xin, Pan, Haobo, Fu, Hailuo, Fu, Qiang, Rahaman, Mohamed N, & Huang, Wenhai, *"Conversion of borate-based glass scaffold to hydroxyapatite in a dilute phosphate solution"*, This work was presented at the Materials Science and Technology (MS&T'09) Conference Symposium: Next Generation Biomaterials, Pittsburgh, PA, 2529 October 2009. Biomedical Materials, 5(1), 6, (2010).

[46] W. Huang, D.E. Day, K. Kittiratanapiboon, M.N. Rahaman, *"Kinetics and mechanisms of the conversion of silicate (45S5), borate, and borosilicate glasses to hydroxyapatite in dilute phosphate solutions"*, J. Mater. Sci. Mater. Med. 17 (2006) 583–596.

[47] Baino, F.; Hamzehlou, S.; Kargozar, S. *"Bioactive Glasses: Where Are We and Where Are We Going?"*, J. Funct. Biomater. 2018, 9, 25.

[48] Jones, J. *"Reprint of: Review of bioactive glass: From Hench to hybrids"*, Acta Biomaterialia, 23, S53-S82, (2015).

[49] Hench, L. *"Bioglass: 10 milestones from concept to commerce"*, Journal of Non-Crystalline Solids, 432(PA), 2-8, (2016).

[50] Henkel, J., Woodruff, M., Epari, D., Steck, R., Glatt, V., Dickinson, I., Choong, P., Schuetz, M., Hutmacher, D., *"Bone Regeneration Based on Tissue Engineering Conceptions - A 21st Century Perspective"*, Bone Research, 1(3), 216-48 (2013).

[51] Tong Wu, Suihuai Yu, Dengkai Chen, & Yanen Wang. *"Bionic Design, Materials and Performance of Bone Tissue Scaffolds"*, Materials, 10(10), (2017).

[52] Akeda, K.; An, H.S.; Okuma, M.; Attawia, M.; Miyamoto, K.; Thonar, E.J.; Lenz, M.E.; Sah, R.L.; Masuda, K. *"Platelet-rich plasma stimulates porcine articular chondrocyte proliferation and matrix biosynthesis"*, Osteoarthr. Cartil. 2006, 14, 1272–1280.

[53] Elisa Fiume, Jacopo Barberi, Enrica Verné, & Francesco Baino, *"Bioactive Glasses: From Parent 45S5 Composition to Scaffold-Assisted Tissue-Healing Therapies"*, Journal of Functional Biomaterials, 9(1), (2018).

[54] Li, P, Yang, Q, Zhang, F, Kokubo, T 1992/11/01 452 456, *" The Effect of Residual Glassy Phase in a Bioactive Glass Ceramic on the Formation of its Surface Apatite Layer In Vitro"*, VL 10.1007/BF00701242 Journal of Materials Science-materials in Medicine.

[55] Siqueira, L., Gouveia, R., Grenho, F., Monteiro, L., Fernandes, F., & Trichês, J. *"Highly porous 45S5 bioglass®-derived glass–ceramic scaffolds by gelcasting of foams"*, Journal of Materials Science, 53(15), 10718-10731, (2018).

[56] J. R. Jones, L.L. Hench, *"Regeneration of trabecular bone using porous ceramics"*, Curr. Opin. Solid State Mater. Sci., vol. 7, no. 4-5, pp. 301-307, 2003.

[57] Wu, S., Hsu, H., Hsiao, S., & Ho, W. *"Preparation of porous 45S5 Bioglass®-derived glass–ceramic scaffolds by using rice husk as a porogen additive"*, Journal of Materials Science: Materials in Medicine, 20(6), 1229-1236, (2009).

[58] Bellucci, Cannillo, Sola, Chiellini, Gazzarri, & Migone. *Macroporous Bioglass®-derived scaffolds for bone tissue regeneration"* Ceramics International, 37(5), 1575-1585, (2011).

[59] Deb, S., Mandegaran, R., & Di Silvio, L. *"A porous scaffold for bone tissue engineering/45S5 Bioglass® derived porous scaffolds for co-culturing osteoblasts and endothelial cells"*, Journal of Materials Science: Materials in Medicine, 21(3), 893-905, (2010).

[60] Boccardi, E ; Philippart, A ; Melli, V ; Altomare, L ; De Nardo, L ; Novajra, G ; Vitale-Brovarone, C ; Fey, T ; Boccaccini, A R, *"Bioactivity and Mechanical Stability of 45S5 Bioactive Glass Scaffolds Based on Natural Marine Sponges"*, Annals of Biomedical Engineering, 44(6), 1881-93, (2016).

[61] Chen Q, Baino F, Spriano S, Pugno N.M, & Vitale-Brovarone C. *"Modelling of the strength-porosity relationship in glass-ceramic foam scaffolds for bone repair"*, In: JOURNAL OF THE EUROPEAN CERAMIC SOCIETY, - ISSN: 0955-2219, (2014).

[62] Tesavibul, Felzmann, Gruber, Liska, Thompson, Boccaccini, & Stampfl, *"Processing of 45S5 Bioglass® by lithography-based additive manufacturing"* Materials Letters, 74(C), 81-84 (2012).

[63] Eqtesadi, Motealleh, Miranda, Pajares, Lemos, & Ferreira, *"Robocasting of 45S5 bioactive glass scaffolds for bone tissue engineering"*, Journal of the European Ceramic Society, 34(1), 107-118, (2014).

[64] Motealleh, A., Eqtesadi, S., Civantos, A., Pajares, A., & Miranda, P. *"Robocast 45S5 bioglass scaffolds: In vitro behavior"*, Journal of Materials Science, 52(15), 9179-9191, (2017).

[65] Jinglin Liu , Huanlong Hu , Pengjian Li , Cijun Shuai & Shuping Peng, *"Fabrication and Characterization of Porous 45S5 Glass Scaffolds via Direct Selective Laser Sintering"*, Materials and Manufacturing Processes, 28:6, 610-615.

[66] Rezwan, Chen, Blaker, & Boccaccini, *"Biodegradable and bioactive porous polymer/inorganic composite scaffolds for bone tissue engineering"*, Biomaterials, 27(18), 3413-3431, (2006).

[67] Mohamad Yunos, D., Bretcanu, O., & Boccaccini, A. *"Polymer-bioceramic composites for tissue engineering scaffolds"*, Journal of Materials Science, 43(13), 4433-4442, (2008).

[68] F. Asghari, M. Samiei, K. Adibkia, A. Akbarzadeh, and S. Davaran, *"Biodegradable and biocompatible polymers for tissue engineering application: a review"*, Artif. Cells, Nanomedicine, Biotechnol., vol. 1401, no. February, pp. 1–8, 2016.

[69] Chen, Thompson, & Boccaccini, "45S5 Bioglass®-derived glass–ceramic scaffolds for bone tissue engineering", Biomaterials, 27(11), 2414-2425, (2006).

[70] Bretcanu, O., Misra, S., Roy, I., Renghini, C., Fiori, F., Boccaccini, A., & Salih, V. *"In vitro biocompatibility of 45S5 Bioglass®-derived glass–ceramic scaffolds coated with poly(3-hydroxybutyrate"*, Journal of Tissue Engineering and Regenerative Medicine, 3(2), 139-148, (2009).

[71] Li, Nooeaid, Roether, Schubert, & Boccaccini, *"Preparation and characterization of vancomycin releasing PHBV coated 45S5 Bioglass®-based glass–ceramic scaffolds for bone tissue engineering"*, Journal of the European Ceramic Society, 34(2), 505-514, (2014).

[72] Yao, Qingqing & Nooeaid, Patcharakamon & Roether, Judith & Dongd, Yanming & Zhange, Qiqing & Boccaccini, Aldo, *"Bioglass®-based scaffolds incorporating polycaprolactone and chitosan coatings for controlled vancomycin delivery"*, Ceramics International, (2013).

[73] Han, Jian & Chen, Bing & Ye, Lin & Zhang, Ai-ying & Zhang, Jian & Feng, Zeng-gu, *"Synthesis and characterization of biodegradable polyurethane based on poly(ϵ-caprolactone) and L-lysine ethyl ester diisocyanate"*, Front. Mater. Sci. China. 3. 25-32. 10.1007/s11706-009-0013-4, (2009).

[74] Ryszkowska, J & Wasniewski, Bartlomiej, '*"Quantitative description of the morphology of polyurethane nanocomposites for medical applications"*, WIT Transactions on Engineering Sciences. 72. 377-386, (2011).

[75] Cooper, Stuart L. Guan, Jianjun, *"Advances in Polyurethane Biomaterials"*, Elsevier (2016).

[76] Sisson, Ekinci, & Lendlein, *"The contemporary role of ϵ-caprolactone chemistry to create advanced polymer architectures"*, Polymer, 54(17), 4333-4350, (2013).

[77] Woodruff MA, Hutmacher DW. *"The return of a forgotten polymer—Polycaprolactone in the 21st century"*, Prog Polym Sci (2010).

[78] S. Sartori, M. Boffito, P. Serafini, A. Caporale, A. Silvestri, E. Bernardi, M. P. Sassi, F. Boccafoschi, G. Ciardelli, *"Synthesis and structure-property relationship of polyester- urethanes and their evaluation for the regeneration of contractile tissues"*, React. Funct. Polym., vol. 73, no. 10, pp. 1366-1376.

[79] Hong Y, Guan JJ, Fujimoto KL, Hashizume R, Pelinescu AL and Wagner WR, "Tailoring the degradation kinetics of poly(ester carbonate urethane)urea thermoplastic elastomers for tissue engineering scaffolds", Biomaterials, 2010, 31, 4249–4258.

[80] Yang, Haiqing; Mouazen, Abdul, *"Vis/Near- and Mid- Infrared Spectroscopy for Predicting Soil N and C at a Farm Scale"*, 2012/04/25 978-953-51-0538-1 10.5772/36393

[81] García, Rosa & Codoñer, Armando & Bañó, María & Abad, Concepción & Campos, Agustín, *"Size-Exclusion Chromatographic Determination of Polymer Molar Mass Averages Using a Fractal Calibration"*, Journal of chromatographic science. 43. 226-34. (2005).

[82] Q. Z. Chen, I. D. Thompson, A. R. Boccaccini, *"45S5 Bioglass®-derived glass ceramic scaffolds for bone tissue engineering"*, Biomaterials, vol. 27, pp. 2414-2425, 2006.

[83] Q.Z. Chen, D. Mohn, W.J. Stark,*"Optimization of Bioglass® scaffold fabrication process"*, Journal of the American Ceramic Society, 94 (12) (2011), pp. 4184-4190.

[84] L.L Hench, Ji Wilson ,*"Surface-active biomaterials."* Science 1984;226:630–6.

[85] C. Vitale-Brovarone, E. Verne, L. Robiglio, P. Appendino, F. Bassi, G. Martinasso, G. Muzio, R. Canuto, *"Development of glass-ceramic scaffolds for bone tissue engineering: characterisation, proliferation of human osteoblasts and nodule formation"*, ActaBiomater.3,199–208.

[86] Z. Fereshteh, P. Nooeaid, M.H. Fathi, A. Bagri, A.R. Boccaccini, *"The effect of coating type on mechanical properties and controlled drug release of PCL/zein coated 45S5 bioactive glass scaffolds for bone tissue engineering"*, Mater. Sci. Eng. C54 (2015) 50–60.

[87] S. Miglietta, *"Reinforcement of Bioactive Glass scaffolds by tailor-made, degradable biomedical polymers"*, Master thesis in Biomedical Engineering, 2017.

[88] Q.Z. Chen, A.R. Boccaccini, *"Poly(D,L-lactic acid) coated 45S5 Bioglass-based scaffolds: processing and characterization"*, J. Biomed. Mater. Res. A, 77 (2006), pp. 445-457.

[89] Baskaran, Sulochanadevi, *"Structure and Regulation of Yeast Glycogen Synthase"*, 2010/01/01.

[90] T. Kokubo and H. Takadama, *"How useful is SBF in predicting in vivo bone bioactivity?"*, Biomaterials, vol. 27, no. 15, pp. 2907-2915, 2006.

[91] Li W., Garmendia N., de Larraya U.P., Ding Y., Detsch R., Grünewald A., Roether J.A., Schubert D.W., Boccaccini A.R., *"45S5 bioactive glass-based scaffolds coated with cellulose nanowhiskers for bone tissue engineering"*, RSC Adv. 2014;4:56156–56164

[92] Maquet V., Boccaccini A.R., Pravata L., Notingher I., Jerome R., *"Porous poly(a-hydroxyacid)/Bioglasss composite scaffolds for bone tissue engineering. I: Preparation and in vitro characterisation"*, Biomaterials 2004;25:4185–94.

[93] F. E. Ciraldo, E. Boccardi, V. Melli, F. Westhauser, A.R. Boccaccini, *" Tackling bioactive glass excessive in vitro bioreactivity: Preconditioning approaches for cell culture tests"*, Acta Biomaterialia 75 (2018) 3–10.

[94] K.D. Nisha, M. Navaneethan, B. Dhanalakshmi, K. Saravana Murali, Y. Hayakawa, S. Ponnusamy, C. Muthamizhchelvan, P. Gunasekaran, *"Effect of organic-ligands on the toxicity profiles of CdS nanoparticles and functional properties"*, Colloids and Surfaces B: Biointerfaces, 2015

[95] Terry L Riss, Richard A Moravec, Andrew L Niles, Sarah Duellman, Hélène A Benink, Tracy J Worzella, Lisa Minor, *"Cell Viability Assays"*, 2013 May 1 . In: Sittampalam GS, Coussens NP, Brimacombe K, et al., editors. Assay Guidance Manual. Bethesda (MD): Eli Lilly & Company and the National Center for Advancing Translational Sciences; 2004.

[96] Jing Wang , Zhen Zheng , Liang Chen , Xiaoxiong Tu & Xinling Wang (2013), *" Glutathione-responsive biodegradable poly(urea-urethane)s containing L-cystinebased chain extender"*, Journal of Biomaterials Science, Polymer Edition, 24:7, 831-848.

[97] Guan JJ,Sacks MS, Beckman EJ,Wagner WR., *"Synthesis, characterization,and cytocompatibility of elastomeric,biodegradable poly(ester-urethane)ureas based on poly(caprolactone) and putrescine"*, J Biomed Mater Res 2002;61:493–503.

[98] ZhangC, RenZ, YinZ, JiangL, FangS, *" Experimental FTIR and simulation studies on H-bonds of model polyurethane in solutions. I: in dimethylformamide (DMF)"*, Spectrochimi Acta Part A. 2011;81:598–603.

[99] Z. Gan, Q. Liang, J. Zhang and X. Jing, *"Enzymatic degradation of poly(ϵ-caprolactone) film in phosphate buffer containing lipases"*, Polym. Degrad. Stab., 1997, 56, 209–213.

[100] Ponjavic, P.; Nikolic, M.S.; Nikodinovic-Runic, J.; Jeremic, S.; Stevanovic, S.; Djonlagic, J., *"Degradation behavior of PCL/PEO/PCL and PCL/PEO block copolymers under controlled hydrolytic, enzymatic and composting conditions"*, Polym. Test. 2017, 57, 66–77.

[101] M. Tortorici, *"Reinforcement of Bioactive Glass scaffolds by tailor-made, degradable biomedical polymers"*, Master thesis in Biomedical Engineering, 2016.

[102] G.A. Skarja & K.A. Woodhouse (1998), *"Synthesis and characterization of degradable polyurethane elastomers containing an amino acid-based chain extender"*, Journal of Biomaterials Science, Polymer Edition, 9:3, 271-295.

[103] S. Li, H. Garreau, B. Pauvert, J. McGrath, A. Toniolo, M. Vert, *"Enzymatic degradation of block copolymers prepared from epsilon-caprolactone and poly(ethylene glycol)"*, Biomacromolecules, 3 (2002), pp. 525-530.

[104] Ma, Z.; Hong, Y.; Nelson, D.M.; Pichamuthu, J.E.; Leeson, C.E.; Wagner, W.R., *"Biodegradable polyurethane ureas with variable polyester or polycarbonate soft segments: Effects of crystallinity, molecular weight, and composition on mechanical properties"*, Biomacromolecules 2011, 12, 3265–3274.

[105] Felfel, R., Hossain, M., Parsons, K., Rudd, Z., & Ahmed, A. *"Accelerated in vitro degradation properties of polylactic acid/phosphate glass fibre composites"* Journal of Materials Science, 50(11), 3942-3955 (2015).

[106] Heimowska Aleksandra, Morawska Magda, & Bocho-Janiszewska Anita, *"Biodegradation of poly(ϵ-caprolactone) in natural water environments"*, Polish Journal of Chemical Technology, 19(1), 120-126 (2017).

[107] Loh, X. *"The effect of pH on the hydrolytic degradation of poly(ϵ-caprolactone)-block-poly(ethylene glycol) copolymers"*, Journal of Applied Polymer Science, 127(3), 2046-2056 (2013).

[108] Dean-Mo Liu, *"Control of pore geometry on influencing the mechanical property of porous hydroxyapatite bioceramic"* J Mater Sci Lett (1996).

[109] Baino, F., Ferraris, M., Bretcanu, O., Verné, E., & Vitale-Brovarone, C. *"Optimization of composition, structure and mechanical strength of bioactive 3-D glass-ceramic scaffolds for bone substitution"*, Journal of Biomaterials Applications, 27(7), 872–890, (2013).

[110] Bretcanu, Chatzistavrou, Paraskevopoulos, Conradt, Thompson, & Boccaccini, *"Sintering and crystallisation of 45S5 Bioglass® powder"*, Journal of the European Ceramic Society, 29(16), 3299-3306 (2009).

[111] O. P. Filho, G. P. LaTorre, L. L. Hench, *"Effect of Crystallization on apatite-layer formation of bioactive glass 45S5"*, J. Biomed. Mater. Res., vol. 30, no. 4, pp. 509-5144, 1996.

[112] Lefebvre, Chevalier, Gremillard, Zenati, Thollet, Bernache-Assolant, & Govin, *"Structural transformations of bioactive glass 45S5 with thermal treatments"*, Acta Materialia, 55(10), 3305-3313, (2007).

[113] Cerruti, M., Greenspan, D. & Powers, K. *"Effect of pH and ionic strength on the reactivity of Bioglass 45S5"*, Biomaterials 26, 1665–74 (2005).

[114] Wu, Hill, Yue, Nightingale, Lee, & Jones, *"Melt-derived bioactive glass scaffolds produced by a gel-cast foaming technique"*, Acta Biomaterialia, 7(4), 1807-1816, (2011).

[115] Romeis, Hoppe, Detsch, Boccaccini, Schmidt, & Peukert, *"Top-down Processing of Submicron 45S5 Bioglass® for Enhanced in Vitro Bioactivity and Biocompatibility"*, Procedia Engineering, 102(C), 534-541, (2015).

[116] [K. S. K. Lin, Y. H. Tseng, Y. Mou, Y. C. Hsu, C. M. Yang, J. C. C. Chan, *"Mechanistic Study of Apatite Formation on Bioactive Glass Surface Using 31P Solid-State NMR Spectroscopy"*, Chem. Mater., vol. 17, pp. 4493-4501, 2005.

[117] Chen, Q., Efthymiou, A., Salih, V., & Boccaccini, A. *"Bioglass®-derived glass–ceramic scaffolds: Study of cell proliferation and scaffold degradation in vitro"*, Journal of Biomedical Materials Research Part A, 84(4), 1049-1060 (2008).

[118] J. S. Temenoff, L. Lu, A. G. Mikos, *"Bone tissue engineering using synthetic biodegradable polymer scaffolds"*, Davies JE, editor. Bone engineering. Toronto: EM Squared, pp. 455-462, 2000.

[119] Farag, & Rüssel, *"Glass-ceramic scaffolds derived from Bioglass® and glass with low crystallization affinity for bone regeneration"*, Materials Letters, 73, 161-165 (2012).

[120] Li, Ding, *"Localized mechanical deformation and dissolution of 45S5 Bioglass®"*, University of Kentucky Doctoral Dissertations. 91 (2010).

[121] Fu, Q., Rahaman, M., & Day, D. *"Accelerated Conversion of Silicate Bioactive Glass (13-93) to Hydroxyapatite in Aqueous Phosphate Solution Containing Polyanions"*, Journal of the American Ceramic Society, 92(12), 2870-2876 (2009).

[122] Fu, Rahaman, Sonny Bal, Brown, & Day, *"Mechanical and in vitro performance of 13–93 bioactive glass scaffolds prepared by a polymer foam replication technique"*, Acta Biomaterialia, 4(6), 1854-1864 (2008).

[123] A. M. Gatti, G. Valdre, O. H. Andersson, *"Analysis of the in vivo reactions of a bioactive glass in soft and hard tissue"*, Biomaterials, vol. 15, pp. 208-212, 1994.

[124] Lossdörfer, Schwartz, Lohmann, Greenspan, Ranly, & Boyan, *"Osteoblast response to bioactive glasses in vitro correlates with inorganic phosphate content"*, Biomaterials, 25(13), 2547-2555, (2004).

[125] Will, Julia & Detsch, Rainer & Boccaccini, Aldo, *"Chapter 7.1. Structural and Biological Characterization of Scaffolds. Characterization of Biomaterials"*, 299-310. 10.1016/B978-0-12-415800-9.00008-5, (2013).

[126] M. Peroglio, L. Gremillard, J. Chevalier, L. Chazeau, C. Gauthier, T. Hamaide *"Toughening of bioceramics scaffolds by polymer coating"*, J. Eur. Ceram. Soc., vol. 27, pp. 2679-2685, 2007.